USING MEMBRANE DISTILLATION CRYSTALLISATION FOR THE TREATMENT OF HYPERSALINE MINING AND INDUSTRIAL WASTEWATER

Report to the
Water Research Commission

by

Jeeten Nathoo, Louie Eggers & Dyllon Randall

NuWater, Cape Town

WRC Report No. 2223/1/16
ISBN 978-1-4312-0867-8

January 2017

Obtainable from
Water Research Commission
Private Bag X03
GEZINA, 0031

orders@wrc.org.za or download from www.wrc.org.za

Executive Summary

South Africa is a water scarce country that is facing increasing stress with regards to the availability of water resources that are environmentally and economically sustainable. This is particularly evident in the mining industry, where issues such as Acid Mine Drainage (AMD) are becoming increasingly detrimental to water security. The viable treatment of these wastewaters is necessary if sustainable growth is to be achieved in alignment with the national developmental goals. Consequently, a systems approach to the wastewater treatment process needs to be adopted that focuses on a complete conversion of the waste material to viable products, using less energy and resources in order for the process to be viewed as truly sustainable.

Membrane Distillation Crystallisation (MDC) offers a sustainable wastewater treatment process, particularly when utilising any available excess heat from peripheral processes to produce pure water as well as salt(s) products, thereby converting a waste material into a product of value that can be reused, recycled or sold to offset water treatment costs. MDC is also an attractive wastewater treatment technique because it requires significantly lower operating temperatures (40-60°C) when compared to evaporative crystallisation, thus enabling the efficient use of waste heat streams or renewable energy sources. Furthermore, MDC requires lower hydrostatic operating pressures when compared to reverse osmosis (RO) and can therefore be constructed from less expensive materials. Other advantages of MDC include: a reduction in membrane fouling compared to other pressure driven processes, improved rejection factors for feed streams containing non-volatile solutes and the ability to treat high total dissolved solids (TDS) feed solutions that are close to their saturation limit (QTAISHAT, M.R. and Banat, F., 2012) (KHAYET, M.). Furthermore, when applied to AMD water treatment, the MDC process is able to operate in very acidic or basic streams (ZENG, L. and Gao, C., 2010), thus the AMD streams would not need to be pre-treated or neutralized beforehand.

The use of MDC for the treatment of mine wastewater has not been a major focus of research even though there is great potential in this field. The focus of this project was therefore on investigating the applicability of MDC for the treatment of industrial wastewater with a specific focus on the treatment of mine wastewater, as this is currently very limited. The project also focused on investigating the impact that the presence of various types of antiscalants had on the MDC process. This was done in two phases:

Phase 1: Aqueous Thermodynamic modelling
Two industrial brines emanating from typical mining related activities in South Africa were selected and the effects of (i) brine composition, (ii) water recovery, and (iii) operating temperature on the crystallisation characteristics of the MDC process were investigated with the use of an aqueous thermodynamic modelling tool.

The study demonstrated the efficacy of using aqueous thermodynamic modelling as a tool for investigating and predicting the crystallisation aspects of the MDC process, including, though not limited to the scaling tendencies, the identities of crystallising salts, and the sequence in which the salts crystallise out as well as identifying subtler crystallisation aspects such as inverse solubilities of specific species, etc.

Based on the two brine specimens investigated, the following general conclusions can be drawn:

i) The propensity for crystallisation increases with an increase in water recovery with the MDC process. This is directly linked to the increase in the supersaturation as more water is removed from the feed side to the product side. This consequently increases the driving force for crystallisation as a result of the removal of permeate water from the brine
ii) Except for species that exhibit an inverse solubility with respect to temperature, a lower operating temperature results in a higher crystal product yield due to the lower solubility of scaling species at lower temperatures
iii) For scaling species exhibiting inverse solubility characteristics, the inverse of (ii) above is true
iv) The purity of the resultant crystallisation product is dependent on the extent of water recovery as the number of additional crystallising species (contaminants/impurities) increases with an increase in the water recovery
v) At the higher MDC operating temperature of 80°C, similar to the 60°C scenario, due to the inverse solubility of calcium sulphate, the dominant crystallising salt at all water recoveries will be calcium sulphate. However, due to the greater driving force of calcium sulphate crystallisation, the purity of the mixed salt is substantially higher with respect to the calcium sulphate
vi) Lastly, different brine compositions produce diverse salts and salt yields, sometimes at the same operating conditions. Consequently, each brine composition should be assessed independently during the process design of an MDC process.

Phase 2: Experimental investigation into MDC

The second phase focussed on the experimental aspects of the investigation, in which a synthetic brine solution was prepared to emulate real brine from a coal mining application in order to:

1. Validate the results obtained from the aqueous thermodynamic modelling. This was achieved by using a laboratory-scale MDC experimental rig to investigate the effects of (i) operating temperature, (ii) feed water concentration, and (iii) flow rates on the permeate flux rates, water recovery, water purity, and salt morphology and composition of the system.
2. Investigate the effect that various antiscalants had on the operating parameters of the MDC process and the performance of the technology. Consequently, the effect of residual antiscalants on the operating parameters as well as: i) permeate flux rates; ii) water purity; and iii) salt morphology and composition were investigated. Two commercially available antiscalants currently used in mining water treatment plants were studied. The distinguishing characteristics between the two antiscalants were:
    a. Antiscalant 1 had organic functional groups
    b. Antiscalant 2 was phosphonic acid based.

The investigations into the effects of (i) operating temperature, (ii) operating feed water concentration, (iii) operating flow rates, and (iv) antiscalant addition on the permeate flux rates all yielded the following results:

i) The higher the feed temperatures and the greater the temperature difference between the feed and product streams, the greater the flux rates
ii) Changes in feed water concentrations (at TDS's of 8000-16000 mg/L) did not have any significant effect on the flux rates, at least within the range of recoveries investigated
iii) Increased flow rates (ranging from 0.15 m/s to 0.49 m/s in the main feed pipe) led to improved flux rates
iv) Phosphonic based antiscalants did not have an effect on the flux rates, whilst the organic based antiscalant resulted in a reduction in the flux rate.

The experiments were performed using three types of polytetrafluoroethylene (PTFE) membranes that had a thickness of 25 µm. All three membranes had different backing layers, with a polyethylene (PE) and polyester non-woven fabric backing layers achieving the highest flux rate. Conversely, the polyester cloth-backing layer achieved the lowest flux rate.

The water purity from all investigations yielded good results with the product water exhibiting extremely low conductivity (<10 µS/cm), which only started to increase once scaling on the membrane surface and pore wetting caused a decrease the flux rate.

Limited distinction could be made with respect to the differences in the morphology between the various factors investigated. This was most likely due to the constant agitation speed in the feed reactor of 600rpm, which had a high shearing effect on the particles as well as due to the milling effect caused by the peristaltic pump. However, the addition of antiscalant did yield good results in that the agglomerates were significantly smaller (up to 50 times smaller with the use of organic based antiscalant) and well dispersed in the presence of an antiscalant.

When looking at the composition of salts formed, only one sample yielded results that were consistent with thermodynamic modelling results.

Importantly, the high flux rates obtained from these experiments are significantly higher than those reported previously in literature and indicates a definite possibility that membrane distillation could be used to increase water recovery from RO brines whilst generating usable salts as a by-product. However, more research needs to go into the development of cheaper membranes for this purpose, since currently hydrophobic membranes are being used more for lab scale experimentation as opposed to large-scale operations.

Acknowledgements

The project team wishes to thank the following Reference Group members for their contributions to the project:

Mr Gerhard Gericke	Eskom
Prof Joe Modise	Vaal University of Technology, VUT
Prof Freeman Ntuli	University of Johannesburg, UJ
Prof Leslie Petrik	University of the Western Cape, UWC
Dr Craig Sheridan	University of the Witwatersrand, WITS
Mr Achim Wurster	Water Treatment Process Engineering
Dr John Ngoni Zvimba	CSIR, Natural Resources and the Environment

This page was left blank intentionally

Table of Contents

List of Figures

List of Tables

CHAPTER 1 - Introduction and Background

South Africa is a water scarce country that is facing increasing stress with regards to the availability of water resources that are environmentally and economically sustainable. This is particularly evident in the mining industry, where issues such as Acid Mine Drainage (AMD) are becoming increasingly detrimental to water security. The sustainable treatment of these wastewaters is necessary if sustainable growth is to be achieved in alignment with the national developmental goals. Consequently, a systems approach to the wastewater treatment process needs to be adopted that focuses on a complete conversion of the waste material to viable products, using less energy and resources in order for the process to be viewed as truly sustainable.

Membrane Distillation Crystallisation (MDC) offers a sustainable wastewater treatment process, particularly when utilising any available excess heat from peripheral processes to produce pure water as well as salt(s) products, thereby converting a waste material into a product of value that can be reused, recycled or sold to offset water treatment costs. Membrane Distillation Crystallisation is also an attractive wastewater treatment technique because it requires significantly lower operating temperatures (40-60°C) when compared to evaporative crystallisation, thus enabling the efficient use of waste heat streams or renewable energy sources. Furthermore, MDC requires lower hydrostatic operating pressures when compared to reverse osmosis (RO) and can therefore be constructed from less expensive materials. Other advantages of MDC include: a reduction in membrane fouling compared to other pressure driven processes, improved rejection factors for feed streams containing non-volatile solutes and the ability to treat high total dissolved solids (TDS) feed solutions that are close to their saturation limit (QTAISHAT, M.R. and Banat, F., 2012) (KHAYET, M.) Furthermore, when applied to AMD water treatment, the MDC process is able to operate in very acidic or basic streams (ZENG, L. and Gao, C., 2010), thus the AMD streams would not need to be pre-treated or neutralized beforehand.

There are however a few disadvantages to MDC, which include: currently a low productivity, a risk of membrane wetting due to the hydrophobic nature of the membrane, the cost of commercial membrane modules and a low membrane flux, but these can all mainly be attributed to the fact that there has been a lack of research done specifically in the design of MDC membranes (KHAYET, M.).

During MDC, MD is used to concentrate a stream to the desired concentration where salt(s) begin to crystallise out in a crystalliser (TUN, C.M. et al., 2005). Many researchers have investigated the use of MDC for the treatment of various industrial wastewater streams but the application of MDC to the treatment of mine wastewaters is currently missing. In fact, a recent review by Alkhudhiri and co-workers (ALKHUDHIRI, A. et al., 2012) found that the application of MDC to different industrial streams is still scarce. Also, research on the influence of high salt concentrations in the feed on the efficiency of the MD process is currently lacking (ALKHUDHIRI, A. et al., 2012).

The development of an MDC process also requires better crystalliser control strategies, since most MDC research is based on a batch process, thereby limiting the crystalliser control (TUN, C.M. et al., 2005). Another key area in MDC that currently needs research is the influence of the type and concentration of various residual antiscalants that are present in RO brines that constitute the feed to MDC processes. The complex nature of mining wastewater, together with the various types of antiscalants used, will likely have different effects on the aqueous chemistry of the MDC process and therefore warrants investigation.

The use of MDC for the treatment of mine wastewater has not been a major focus of research even though there is great potential in this field. The focus of this project was therefore on investigating the applicability of MDC for the treatment of industrial wastewater with a specific focus on the treatment of mine wastewater, as this is currently very limited. The project also focused on investigating the impact that the presence of various types of antiscalants had on the MDC process.

This Water Research Commission funded project K5/2223/3 entitled 'Using membrane distillation crystallisation for the treatment of industrial wastewater' report focuses on the aqueous thermodynamic modelling and experimental aspects of the MDC process investigated within the context of treating RO brines emanating from the South African coal mining sector.

CHAPTER 2 - Literature Review

2.1 Background

Wastewater characterised as containing an elevated level of suspended solids and dissolved solids is usually treated in a multi-stage process before it can be discharged or reused. If there are any large materials or coarse solids in the wastewater, a pre-treatment (such as screening) is required to remove these coarse solids, to avoid these materials causing damage to downstream equipment in the subsequent processes.

Smaller sediment particles may be removed by gravity settling, flotation, filtration (both multi-media and membrane processes) or by skimming, amongst others, during the primary treatment process. For dissolved organic compounds in the wastewater, a biological process can be used during secondary treatment to remove the residual organics and suspended solids. Any further constituents in the wastewater that cannot be removed by the secondary process require individual treatment processes during the tertiary or advanced processes. However, these individual treatments may also be combined with the primary or secondary processes (WORLD BANK GROUP).

When looking specifically at the treatment of mine wastewater, this water is typically characterised as having elevated levels of inorganic and organic suspended matter and variable salinity. Although the general treatment process for these mine waters may be similar to other types of wastewater, the presence of metals as well as a dynamic variability in the feed water composition adds further complexity to the treatment process. Typically, the treatment process will the removal of fines and suspended solids, followed by the removal of dissolved ionic species sometimes including metals, using the appropriate technology in order to achieve the final product water quality specification required.

Desalination processes such as RO and thermal evaporation by and large carry out the removal or reduction of dissolved ionic species. By and large, RO is still currently the most cost-effective method of desalination to remove dissolved ionic species and reduce salinity. However, the reject or retentate from the RO process, referred to in the context of this study as brine, continues to pose both technical and economical challenges towards achieving a sustainable zero liquid discharge (ZLD) scenario.

Some common brine treatment and disposal methods include: Direct surface water discharge, discharge to a sewage treatment plant, deep well injection, evaporation ponds, brine concentrators/Zero liquid discharge, mixing with cooling water discharge, mixing with sewage treatment effluent, electro-dialysis and Vibratory Shear Enhanced Processing (VSEP) Membrane System (BALASUBRAMANIAN, P., 2013). Many of these may be infeasible due to environmental and geological impacts to the area. Importantly, the brine may still contain reusable salts and therefore the management of the brine is an integral part of the process.

One proposed type of brine concentration method is Membrane Distillation (MD), which was the topic of this investigation. Membrane Distillation is a thermally driven separation process that only allows vapour molecules to be transported across a microscopic, hydrophobic membrane, without altering the vapour equilibrium of the different components in the process liquids. The trans-membrane temperature differential (ΔT) creates a vapour pressure gradient for separation, whilst the hydrophobic microporous membrane separates heated feed from the cooled receiving phase, allowing only volatile compounds to pass through it, with the process liquid being in contact with at least one side of the membrane (ALKHUDHIRI, A. et al., 2012; CAMACHO, L.M. et al., 2013).

As the maximum achievable recovery in an RO process is limited by membrane fouling and scaling at concentrations beyond the maximum antiscalant tolerance levels and since precipitation within the RO element is to be avoided, MD could be applicable in zero (or near zero) liquid discharge applications, due to the fact that relatively high fluxes can be obtained at salt concentrations that are higher than for an RO application. However, this requires proper management of precipitating salts to avoid membrane fouling, which is significantly less detrimental to the membrane given that the fouling/scaling does not occur at elevated pressures, as is the case in a RO process. One way of managing these salts is with MD crystallisation. This method has been explored for NaCl and Na_2SO_4 solutions, where it was found that at a certain feed concentration, the flux declines due to crystal formation on the membrane surface. This in turn reduces the membrane's salt rejection characteristic due to the fact that salts can penetrate into the pores. Using MD together with MD crystallisation allows for improved separation of salts from solution and this concept has the potential to expand into other industries, such as drug development (CAMACHO, L.M. et al., 2013).

2.1.1 Types of Membrane Distillation

There are four categories of MD that differ based on how the permeate is processed. These categories are described below and can be seen in Figure 1 (SALEHI, M.A. and Rostamani, R., 2013; CAMACHO, L.M. et al., 2013):

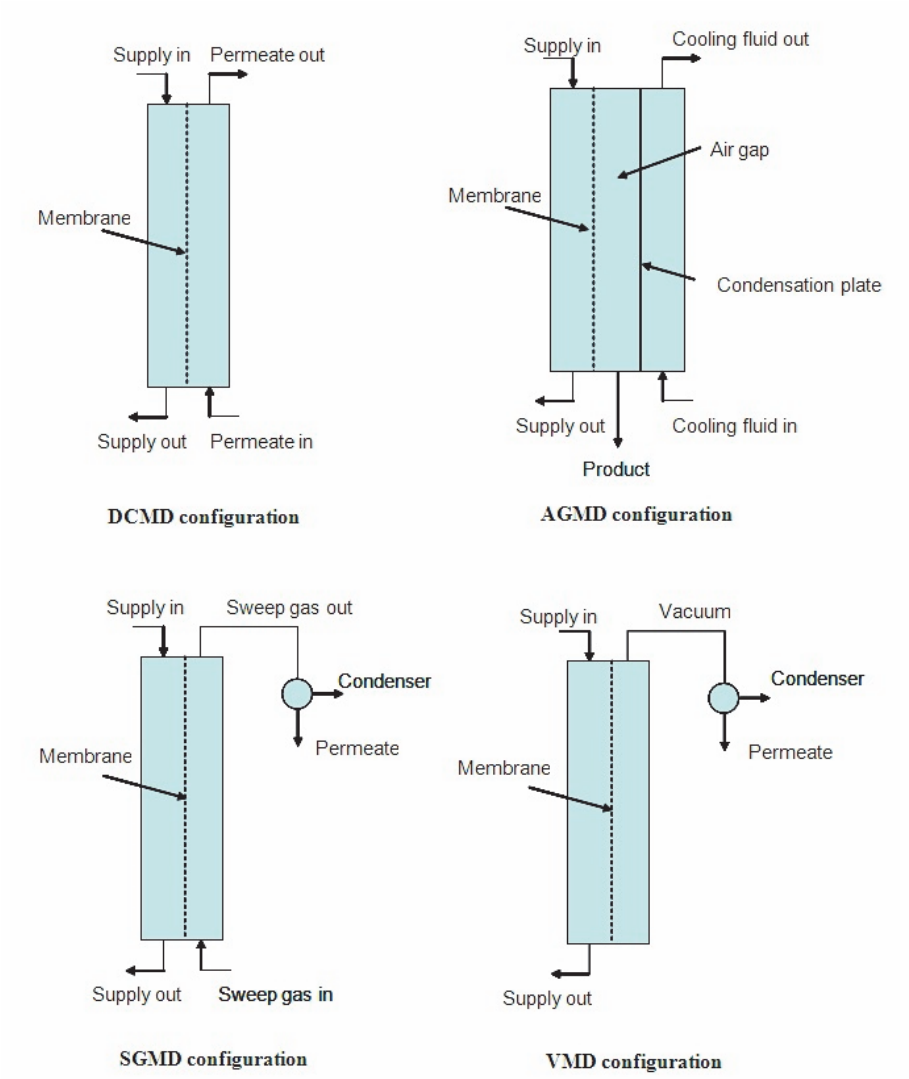

Figure 1: Categories of Membrane Distillation (EMIS, 2010)

Direct Contact Membrane Distillation (DCMD):
Both sides of the membrane are in contact with the hot and cold fluid, producing reasonably high flux, but also resulting in low energy efficiency due to the high heat conduction loss on the permeate side. This type of distillation is best suited to concentrated aqueous solutions and for desalination.

Air Gap Membrane Distillation (AGMD):
The feed liquid is in contact with the membrane, whilst there is an air gap between the membrane and the condensation surface on the product side. This setup has the highest energy efficiency due to a decrease in heat transfer from the feed to the product, but at the same time, the air gap results in a low flux. This type of distillation is particularly suitable for systems that have low energy requirements and is suitable for most MD applications.

Sweep Gas Membrane Distillation (SGMD):
The vapour produced on the product side of the membrane is stripped with an inert gas, which flows to a condenser where the liquid is collected. The flowing gas improves the mass flux by reducing the boundary layer resistance. This type of distillation is particularly suitable for the removal of volatiles from an aqueous solution.

Vacuum Membrane Distillation (VMD):
The product side of the membrane is vapour or air under reduced pressure, thereby creating a vacuum that removes trapped gas in the pores and improves the mass flux. The permeate gas can then be condensed to obtain the product. This distillation is also particularly suitable for the removal of volatiles from an aqueous solution, although the energy costs to create the vacuum are high.

The DCMD configuration was identified to be best suited for the purposes of this project owing to the fact that the brines emanating from RO processes treating mine water are highly saline.

2.1.2 Membrane Distillation Crystallisation Process Parameters

The two main underlying phenomena that govern the efficiency of an MDC process are the heat and mass transfer of the system; these are discussed below along with other parameters that affect an MDC process.

2.1.2.1 Heat and mass transfer

The typical heat and mass transfer phenomena in a DCMD process can be seen in Figure 2. As can be seen, the flux for both the mass and heat is from the heated feed side to the cold product side. The feed temperature T_f decreases to T_1 at the feed membrane wall, whereas the product temperature T_p increases to T_2 at the product membrane wall. Water from the feed evaporates at T_1 and is transported across the membrane where it condenses at T_2 and is absorbed by the cold product flow. This process therefore results in the transfer of heat via convection from the feed to the feed membrane wall and similarly from the product boundary wall to the product. Additionally, heat is conducted through the membrane wall, as well as through stagnant vapour or air in the membrane pores via sensible heat, whilst latent heat is transferred from the feed to the product by the vapour (CAMACHO, L.M. et al., 2013).

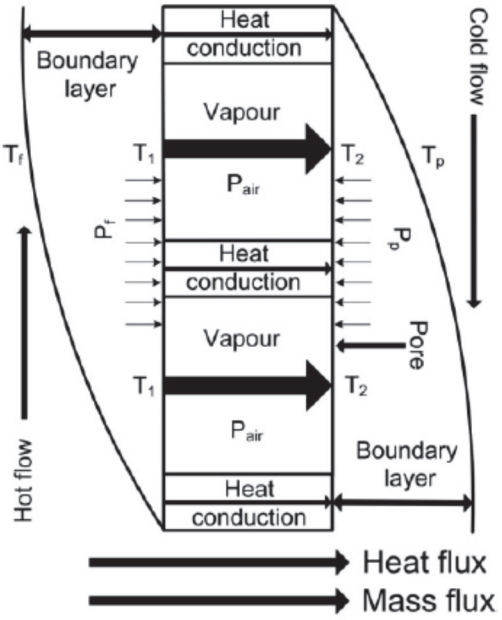

Figure 2: DCMD heat and mass transfer through membrane (CAMACHO, L.M. et al., 2013).

There are three steps involved in the transfer of mass from the feed to the product, namely the vaporisation and condensation on the hot and cold sides of the membrane respectively, and the transfer of vapour from the hot to cold side of the membrane. The vapour is transferred by convection and diffusion through the microporous membrane with a flux rate (J_W), which is dependant on the membrane characteristics (described in Section 2.1.2.6) and the driving force. The mass transfer can be represented by Equation 1 below:

$$J_w = C_w \, \Delta P_m \tag{1}$$

With C_w being the overall mass transfer coefficient and $\Delta P_m = P_{mf} - P_{mp}$ being the vapour pressure difference between the feed and product sides (KHALIFA, A. E. and Lawal, D. U., 2014).

Vapour pressure is the pressure exerted by a vapour in thermodynamic equilibrium with its condensed phase at a given temperature in a closed system. The two factors affecting vapour pressure are temperature and the type of liquid. There are numerous methods in which the vapour pressure is correlated as a function of temperature. These are mainly derived from the Clausius Clapeyron equation given in Equation 2 below:

$$\ln(P^{sat}) = \ln(A) - \frac{\Delta H_{vap}}{RT} \tag{2}$$

From this, Antoine's equation was developed, Equation 3:

$$\ln(P^{sat}) = \mathrm{A} + \frac{B}{T+C} \tag{3}$$

This equation is used mainly for low to moderate vapour pressures and does not fit data accurately above the normal boiling point. Consequently, the modified Riedel equation was developed as given in Equation 4.

Although the constants have been determined for a wide variety of chemicals, we are only interested in the constants specific to water, as given in Equation 5 (LILEY, E.L. et al., 1999):

$$\ln(P^{sat}) = A + \frac{B}{T} + C\ln T + DT^{E} \tag{4}$$

$$\ln(P^{sat}) = 73.649 - \frac{7258.2}{T} - 7.3037\ln T + 4.1653 \times 10^{-6} \times T^{2} \tag{5}$$

The driving force of the vapour transfer rate is the vapour pressure difference at T_2 and T_1 and not T_f and T_p (as shown in Figure 2), as this would have a higher vapour pressure difference, whilst the permeability of the membrane also affects the transfer rate. Due to the evaporation at the feed membrane wall, the feed concentration increases from the feed C_f to the feed membrane wall C_1.

The ratio of the difference between the membrane wall temperatures and the feed and product temperatures is known as temperature polarization, TP (CAMACHO, L.M. et al., 2013).

$$\boldsymbol{TP = \frac{T_1 - T_2}{T_f - T_p}} \tag{6}$$

From Equation 6 it can be seen that the ideal TP would be when the membrane wall temperatures are equalled to their respective bulk fluid temperatures (TP = 1). This would result in a greater difference between the vapour pressures, thereby increasing the flux across the membrane. In order to achieve a TP of 1, the temperature gradient in the thermal boundary layer needs to be decreased, which can be done by enhancing the stream turbulence, which in turn may be done by increasing the flow rate or inserting turbulence promoters. However, the relationship between turbulence and flux is not proportional, as the influence on flux decreases at higher turbulence levels. Therefore, an optimal flow rate has to be determined for a system, so as to reduce the energy cost of pumping whilst still achieving a high flux rate (CAMACHO, L.M. et al., 2013).

Additionally, if the membrane is compressible, the increase in flux due, to higher turbulence, will be negated by an increase in pressure, due to the square relationship between hydrostatic pressure and the flow rate (CAMACHO, L.M. et al., 2013).

2.1.2.2 Temperature

An increase in feed temperature will result in a greater vapour pressure differential, which in turn increases the mass flux through the membrane.

On the other hand, there will be an increase in heat loss in the system due to the fact that there is a linear correlation between the conductive heat loss and the temperature difference. Both of these factors in turn also result in an increase in the TP effect (CAMACHO, L.M. et al., 2013).

Conversely, an increase in the permeate temperature will result in a decrease in mass flux due to a decrease in the vapour pressure differential. A decrease in the permeate temperature should have a smaller increase in the flux than an increase in the feed temperature due to the exponential increase in the vapour pressure with temperature.

2.1.2.3 Feed concentration

Variability in the concentration of solutes in a solvent affects the vapour pressure, which for the purposes of this study is the concentration of salt in water. Raoult's law can be used to approximate the vapour pressure of dilute solutions with Equation 7 (VAN NESS, H. C. and Abott, M. M., 1999):

$$P^{sat} = X_{solv} \times P^{0}_{solv} \tag{7}$$

Where P^{sat} is the vapour pressure of the solution, X_{solv} is the mole fraction of the solvent and P^{0}_{solv} *is the vapour pressure of the pure solvent at a particular temperature.*

From Equation 7 we can see that an increase in feed concentration results in a decrease in vapour pressure of the solution and therefore also a decrease in permeate flux, as vapour pressure is the driving force. Furthermore, an increase in feed concentration also increases the viscosity of the solution, which leads to a smaller Reynolds number indicating less turbulent flow. As mentioned previously, this leads to a decrease in mass flux.

2.1.2.4 Flow rate

An increase in feed flow rate results in a decrease in the thermal boundary layer, thereby reducing the TP effect and improving the mass flux. However, an increase in flow rate also leads to an increase in hydrostatic pressure, which could lead to membrane pore wetting if the liquid entry pressure (LEP) is exceeded (ONSEKIZOGLU, P., 2012). An increase in permeate flow rate has a similar effect in that there is a reduction in the TP effect.

2.1.2.5 Fouling

Fouling will reduce the effective membrane area and therefore result in a decrease in mass flux. Furthermore, due to the reduced flow there will also be an increase in temperature polarisation effect. Fouling may also introduce wettability of the pores, thereby allowing solutes to pass through the membrane (GRYTA, M., 2001).

2.1.2.6 Membrane characteristics

There are two common types of DCMD membrane configurations, namely hollow fibre or tubular, wherein the membrane is normally made from PP, PVDF, and PVDF-PTFE composite material, and flat sheet or plate, where the membrane is normally made from PP, PTFE, and PVDF (CAMACHO, L.M. et al., 2013). The plate configuration has a much smaller contact area than the tubular configuration, but it is a lot easier to construct and clean, and thereby easier to experiment on.

The correlation between trans-membrane flux and membrane characteristics is given by the following relationship (KULLAB, A., 2011):

$$N \propto \frac{r^{\alpha}\varepsilon}{\tau\delta_m}$$

where r^{α} is the average pore size for Knudsen diffusion (α = 1) or the average squared pore size for viscous flux (α = 2), ε is the membrane porosity, τ is the membrane tortuosity, and δ_m is the membrane thickness.

The membranes in MD should ideally have a relatively large pore size, although this pore size has an upper limit that is dependent on the hydrophobicity of the material, as there is a minimum pressure at which point water will enter the pores and pass through the membrane. This pressure limit is known as the Liquid Entry Pressure (LEP) and is determined by Equation (8) below (DOW, N. et al., 2008).

$$LEP = \frac{-2B\gamma_L cos\theta}{r_{max}} \quad (8)$$

where γ_L is the liquid surface tension, θ is the liquid-solid contact angle, r_{max} is the largest pore radius, and B is a geometric factor determined by pore structure.

The effect of pore size becomes clear when a solution of low surface tension is processed. In order to avoid wetting of membrane pores, the pore size must be as small as possible, which contradicts the requirement of higher MD permeability. An optimum value is needs to be determined for each MD application depending on the type of the feed solution to be treated relation (KULLAB, A., 2011).

According to one study on membrane distillation of brine water, the membrane that produced the highest flux out of those that were studied was made of Polytetrafluoroethylene (PTFE) with a pore size of 1.0 μm and a thickness of 0.01 mm. Furthermore, the conditions that produced the highest flux were found to be at the greatest economically feasible temperature difference across the membrane, with the highest practical turbulent flow across the membrane, while maintaining a safe margin below the LEP. The study also showed that a thin layer of open mesh-like material should be used as a membrane backing (DOW, N. et al., 2008).

The type of membrane and also the membrane configuration used will have a major impact on the efficiency of the process; however this report focuses on the best operating parameters to improve crystallisation of the feed, which should be similar in either configuration.

2.1.3 Brine Chemistry

Brine is classified as water with a TDS above 35 000 ppm (or 35 g/l) (ECOLOGYDICTIONARY.ORG, 2008). The chemistry of brine is complex and suitable chemical speciation methods need to be carried out before the chemical composition of any particular brine can be fully understood. Furthermore, chemical speciation requires the thorough knowledge of thermodynamic properties such as activity coefficients – the modelling of which is rather complex (MARIAH, L., 2006). This was the basis for extensive aqueous thermodynamic modelling aspects of this project, with particular emphasis on two typical mining brines and the effect that the water

recovery and operating temperature have on the salts that are predicted to crystallise out, the sequence in which they will crystallise out and purities (mixed salt composition) as a function of the water recovery.

2.1.4 Crystallisation

Crystallisation is a method that is used to purify a solid compound, which for the purpose of this research project, is salt. Two steps are required for a crystal to form, namely nucleation, which is when a particle is formed in solution, and the growth of that particle. The rate at which the crystallisation process for a particular species takes place is largely dependent on the difference between how supersaturated the solution is with respect to the species in question and its equilibrium solubility limit.

Every salt has a particular solubility in water at a specific temperature and salts are generally more soluble at higher temperatures. However, there are a number of exceptions to this rule such as calcium sulphate, which has an inverse solubility and consequently exhibits a higher solubility at lower temperatures. When the solubility limit is reached, the solution will become saturated and no additional salt can dissolve in the solvent (water) and any further change in temperature in the direction of decreased solubility will generate a supersaturated solution. Similarly, if enough water is removed from a salt solution so that the saturation point is reached and exceeded, the solution becomes supersaturated with respect to the salt in question and it starts crystallising out of solution. A third method of generating supersaturation is called salting and achieved by the addition of another component, which may form a mixed solvent in which the solute has a reduced solubility compared to the original solvent. Similarly a third component may be added that will react with the solute to form an insoluble substance, which is called precipitation (MCCABE, W. L. et al., 1993).

Crystal shape, size and purity depend strongly on the level of local supersaturation. Fast crystallisation kinetics usually lead to the formation of crystals that are small, needle like in shape and impure and often have unstable modifications, rather than the slower growth-based size enlargement mechanism which would arise as a result from the solution being at significantly lower level of supersaturation or within the metastable zone. Therefore by controlling the crystallisation kinetics, the crystal characteristics can be controlled to a certain degree. This can be done with the use of membrane distillation by limiting the mass transfer across the membrane and thereby limiting the level of supersaturation (KONIG, A. and Weckesser, D., 2005).

2.1.4.1 Crystal size and rate of growth

Crystal size is important for marketing and handling purposes, since a reasonable size is required to improve the filterability and wash-ability of the crystals. Furthermore, if the crystals are of reasonable size, they are easier to handle and store and in some cases react better with other chemicals. Therefore, it is important to have a crystalliser design that takes this into account (MCCABE, W. L. et al., 1993).

Crystals grow by the diffusion of solute molecules or ions through the liquid phase to the surface of the crystal, at which point the molecule or ion must be accepted by the crystal and organised into the space lattice. This process will only occur if the solution is supersaturated (MCCABE, W. L. et al., 1993).

As mentioned previously, there are two steps for crystal formation, namely nucleation and crystal growth. If there is a high level of supersaturation, there will be a greater tendency for nucleation compared to crystal growth, resulting in smaller crystal sizes due to the overall higher surface area of the crystals. Whereas at lower supersaturation, they crystals tend to grow faster than they nucleate, resulting in larger crystal sizes. Furthermore, if the system is turbulent, crystal growth is slowed due to a reduction in the probability of a molecule of solute coming into contact with an existing crystal and integrating into the crystal lattice as compared to when the flow is laminar, i.e. no stable nuclei can form (MCCABE, W. L. et al., 1993).

2.1.4.2 Purity

Generally a well-formed crystal is pure, but due to the fact that the crystal was formed in a solution, it may retain some of the mother liquid, especially when there are crystalline aggregates. Since this mother liquor may contain other impure substances, when it dries on the product, it results in a contaminated product. Filtering or centrifuging the crystals may negate this issue to certain degree (MCCABE, W. L. et al., 1993).

The rate of crystallisation may also affect the purity of the crystals, since a high crystallisation rate may lead to the entrapment of impurities with the crystal lattice, whereas if the crystallisation rate is slower, the impurities have an opportunity to diffuse away from the surface of the crystal into the bulk before becoming entrapped. Due to the fact that the level of supersaturation drives the rate of crystallisation, the purity of the crystals can, to a certain degree, be controlled by controlling the level of supersaturation (UNIVERSITY OF COLORADO AT BOULDER, 2015).

2.1.5 Antiscalant

Antiscalants are employed in processes such as RO in order to increase the water recovery by controlling crystallisation out of solution and subsequent scaling within an RO element despite the feed water having exceeded its thermodynamic solubility limit. Scaling within RO elements results in increasing operating pressures and decreased salt rejection, leading to the requirement for Cleaning in Place (CIP), which is costly and time consuming. There is also the risk that scaling will damage the membrane surface.

Antiscalants interfere with the crystallisation/precipitation reactions in three primary ways (LENNTECH, B.V.):

- Threshold inhibition: the addition of antiscalant may allow a solution to remain supersaturated thereby keeping sparingly soluble salts in solution, thereby inhibiting the crystallisation threshold
- Crystal modification: the antiscalant may affect the growth of crystal structures resulting in crystals that appear distorted, generally more oval in shape, and less compact. This is due to the fact that antiscalant interrupts the electronic charge balance necessary to propagate crystal growth at the nanoscopic scale, with the negative groups located on the antiscalant molecule attacking the positive charges on scale nuclei.
- Dispersion: antiscalants can also keep crystals dispersed by adsorbing on crystals or colloidal particles and imparting a high anionic charge. This property also separates particles from fixed anionic charges present on the membrane surface.

Due to these effects, it is expected that the antiscalant will affect the crystal structure of the salts, in that smaller salt crystals will be formed, and also that it will delay the effects of scaling as there will be a delay in salt crystal formation.

On the other hand, antiscalants could have a negative impact on the membrane flux rates of an MDC process for the treatment of RO brines owing to the fact that some of them contain organic functional groups and because these antiscalants are almost entirely rejected by the RO membrane, their elevated concentration in the RO brine could result in organic fouling of the MDC membranes.

CHAPTER 3 - Aims

The main aim of this project was to investigate the effect of key operating parameters on the treatment of mine wastewater using MDC. The investigation was divided into two phases. The first was an aqueous thermodynamic modelling investigation in which the objectives were:

1. To select two industrial brines emanating from typical mining related activities in South Africa that could be used to investigate the capability and efficacy of using aqueous modelling as a process design tool for MDC with specific emphasis on the crystallisation aspects.
2. For each of the two sample brines; to investigate the effect of (i) Brine composition (ii) Water recovery (iii) Operating temperature on the crystallisation characteristics of the MDC process such as:
    a. The identity of crystallising salts
    b. The sequence in the which the salts crystallise out
    c. The purity (composition) of any mixed salts produced
3. To highlight the key outcomes from the aqueous thermodynamic studies that informs the process design of the MDC process.

The second phase focussed on the experimental aspects of the investigation, where the objectives were:

1. To prepare and investigate a simple NaCl based brine to develop a performance base-line for the MDC process
2. To prepare and investigate a synthetic brine that emulates the actual brine from the mine wastewater test samples
3. To validate the results obtained from the aqueous thermodynamic modelling by using a laboratory-scale MDC experimental rig to investigate the effects of operating (i) temperature, (ii) feed water concentration, and (iii) flow rates on the permeate flux rates, water recovery, water purity, and salt morphology and composition of the system.
4. To investigate the effect that various antiscalants had on the operating parameters of the MDC process and the performance of the technology. Consequently, the effect of residual antiscalants on the operating parameters as well as: i) Permeate flux rates; ii) Water purity; and iii) Salt morphology and composition were investigated. Two commercially available and commonly used antiscalants in mining water treatment plants were used for the study, which could be described as:
    c. Antiscalant with organic functional groups
    d. Antiscalant that is aqueous phosphonic acid based

Finally, the key outcomes from the experimental work are highlighted and recommendations made on how additional studies could assist in improving the MDC process for the treatment of mining brines.

CHAPTER 4 - Aqueous Thermodynamic Modelling

4.1 Methodology

4.1.1 Modelling Framework

The aqueous thermodynamic modelling was performed using OLI Systems Inc. Stream Analyzer (2012). OLI's electrolyte thermodynamic framework allows single point calculations and multiple point survey calculations for trend analysis related to temperature, pressure, pH and composition effects.

OLI's basic electrolyte thermodynamic model (AQ model) is based on a true speciation model, a predictive equation of state (Helgeson Equation of State), and an activity coefficient model and convergence heuristics. Where the AQ model is valid to a concentration limit of 30 molal ionic strength, the Mixed Solvent Electrolyte (MSE) model predicts electrolyte behaviour from infinite dilution to molten salts, making it well suited for hypersaline brines.

The MSE model incorporates the Helgeson Equation of State and supporting databank through a conversion of the standard-state chemical potentials provided for aqueous systems. Thus, the equilibrium constants and other standard state partial molal thermodynamic properties are readily predicted for mixed solvent environments. The activity coefficient model is based on the extended Debye-Huckel term, a Uniquac term, and a middle-range electrolyte term.

Using OLI's MSE thermodynamic framework, firstly the brine composition analysis was evaluated to determine the completeness of the analysis with respect to the balance between the anions and cations. The scaling tendencies were then calculated. Lastly, a range of water recoveries and operating temperatures were investigated to determine their implication on the key crystallisation characteristics of the two systems investigated.

4.1.2 Selection of key MDC process parameters

The key MDC process parameters were determined to be the feed composition / concentration, the feed temperature, the feed flow rate, the extent of agitation, the permeate temperature and the condensation sweep solution flow rate. For the purposes of this aqueous thermodynamic modelling study, the feed composition / concentration and the feed temperature were identified as being the most important. These are discussed in greater detail below.

4.1.2.1 Brine feed composition / concentration

The driving force for membrane distillation is the vapour pressure difference between the feed and permeate sides of the membrane. As there is a direct relationship between the feed solution concentration and the vapour pressure, the permeate flux decreases with an increase in the feed concentration.

4.1.2.2 Brine feed temperature

An increase in feed temperature results in a corresponding increase in the vapour pressure on the feed side, which in turn increases the driving force and results in an exponential increase in flux through the membrane.

4.1.3 Selection of model brines for the study

Two brines characterised as being broadly representative of typical brine specimens emanating from coal mining operations and platinum processing operations were selected for the purposes of this aqueous thermodynamic modelling study. The source of the coal mining brine (CMB) specimen was the brine generated from the desalination (via RO) of coal mine pit water. This multicomponent brine was significantly more complex when compared to the brine specimen originating from the platinum processing operation. The brine emanating from the platinum processing operation (PPB), although more concentrated than that of the CMB, was less complex in that the number of individual aqueous species was notably less. Furthermore, the concentration of the dominant ions in the PPB far exceeded that of the minor species. Consequently, these minor species were excluded from thermodynamic modelling exercise to reduce the computational time.

The compositions of the CMB and PPB are presented in Table 1 and Table 2 respectively:

Table 1: Coal mine brine (CMB) analysis used in the aqueous thermodynamic modelling study

Species	*mg/L*
Silicic acid	18.20
Sodium ion(+1)	2456
Potassium ion(+1)	96.33
Calcium ion(+2)	528.42
Magnesium ion(+2)	451.74
Iron ion(+2)	0.04
Manganese ion(+2)	0.09
Copper(II) ion(+2)	1.00E-03
Zinc ion(+2)	5.00E-03
Ammonium ion(+1)	4.00
Barium ion(+2)	0.05
Strontium ion(+2)	14.95
Chloride ion(-1)	481.12
Carbonate ion(-2)	39.16
Bicarbonate ion(-1)	695.12
Sulphate ion(-2)	7413.63
Phosphate ion(-3)	0.619
Nitrate ion(-1)	4.78
Fluoride ion (-1)	1.62

Table 2: Platinum Processing Brine (PPB) analysis used in the aqueous thermodynamic modelling study

Species	*mg/L*
Sodium ion(+1)	70297
Carbonate ion(-2)	32821
Sulphate ion(-2)	37363
Chloride ion(-1)	46963

4.2 Results and Discussion

The results of the aqueous thermodynamic study into the crystallisation characteristics of the brines investigated are presented as follows:

i) Analysis of the feed water data in terms of the charge balance and the scaling tendencies
ii) Crystallisation characteristics of the CMB as a function of the water recovery and operating temperature of the MDC process
iii) Crystallisation characteristics of the PPB as a function of the water recovery and operating temperature of the MDC process
iv) Total solids predicted to crystallise out for the CMB as a function of the water recovery and operating temperature of the MDC process
v) Total solids predicted to crystallise out for the PPB as a function of the water recovery and operating temperature of the MDC process
vi) Single salt / mixed salt purities as a function of the water recovery and operating temperature of the MDC process

4.2.1 Feed water data analysis

The feed water composition analysis focused primarily on calculating the charge balance to confirm that the analysis used for the study met the requirement that the charge imbalance was less than or equal to 10%. In addition to this, the feed water composition analysis also focused on determining the scaling tendencies of the species that were close to exceeding or had already exceeded their solubility limits.

4.2.1.1 CMB Feed water data analysis

Based on the feed water analysis provided in Table 1, the feed water can be characterised as brackish water with sodium, potassium, calcium and magnesium ions as the dominant cationic species and chloride, sulphate and bicarbonate ions as the dominant anionic species. This is broadly representative of expected characteristics of high sulphate content coal mining effluent brines.

The charge balance characteristics of the water analysis are as follows:

Cation charge : 0.173403 eq/L
Anion charge : -0.180798 eq/L
Imbalance : -0.007395 eq/L
Imbalance % : 2.09%

The anionic charge imbalance was rectified by the addition of 170 mg/L of the dominant cation species, i.e. sodium ions.

In Table 3 the scaling tendency of the CMB can be seen. A scaling tendency value greater than one means that the feed water is supersaturated with respect to the species in question, and would consequently crystallise out to a species concentration that is in equilibrium with its corresponding solubility limit at that specific temperature.

Table 3: CMB feed water-scaling tendencies at 25°C

Scaling Tendencies	
Fluorapatite	2.76E+17
Pentacalcium hydroxide phosphate	1.28E+05
Barium sulphate	14.283
Calcium carbonate	8.849
Calcium carbonate (aragonite)	6.513
Strontium sulphate	2.522
Strontium carbonate	1.502
Calcium sulphate dihydrate	1.113
Calcium sulphate	0.855
Calcium orthophosphate	0.468
Calcium sulphate hemihydrate	0.259
Iron(II) carbonate	0.256
Magnesium carbonate	0.021
Calcium hydrogen orthophosphate	0.014
Calcium hydrogen orthophosphate dihydrate	0.011

Importantly, the reason for various species' scaling tendencies being in excess of 1 in the case of the CBM is that the brine emanates from an RO process that uses an antiscalant to drive up the RO plant's recovery by suppressing the scaling potential. Consequently, the antiscalant enables the thermodynamic solubility limit to be extended further than would be the case without an antiscalant.

Based on the scaling potential of CMB, the identity of the dominant salts that are thermodynamically predicted to crystallise out as an increasing amount of water is removed by the MDC process are calcium sulphate dihydrate, calcium carbonate and strontium sulphate with fluorapatite, pentacalcium hydroxide phosphate and barium sulphate in smaller quantities.

4.2.1.2 PPB Feed water data analysis

Based on the feed water analysis provided in Table 2, the feed water can be characterised as a hyper-saline brine with sodium as the dominant cationic species and chloride, sulphate and carbonate ions as the dominant anionic species.

The charge balance characteristics of the water analysis are as follows:

Cation charge : 3.057725 eq/L
Anion charge : -3.196399 eq/L
Imbalance : -0.138675 eq/L
Imbalance % : 2.22%

The anionic charge imbalance was rectified by the addition of 3188 mg/L of the dominant cation species, i.e. sodium ions. In Table 4 the scaling tendency of the PPB can be seen.

Table 4: PPB feed water-scaling tendencies 25°C

Scaling Tendencies	
Sodium sulphate decahydrate	0.316
Sodium carbonate decahydrate	0.200
Sodium carbonate heptahydrate	0.128
Sodium sulphate	0.096
Sodium chloride	0.049
Salt	0.043
Sodium carbonate monohydrate	0.030
Sodium bicarbonate	0.008
Sodium carbonate	0.006
sodium sesquicarbonate dihydrate	0.002
Sodium sulphate (monoclinic)	0.002
Hexasodium carbonate bissulphate	0.001

Based on the scaling potential of PPB, it is evident that the brine is still under-saturated and could be further concentrated by using a process such as RO in order to reduce the volume of brine that needs to be treated. The identities of the dominant salts that are thermodynamically predicted to crystallise out as the MDC process removes water are listed in Table 4.

4.2.2 Crystallisation characteristics of the CMB in an MDC process

The crystallisation characteristics of the CMB in an MDC process was investigated at a water recovery range between 0 – 90% and an operating temperature range of 40 - 80°C.

4.2.2.1 Crystallisation characteristics of the CMB in an MDC process as a function of the water recovery at an operating temperature of 40°C

In Figure 3 the results of thermodynamically calculated crystallisation characteristics of the CMB in an MDC process with respect to the identities of the crystallising species can be seen.

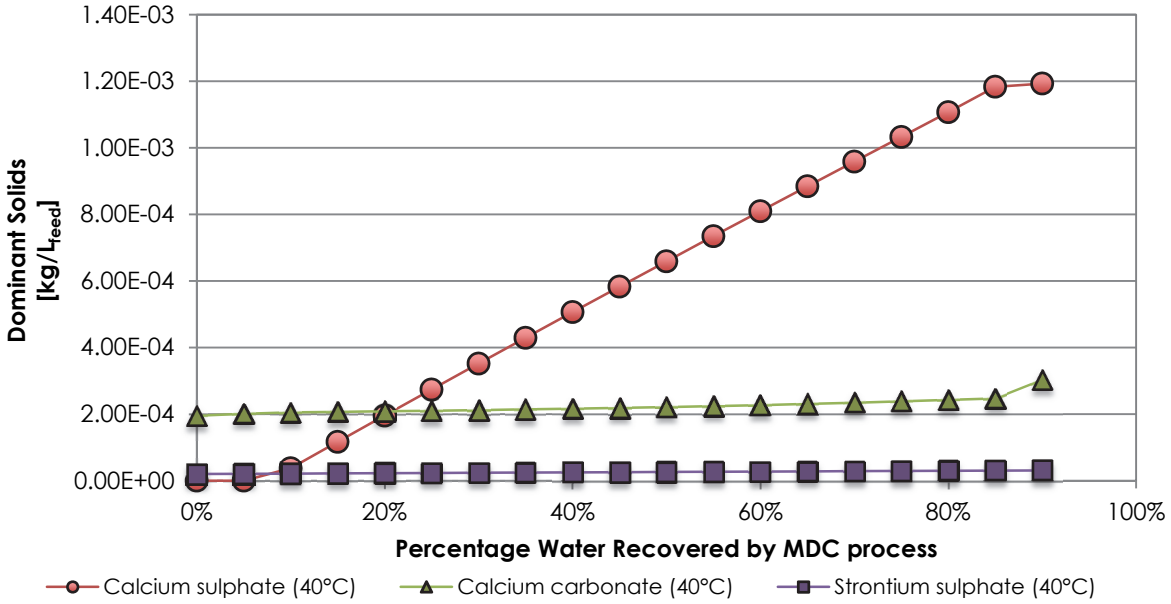

Figure 3: Dominant crystallising solids from CMB in an MDC process operated at 40°C

From Figure 3, it can be seen that the salts would start to crystallise out immediately after deactivation of the antiscalant with the dominant crystallising salts being calcium sulphate, calcium carbonate and strontium sulphate. Furthermore, the total mass of the three salts that crystallise out increases with an increase in the overall water recovery. This is to be expected, as the removal of water in the form of permeate from the system results in a corresponding increase in the relative supersaturation of the scaling species, thereby increasing the driving force for further crystallisation.

The combined mass of the crystallising salts as a function of the water recovery at 40°C is presented in Figure 4:

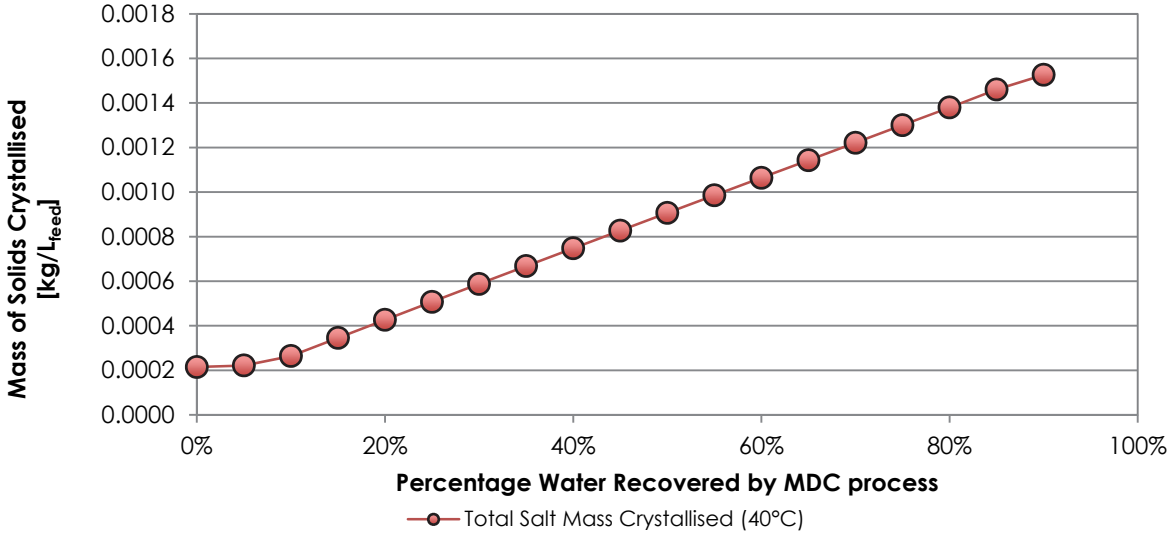

Figure 4: Total mass of crystallising solids from CMB in an MDC process as function of water recovery operated at 40°C

From Figure 4, it is clear that the combined mass of crystallising salts increases with an increase in the water recovery due to a corresponding increase in the relative supersaturation and hence the driving force for crystallisation.

The purity, defined as the relative contributions of the dominant crystallising salts to a mixed salt product, as a function of the sequential increase in the overall water recovery of the MDC process on CMB is presented in Figure 5:

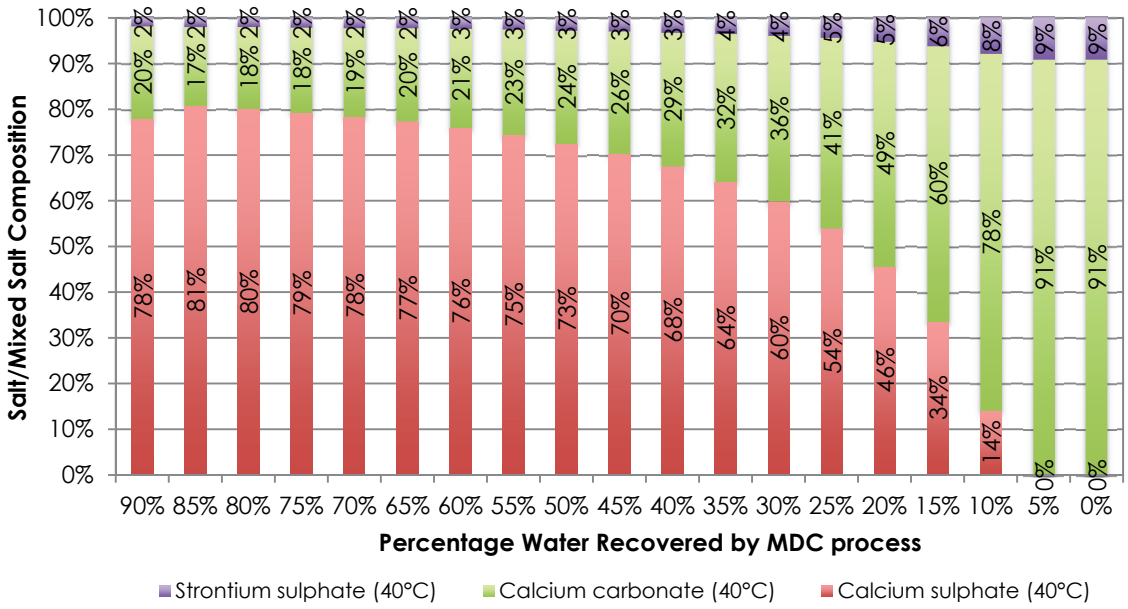

Figure 5: Purity (relative composition) of the dominant crystallising salts from CMB in an MDC process as function of water recovery operated at 40°C

From Figure 5 it can be seen that up to a 5% water recovery, the dominant crystallising salt will be calcium carbonate with a purity of 91%. The impurity will be strontium sulphate at 9% composition. Calcium sulphate begins to crystallise out after a water recovery of 10% and its relative contribution to the overall mixed salt increases with a sequential increase in the water recovery. At 90% water recovery, the mixed salt has a composition of 78% calcium sulphate, 20% calcium carbonate and 2% strontium sulphate.

4.2.2.2 Crystallisation characteristics of the CMB in an MDC process as a function of the water recovery at an operating temperature of 60°C

In Figure 6 the results of thermodynamically calculated crystallisation characteristics of the CMB in an MDC process with respect to the identities of the crystallising species can be seen.

In Figure 6 it can be seen that the salts would start to crystallise out immediately after deactivation of the antiscalant, similarly to the 40°C case, with the dominant crystallising salts being calcium sulphate, calcium carbonate and strontium sulphate. Furthermore, the total mass of the three salts that crystallise out increases with an increase in the overall water recovery. This is to be expected as the removal of water in the form of permeate from the system results in a corresponding increase in the relative supersaturation of the scaling species, thereby increasing the driving force for further crystallisation. The slight drop in the calcium sulphate at recoveries above 80% is explained by the equivalent uptake in the calcium ions for the crystallisation of calcium carbonate, which shows an increase in crystallisation beyond 80% water recovery.

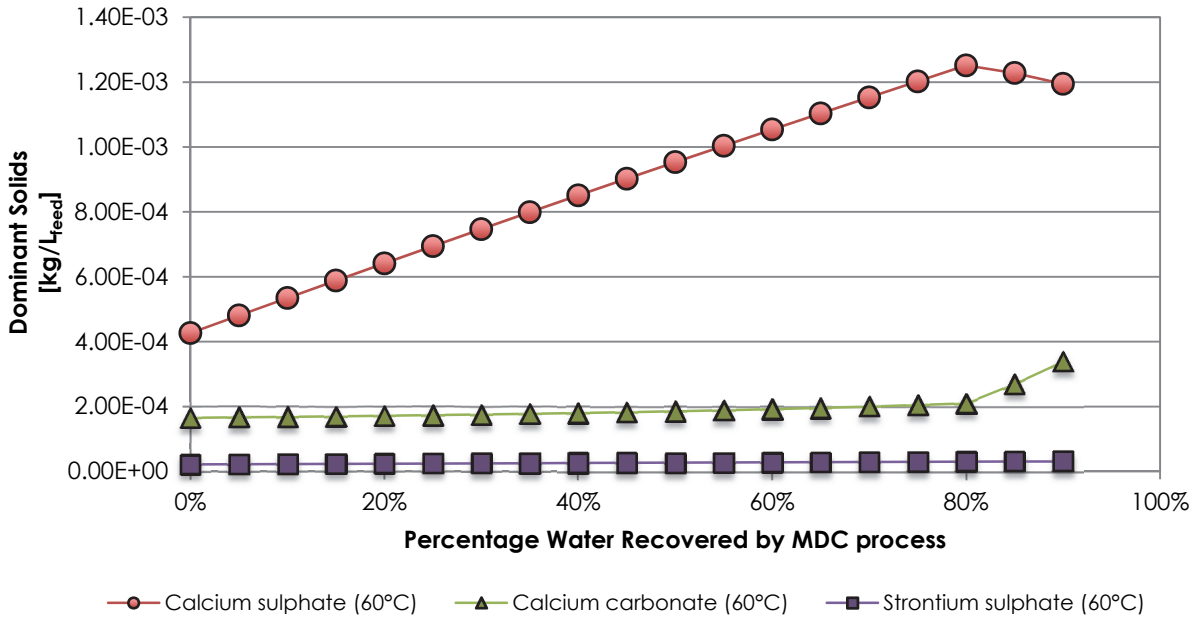

Figure 6: Dominant crystallising solids from CMB in an MDC process operated at 60°C

The combined mass of the crystallising salts as a function of the water recovery at 60°C is presented in Figure 7:

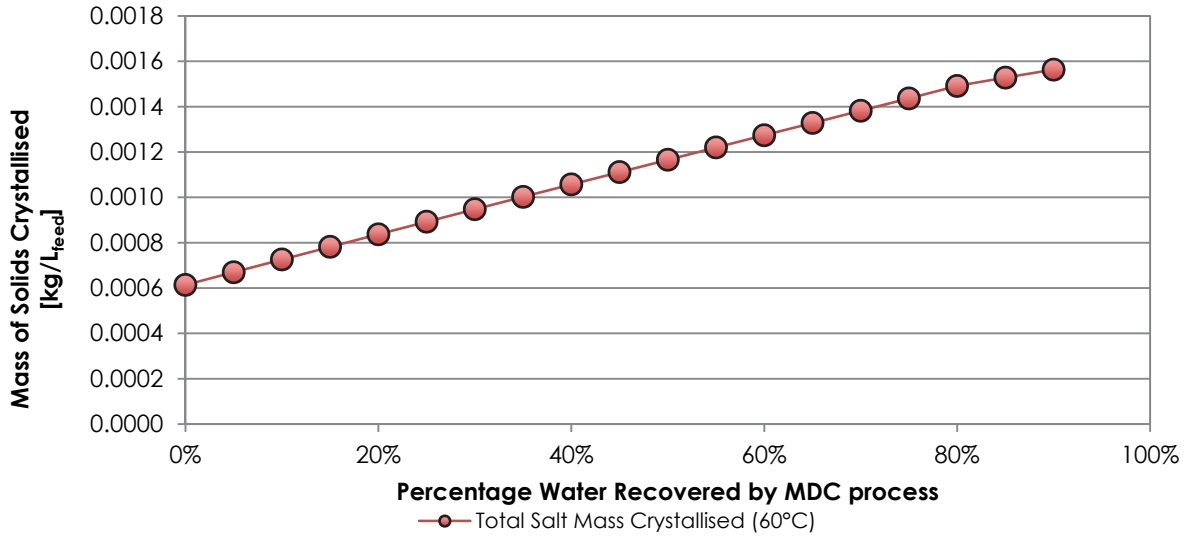

Figure 7: Total mass of crystallising solids from CMB in an MDC process as function of water recovery operated at 60°C

From Figure 7, it is clear that the combined mass of crystallising salts increases with an increase in the water recovery due to a corresponding increase in the relative supersaturation and hence the driving force for crystallisation.

The purity, defined as the relative contributions of the dominant crystallising salts to a mixed salt product, as a function of the sequential increase in the overall water recovery of the MDC process on CMB is presented in Figure 8:

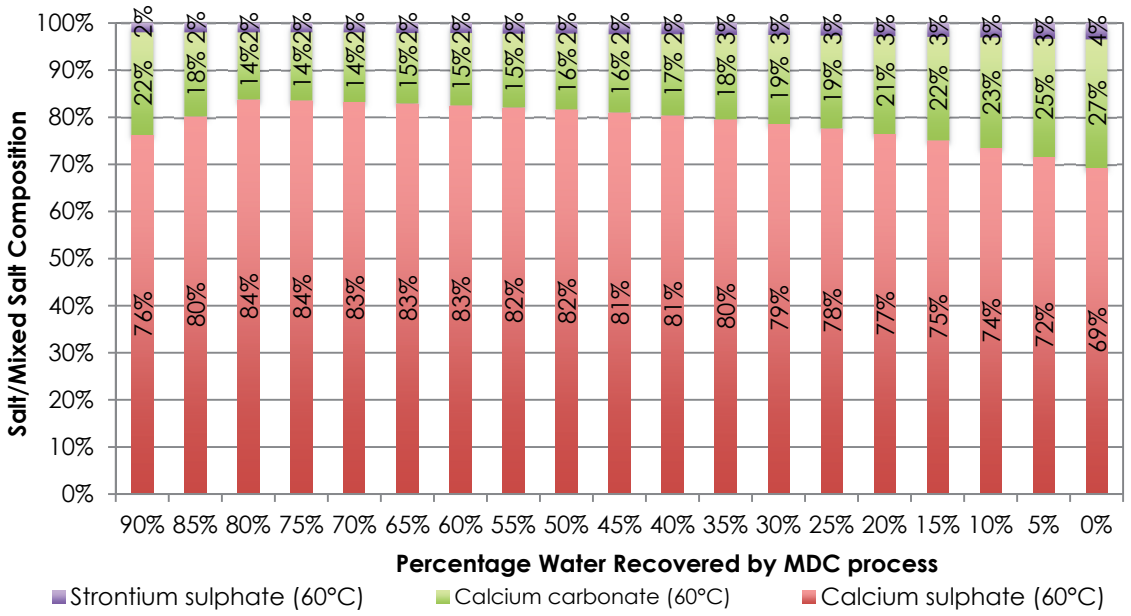

Figure 8: Purity (relative composition) of the dominant crystallising salts from CMB in an MDC process as function of water recovery operated at 60°C

In Figure 8, it can be seen that at a higher MDC operating temperature of 60°C, due to the inverse solubility of calcium sulphate, the dominant crystallising salt at all water recoveries will be calcium sulphate with a relative composition in the mixed salt ranging between 69% at 0% water recovery to 76% at 90% water recovery. The other contributing salts to the mixed salt product are calcium carbonate (14% - 27%) and to a much lesser degree strontium sulphate (2% - 4%).

4.2.2.3 Crystallisation characteristics of the CMB in an MDC process as a function of the water recovery at an operating temperature of 80°C

In Figure 9 the results of thermodynamically calculated crystallisation characteristics of the CMB in an MDC process with respect to the identities of the crystallising species can be seen.

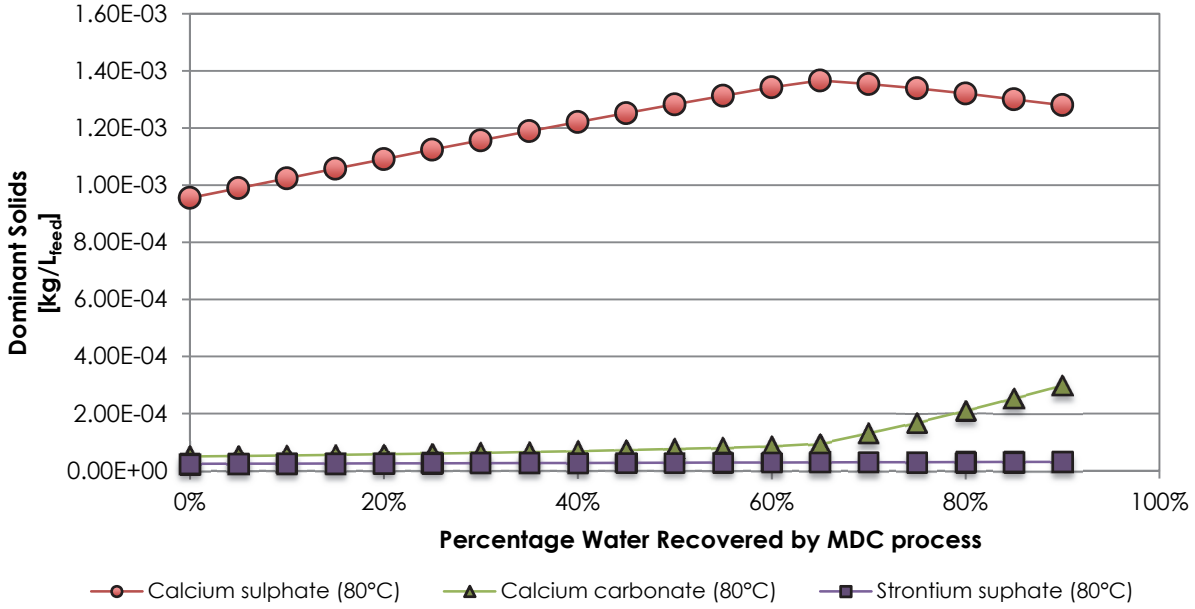

Figure 9: Dominant crystallising solids from CMB in an MDC process operated at 80°C

From Figure 9, it can be seen that, similar to the 40°C and 60°C scenarios, the salts would start to crystallise out immediately after deactivation of the antiscalant. The dominant crystallising salts would again be calcium sulphate, calcium carbonate and strontium sulphate. Furthermore, the total mass of the three salts that crystallise out increases with an increase in the overall water recovery. This is to be expected as the removal of water in the form of permeate from the system results in a corresponding increase in the relative supersaturation of the scaling species, thereby increasing the driving force for further crystallisation. The slight drop in the calcium

sulphate at recoveries above 70% is explained by the equivalent uptake in the calcium ions for the crystallisation of calcium carbonate, which shows an increase in crystallisation beyond 70% water recovery.

The combined mass of the crystallising salts as a function of the water recovery at 80°C is presented in Figure 10:

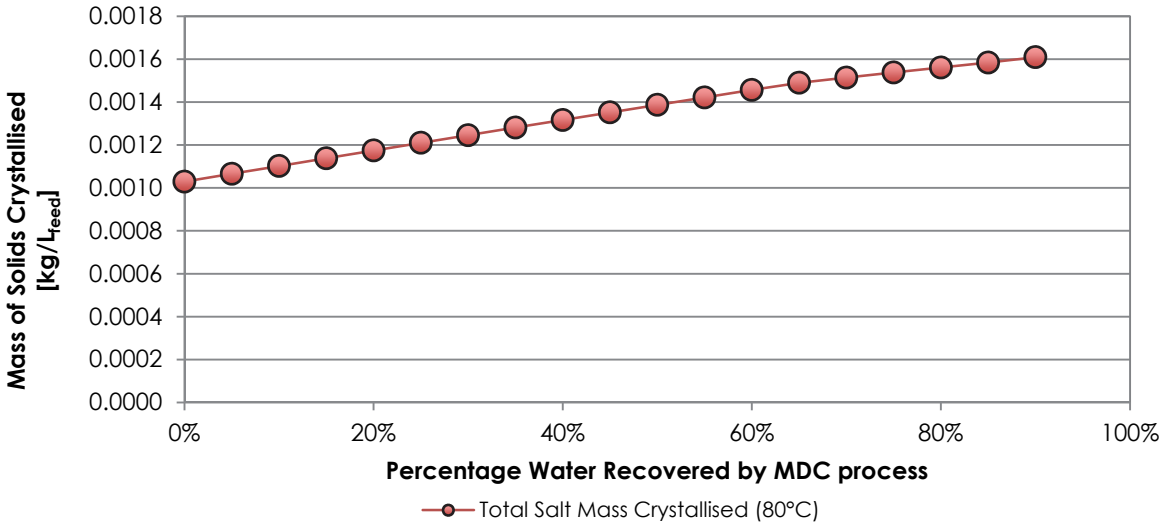

Figure 10: Total mass of crystallising solids from CMB in an MDC process as function of water recovery operated at 80°C

From Figure 10, it is clear that the combined mass of crystallising salts increases with an increase in the water recovery due to a corresponding increase in the relative supersaturation and hence the driving force for crystallisation.

The purity, defined as the relative contributions of the dominant crystallising salts to a mixed salt product, as a function of the sequential increase in the overall water recovery of the MDC process on CMB is presented in Figure 11:

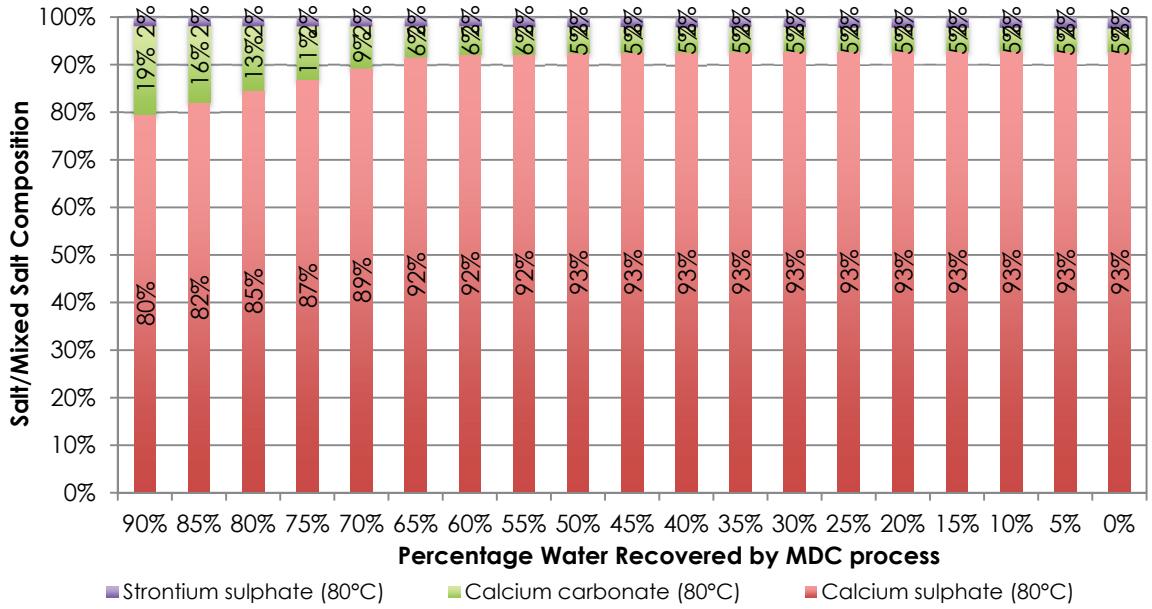

Figure 11: Purity (relative composition) of the dominant crystallising salts from CMB in an MDC process as function of water recovery operated at 80°C

In Figure 11, it can be seen that at the higher MDC operating temperature of 80°C, similar to the 60°C scenario, due to the inverse solubility of calcium sulphate, the dominant crystallising salt at all water recoveries will be calcium sulphate. However, due to the greater driving force of calcium sulphate crystallisation, the purity of the mixed salt is substantially higher with respect to the calcium sulphate with a relative composition of the calcium sulphate in the mixed salt ranging between 93% at 0% water recovery to 80% at 90% water recovery. The other contributing salts to the mixed salt product are calcium carbonate (5% - 19%) and to a much lesser degree strontium sulphate (1% - 5%).

4.2.2.4 *A comparison of the effect of operating temperature on the crystallisation behaviour of the dominant solids*

In Figure 12 the comparative differences in the amount of each of the dominant solids that crystallise out as a function of an increase in water recovery in the MDC of CMB can be seen.

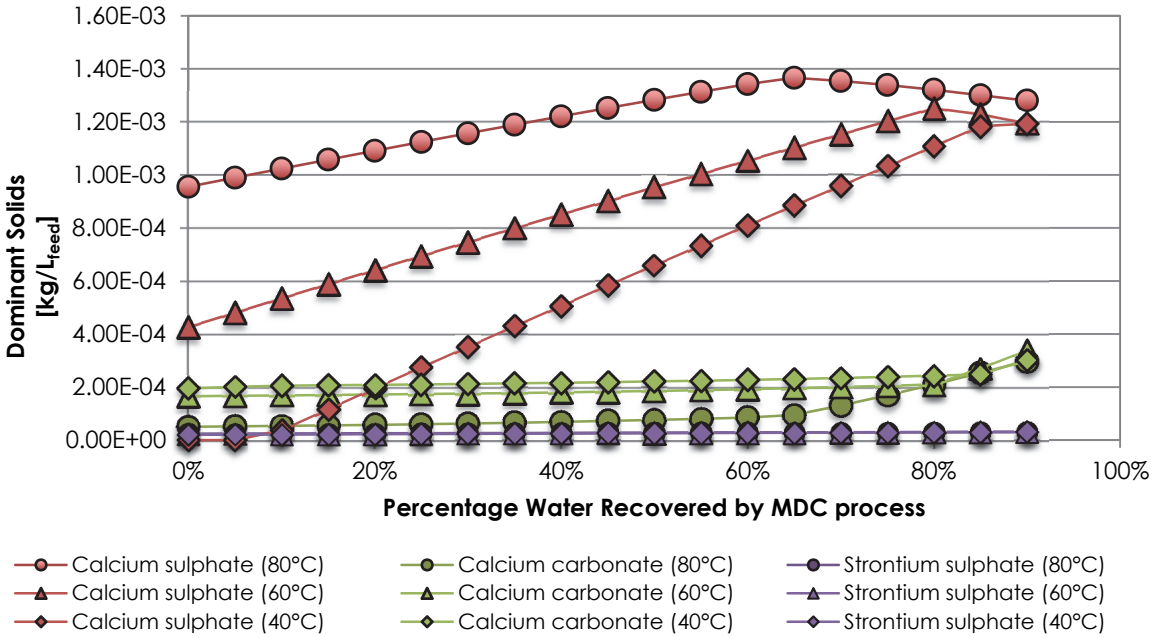

Figure 12: Effect of MDC operating temperature on the comparative amounts of each of the dominant solids that crystallise out as a function of an increase in water recovery

From Figure 12 it can be seen that the propensity for calcium sulphate crystallisation is higher at a higher operating temperature. This is counter-intuitive to the norm as the solubility of most solids increases at a higher temperature and would result in a reduction in the crystallisation. This is explained by calcium sulphate's characteristic inverse solubility.

In the case of the calcium carbonate and strontium sulphate, the propensity of crystallisation decreases at a higher operating temperature, which is in line with the expected increase in solubility at elevated temperatures that consequently reduce the supersaturation driving force for crystallisation.

In Figure 13 the comparative differences in the combined amount of mixed salt that crystallises out as a function of the selected operating temperature at increasing levels of water recovery in the MDC of CMB can be seen.

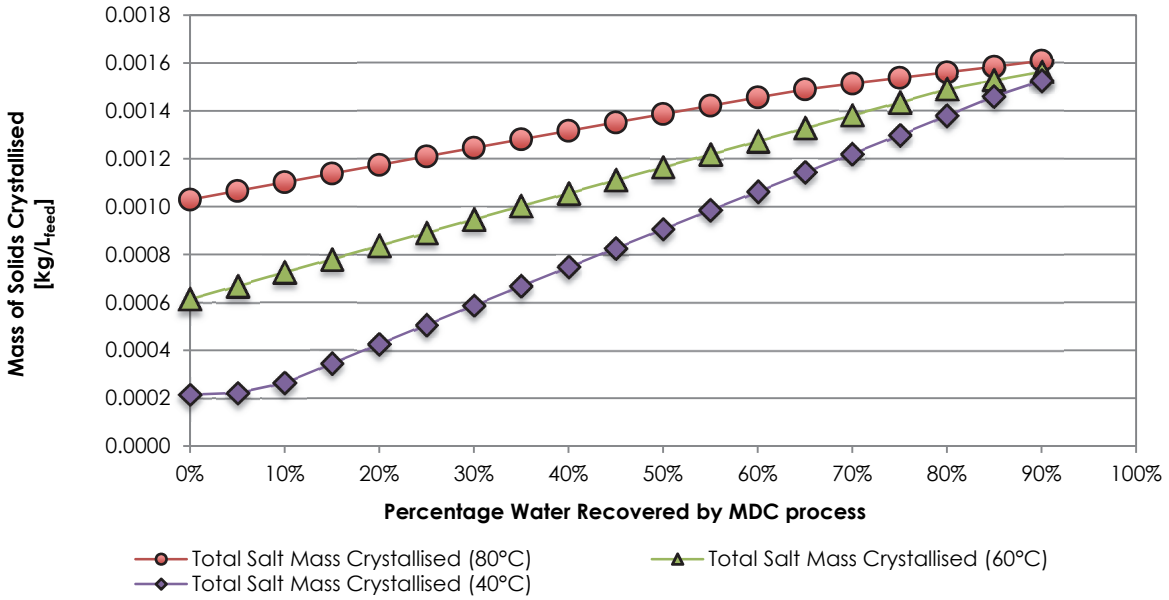

Figure 13: Total mass of crystallising solids from CMB in an MDC process as function of water recovery operated at 40°C, 60°C and 80°C

In Figure 13, it can be seen that due to the fact that the calcium sulphate is the largest contributing component to the mixed salt, its inverse solubility characteristics of a higher propensity towards crystallisation at a higher operating temperature supersedes the conventional crystallisation characteristics of the two less dominant species, i.e. calcium carbonate and strontium sulphate.

4.2.3 Crystallisation characteristics of the PPB in an MDC process

The crystallisation characteristics of the PPB in an MDC process was investigated at a water recovery range between 0 – 90% and an operating temperature range of 40 - 80°C.

4.2.3.1 Crystallisation characteristics of the PPB in an MDC process as a function of the water recovery at an operating temperature of 40°C

In Figure 14 the results of thermodynamically calculated crystallisation characteristics of the PPB in an MDC process with respect to the identities of the crystallising species can be seen.

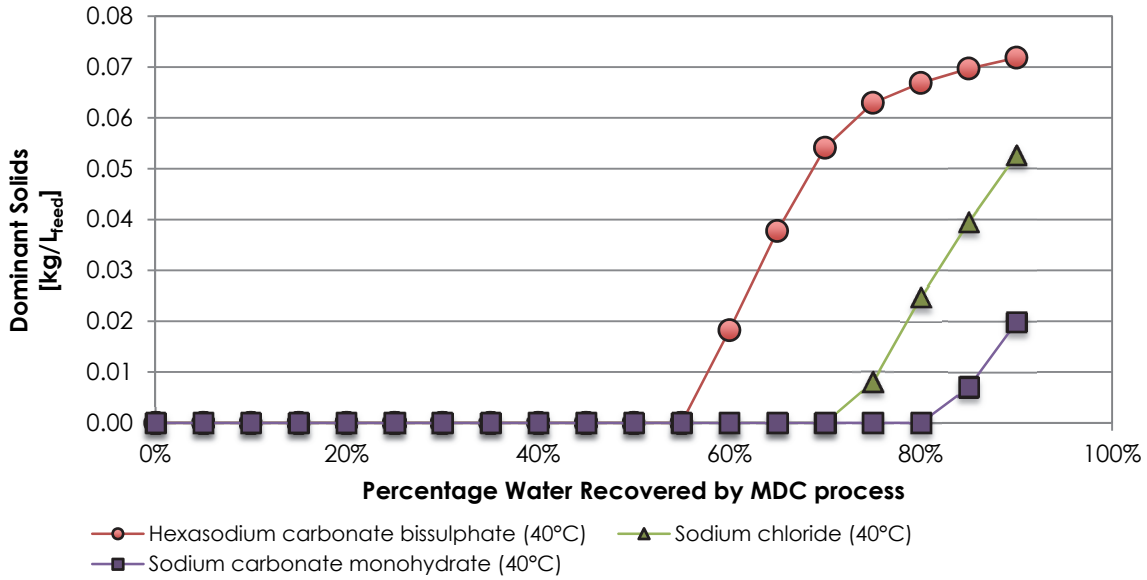

Figure 14: Dominant crystallising solids from PPB in an MDC process operated at 40°C

From Figure 14, it can be seen that the brine is under-saturated and that crystallisation only occurs at water recoveries greater than 55%. The dominant crystallising salts are hexasodium carbonate bisulphate, sodium chloride and sodium carbonate monohydrate. Furthermore, the total mass of the three salts that crystallise out increases with an increase in the overall water recovery. This is to be expected as the removal of water in the form of permeate from the system results in a corresponding increase in the relative supersaturation of the scaling species, increasing the driving force for further crystallisation.

The combined mass of the crystallising salts as a function of the water recovery at 40°C is presented in Figure 15:

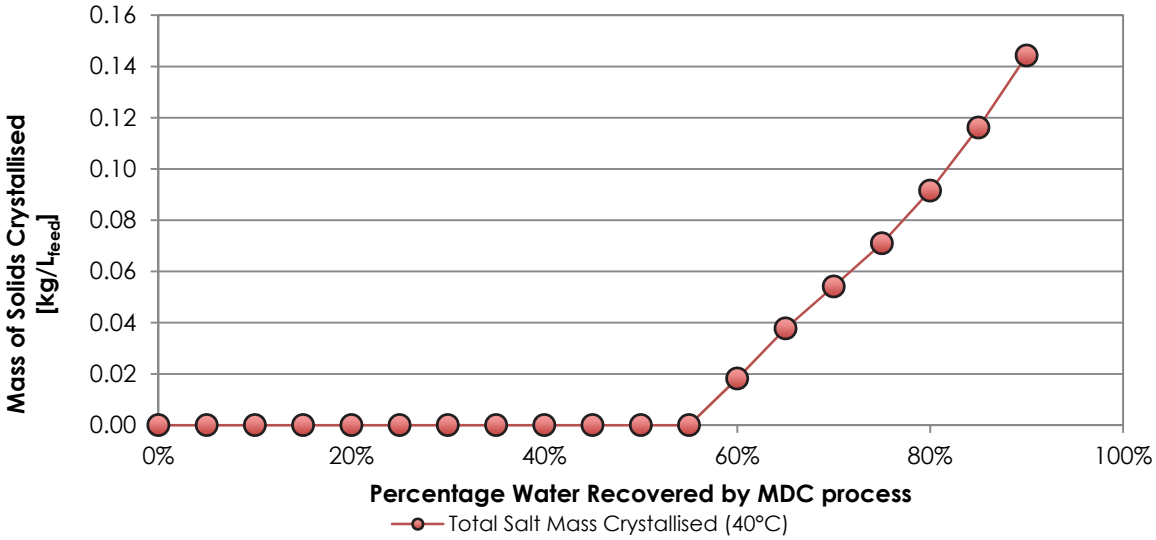

Figure 15: Total mass of crystallising solids from PPB in an MDC process as function of water recovery operated at 40°C

From Figure 15, it is clear that the combined mass of crystallising salts increases with an increase in the water recovery due to a corresponding increase in the relative supersaturation and hence the driving force for crystallisation.

The purity, defined as the relative contributions of the dominant crystallising salts to a mixed salt product, as a function of the sequential increase in the overall water recovery of the MDC process on PPB is presented in Figure 16:

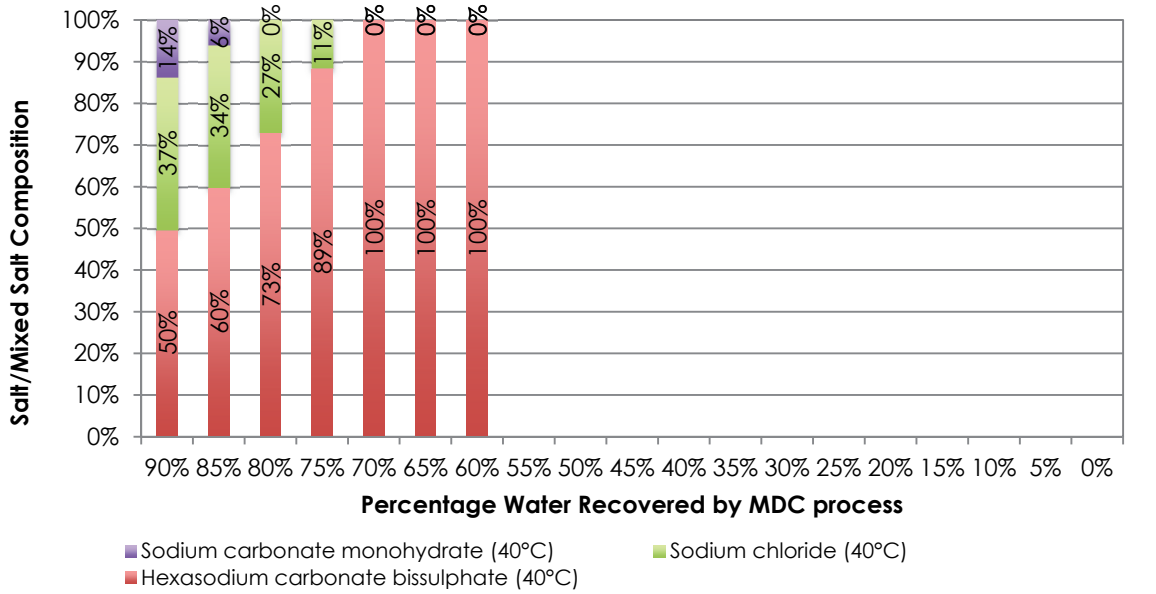

Figure 16: Purity (relative composition) of the dominant crystallising salts from PPB in an MDC process as function of water recovery operated at 40°C

In Figure 16 it can be seen that up to a water recovery of 70%, the only crystallising salt will be hexasodium carbonate bisulphate at 100% purity. This is followed by sodium chloride at 75% water recovery and sodium carbonate bisulphate at 85% water recovery. The contribution of the sodium chloride and sodium carbonate bisulphate to the mixed salt ranges between 11-37% and 6-14% respectively.

4.2.3.2 Crystallisation characteristics of the PPB in an MDC process as a function of the water recovery at an operating temperature of 60°C

In Figure 17 the results of thermodynamically calculated crystallisation characteristics of the PPB in an MDC process with respect to the identities of the crystallising species can be seen.

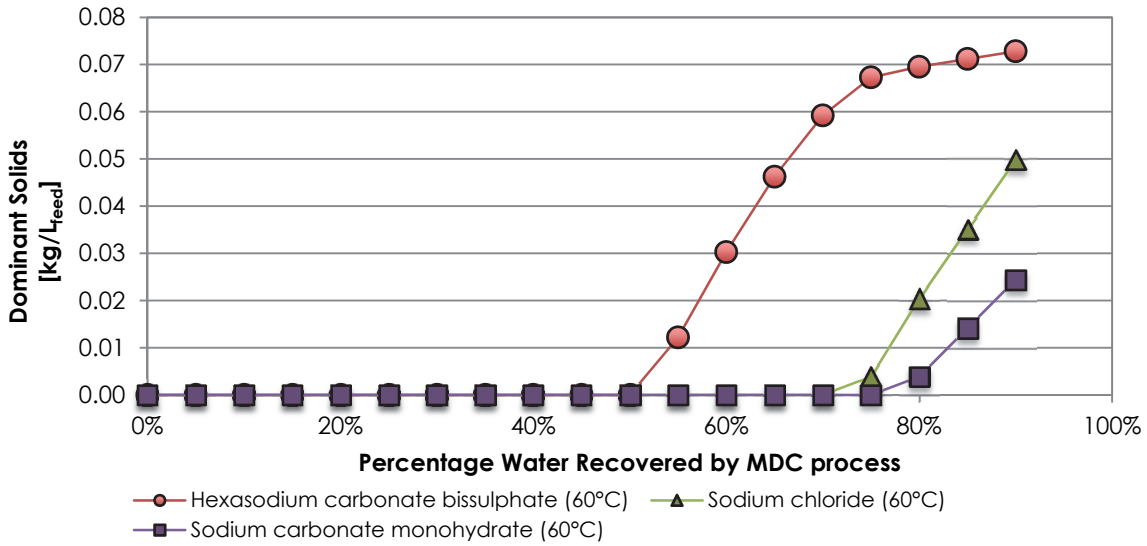

Figure 17: Dominant crystallising solids from PPB in an MDC process operated at 60°C

From Figure 17, it can be seen that the brine is under-saturated and that crystallisation only occurs at after 50% water recovery. The dominant crystallising salts are hexasodium carbonate bisulphate, sodium chloride and sodium carbonate monohydrate. Furthermore, the total mass of the three salts that crystallise out increases with an increase in the overall water recovery. This is to be expected as the removal of water in the form of permeate from the system results in a corresponding increase in the relative supersaturation of the scaling species, increasing the driving force for further crystallisation.

The combined mass of the crystallising salts as a function of the water recovery at 60°C is presented in Figure 18:

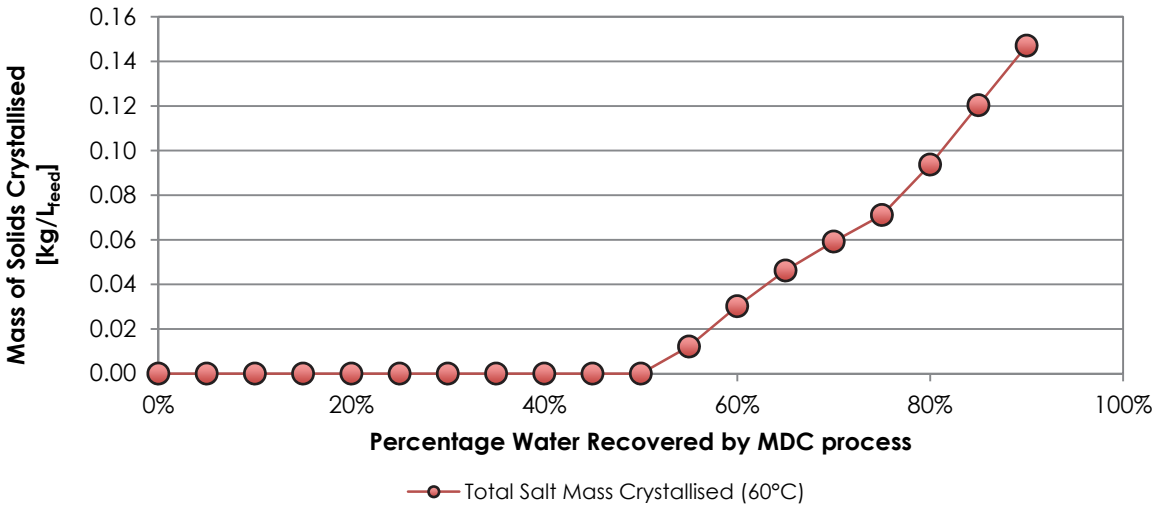

Figure 18: Total mass of crystallising solids from PPB in an MDC process as function of water recovery operated at 60°C

From Figure 18, it is clear that the combined mass of crystallising salts increases with an increase in the water recovery due to a corresponding increase in the relative supersaturation and hence the driving force for crystallisation.

The purity, defined as the relative contributions of the dominant crystallising salts to a mixed salt product, as a function of the sequential increase in the overall water recovery of the MDC process on PPB is presented in Figure 19:

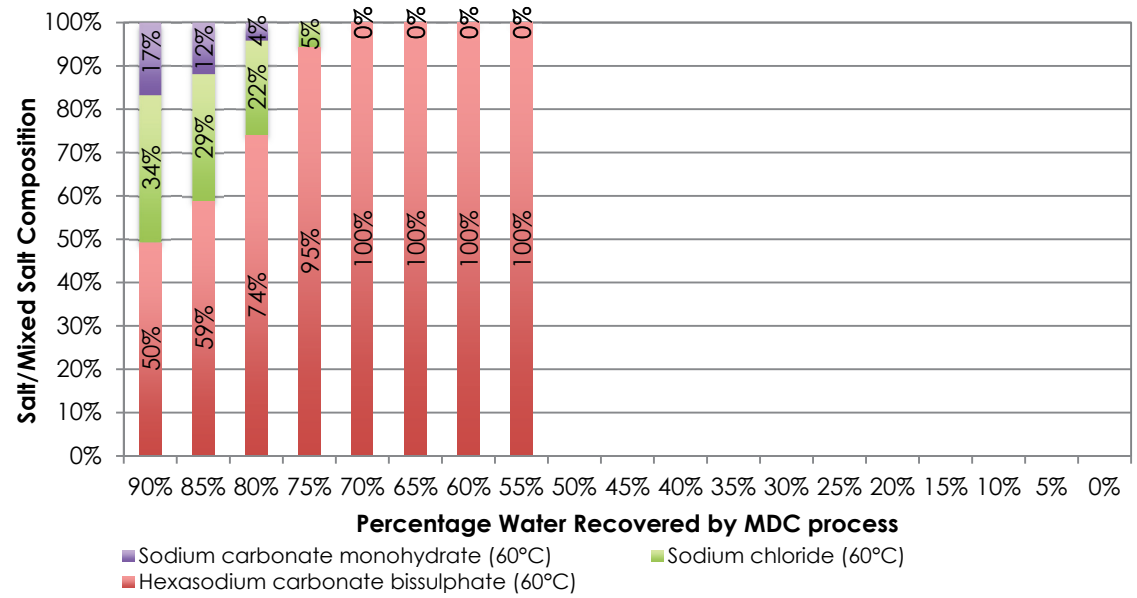

Figure 19: Purity (relative composition) of the dominant crystallising salts from PPB in an MDC process as function of water recovery operated at 60°C

In Figure 19 it can be seen that up to a water recovery of 70%, the only crystallising salt will be hexasodium carbonate bisulphate at 100% purity. This is followed by sodium chloride at 75% water recovery and sodium carbonate bisulphate at 80% water recovery. The contribution of the sodium chloride and sodium carbonate bisulphate to the mixed salt ranges between 5-34% and 1-4% respectively.

4.2.3.3 *Crystallisation characteristics of the PPB in an MDC process as a function of the water recovery at an operating temperature of 80°C*

In Figure 20 the results of thermodynamically calculated crystallisation characteristics of the PPB in an MDC process with respect to the identities of the crystallising species can be seen.

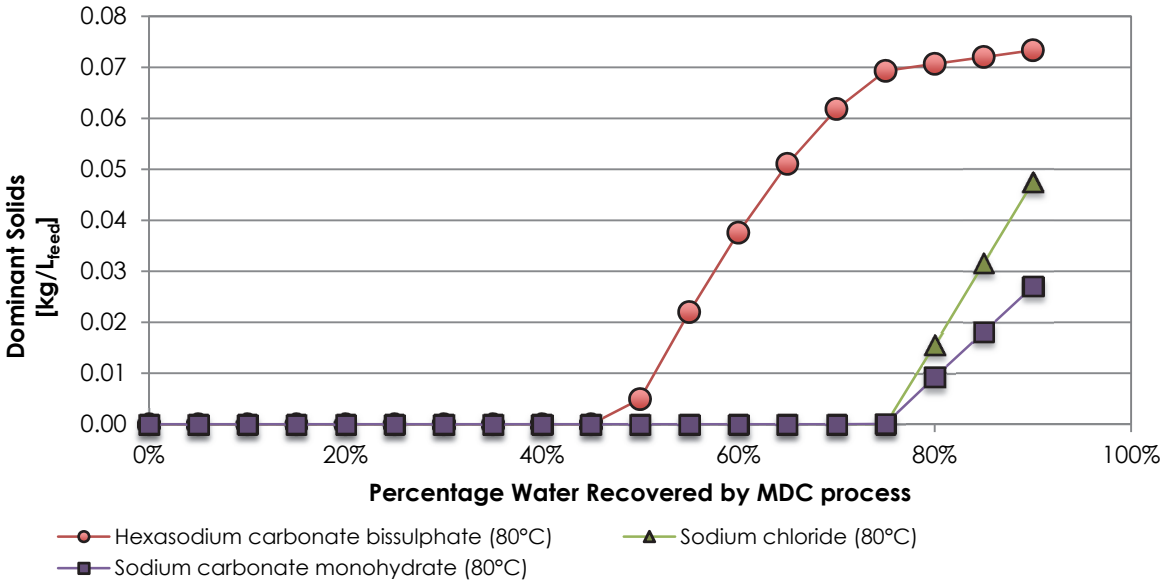

Figure 20: Dominant crystallising solids from PPB in an MDC process operated at 80°C

From Figure 20, it can be seen that the brine is under-saturated and that crystallisation only occurs at after 45% water recovery. The dominant crystallising salts are hexasodium carbonate bisulphate, sodium chloride and sodium carbonate monohydrate. Furthermore, the total mass of the three salts that crystallise out increases with an increase in the overall water recovery. This is to be expected as the removal of water in the form of permeate from the system results in a corresponding increase in the relative supersaturation of the scaling species, increasing the driving force for further crystallisation.

The combined mass of the crystallising salts as a function of the water recovery at 80°C is presented in Figure 21:

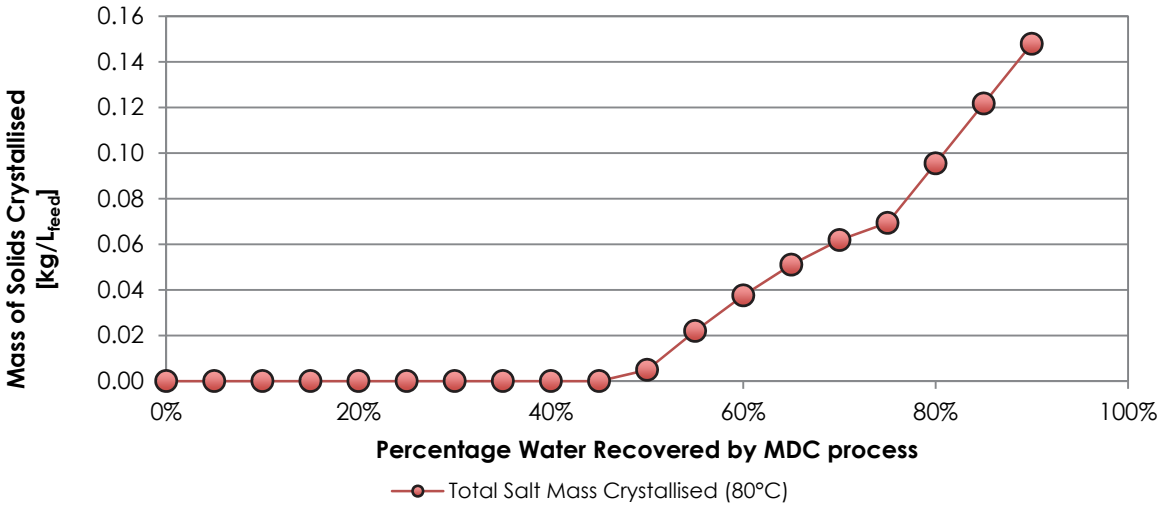

Figure 21: Total mass of crystallising solids from PPB in an MDC process as function of water recovery operated at 80°C

From Figure 21, it is clear that the combined mass of crystallising salts increases with an increase in the water recovery due to a corresponding increase in the relative supersaturation and hence the driving force for crystallisation.

The purity, defined as the relative contributions of the dominant crystallising salts to a mixed salt product as a function of the sequential increase in the overall water recovery of the MDC process on PPB, is presented in Figure 22:

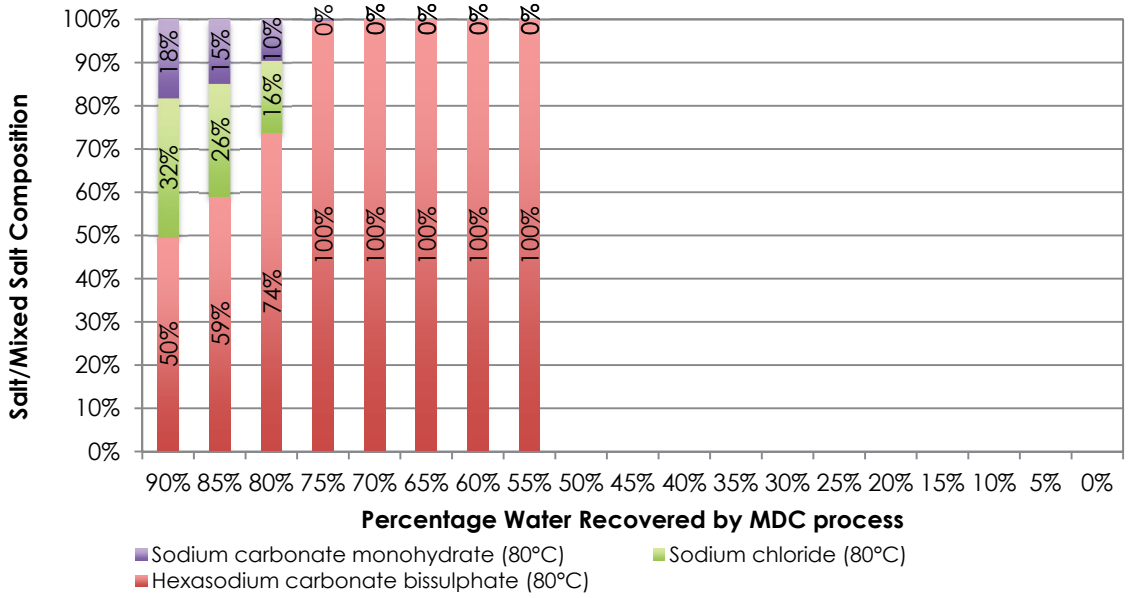

Figure 22: Purity (relative composition) of the dominant crystallising salts from PPB in an MDC process as function of water recovery operated at 80°C

In Figure 22 it can be seen that up to a water recovery of 75%, the only crystallising salt will be hexasodium carbonate bisulphate at 100% purity. This is followed by sodium chloride and sodium carbonate bisulphate at 80%. The contribution of the sodium chloride and sodium carbonate bisulphate to the mixed salt ranges between 16-32% and 10-18% respectively.

4.2.3.4 A comparison of the effect of operating temperature on the crystallisation behaviour of the dominant solids

In Figure 23 the comparative differences in the amount of each of the dominant solids that crystallise out as a function of an increase in water recovery in the MDC of PPB can be seen.

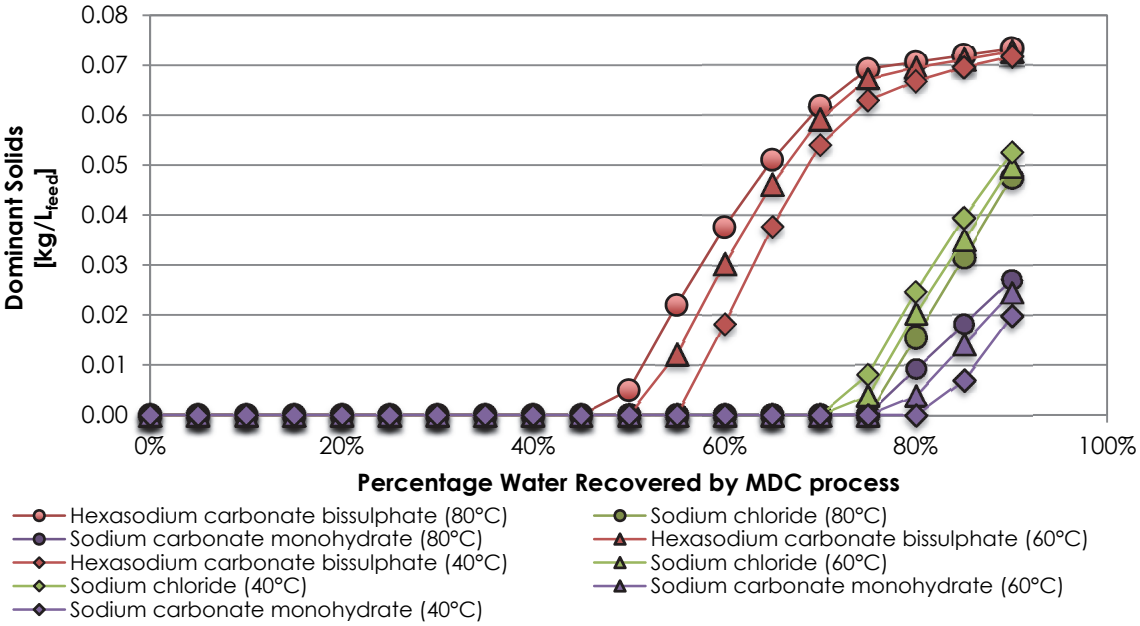

Figure 23: Effect of MDC operating temperature on the comparative amounts of each of the dominant solids that crystallise out as a function of an increase in water recovery

From Figure 23 it can be seen that the propensity for hexasodium carbonate bisulphate and sodium carbonate bisulphate crystallisation is higher at a higher operating temperature. This suggests that both of these species exhibit an inverse solubility characteristic similar to calcium sulphate.

In the case of the sodium chloride, the propensity of crystallisation decreases at a higher operating temperature, which is in line with the expected increase in solubility at elevated temperatures that consequently, reduces the supersaturation driving force for crystallisation.

In Figure 24 the comparative differences in the combined amount of mixed salt that crystallises out as a function of the selected operating temperature at increasing levels of water recovery in the MDC of PPB can be seen.

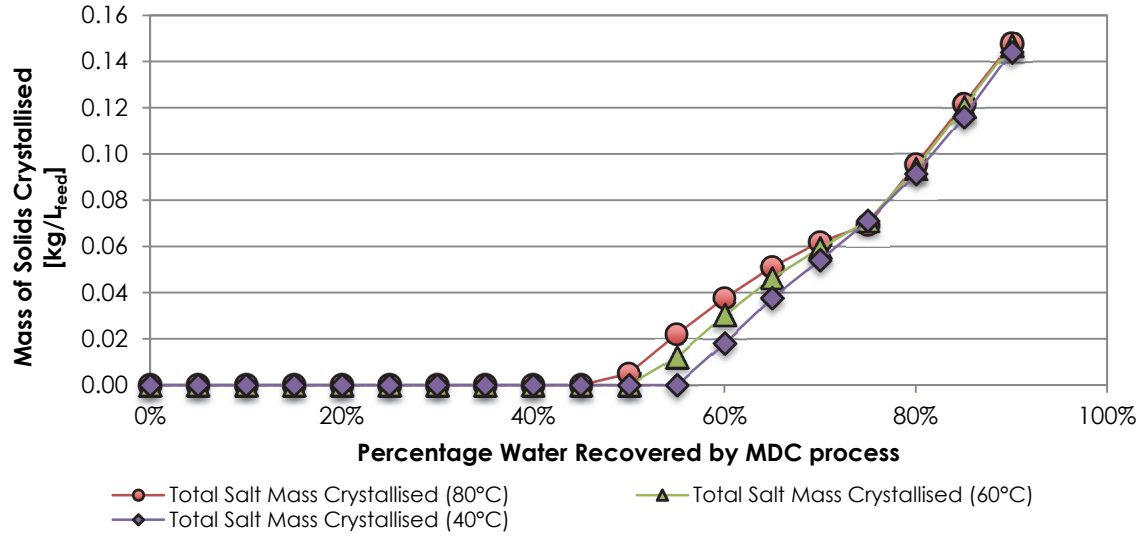

Figure 24: Total mass of crystallising solids from PPB in an MDC process as function of water recovery operated at 40°C, 60°C and 80°C

In Figure 24 it can be seen that the operating temperature has a small positive influence when operating at higher temperatures between water recoveries of 50-70% due to the inverse solubility characteristics and higher propensity towards crystallisation at a higher operating temperature for hexasodium carbonate bisulphate and sodium carbonate. However, beyond a water recovery of 75%, the effect is almost negligible.

4.3 Conclusions

This study demonstrates the efficacy of using aqueous thermodynamic modelling as a tool for investigating and predicting the crystallisation aspects of the MDC process, including, though not limited to the scaling tendencies, the identities of crystallising salts, and the sequence in which the salts crystallise out as well as identifying subtler crystallisation aspects such as inverse solubilities of specific species, etc.

Based on the two brine specimens investigated, the following general conclusions can be drawn:

i) The propensity for crystallisation increases with an increase with water recovery in the MDC process. This is directly linked to the increase in the supersaturation and consequently the driving force for crystallisation as a result of the removal of permeate water from the brine.

ii) Except for species that exhibit an inverse solubility, a lower operating temperature results in a higher crystal product yield due to the lower solubility of scaling species at lower temperatures

iii) For scaling species exhibiting inverse solubility characteristics, the inverse of (ii) above is true

iv) The purity of the resultant crystallisation product is dependent on the extent of water recovery as the number of additional crystallising species (contaminants/impurities) increases with an increase in the water recovery

v) At the higher MDC operating temperature of 80°C, similar to the 60°C scenario, due to the inverse solubility of calcium sulphate, the dominant crystallising salt at all water recoveries will be calcium sulphate. However, due to the greater driving force of calcium sulphate crystallisation, the purity of the mixed salt is substantially higher with respect to the calcium sulphate

vi) Lastly, different brine compositions produce diverse salts and salt yields, sometimes at the same operating conditions. Consequently, each brine composition should be assessed independently during the process design of an MDC process.

CHAPTER 5 - Experimental Set-up and Methodology

5.1 Experiment set-up

Direct Contact Membrane Distillation (DCMD) was selected as the MD configuration for this project. With DCMD, the membrane is in direct contact with the liquid phases and is best suited for desalination and concentration of aqueous solutions. In addition, it is characterised by an increased flux when compared to other configurations such as Air Gap Membrane Distillation (AGMD), Vacuum Membrane Distillation (VMD) and Sweep Gas Membrane Distillation (SGMD).

The MDC setup as described by (KHAYET, M.) and (TUN, C.M. et al., 2005) was adopted such that the working volume for the crystalliser was 4 L for this study. In Figure 25 the general configuration of the DCMD experimental set up that was used can be seen, whilst in Figure 26 the basic design of the membrane element cell that was used can be seen.

A list of the key equipment components and their specific function is provided in Table 5:

Table 5: Direct Contact Membrane Distillation set up key equipment components and their specific function

Equipment Description	Purpose
Membrane distillation unit	To concentrate the stream by producing pure water
Jumo Conductivity meters	Measures the conductivities and temperatures of the feed and product
Thermo Scientific Chiller x 2	Maintains solution temperature at predetermined level
Level indicators	Needed to record the change in volume of the permeate and feed
Watson Marlow 620S/R Peristaltic pumps x 2	Necessary to pump solution to and from the crystalliser & membrane unit
4 L Jacketed crystalliser x 2	To crystallise out salts from solution
Overhead agitator with variable speed drive x 2	Provides adequate mixing of the solution
Equipment frame	Needed to house equipment
Programmable Logic Controller (PLC) system	To record all the relevant data in real time (Temperature, pressure, conductivity, etc.)
Auxiliary equipment (piping, valves, tubing, insulation, clamps, etc.)	

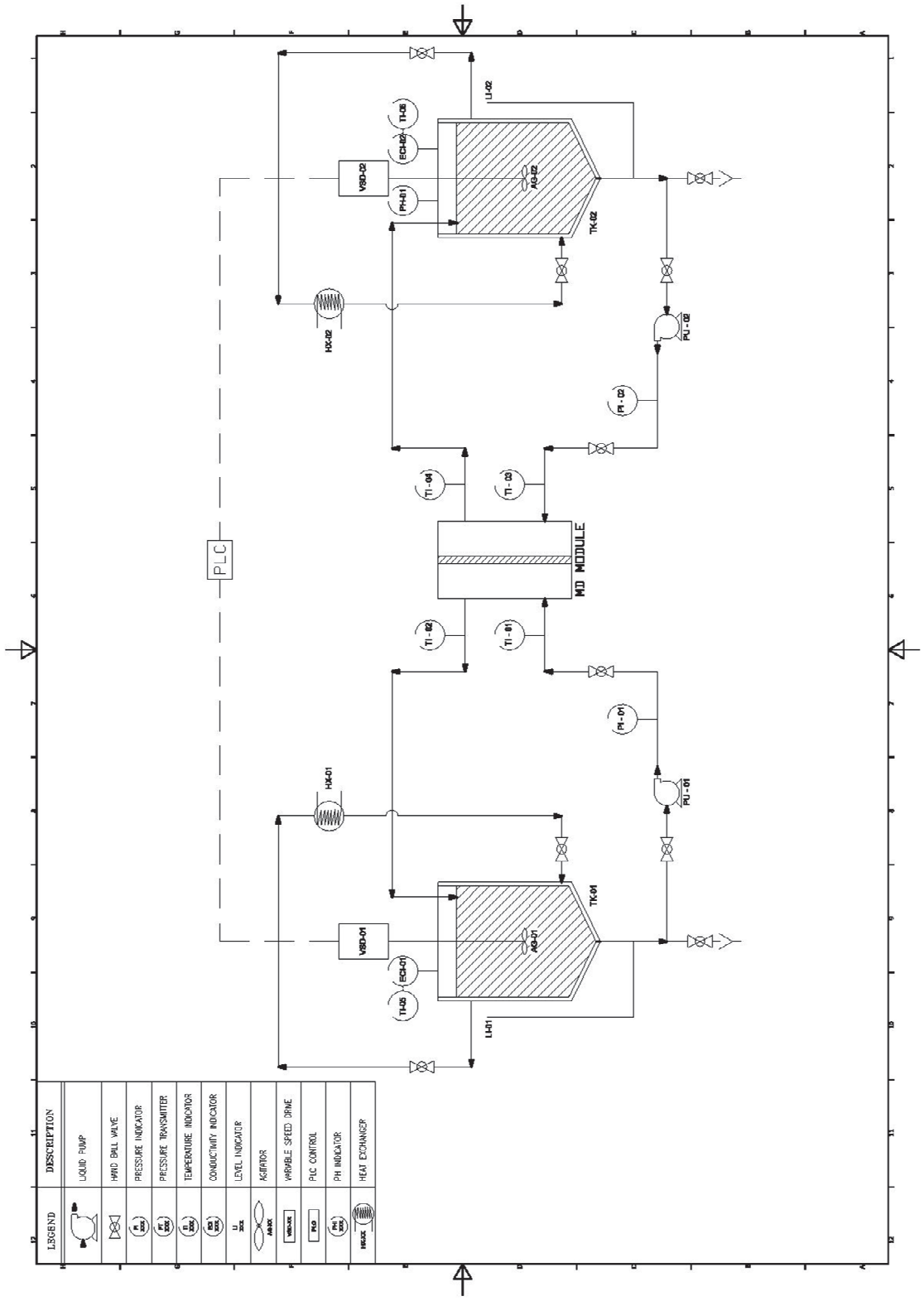

Figure 25: General configuration of the DCMD experimental set up

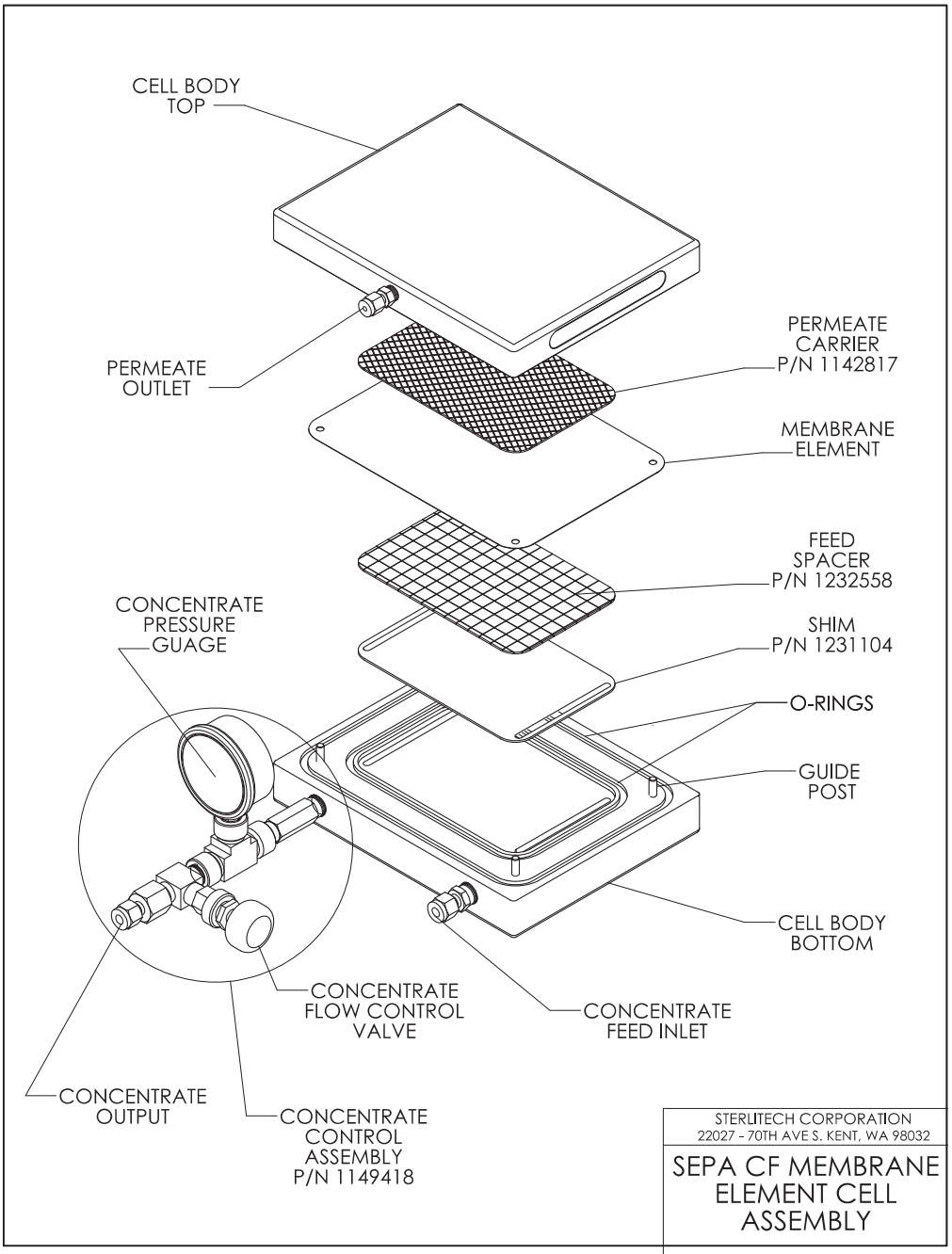

Figure 26: Membrane element cell assembly of the DCMD experimental set up

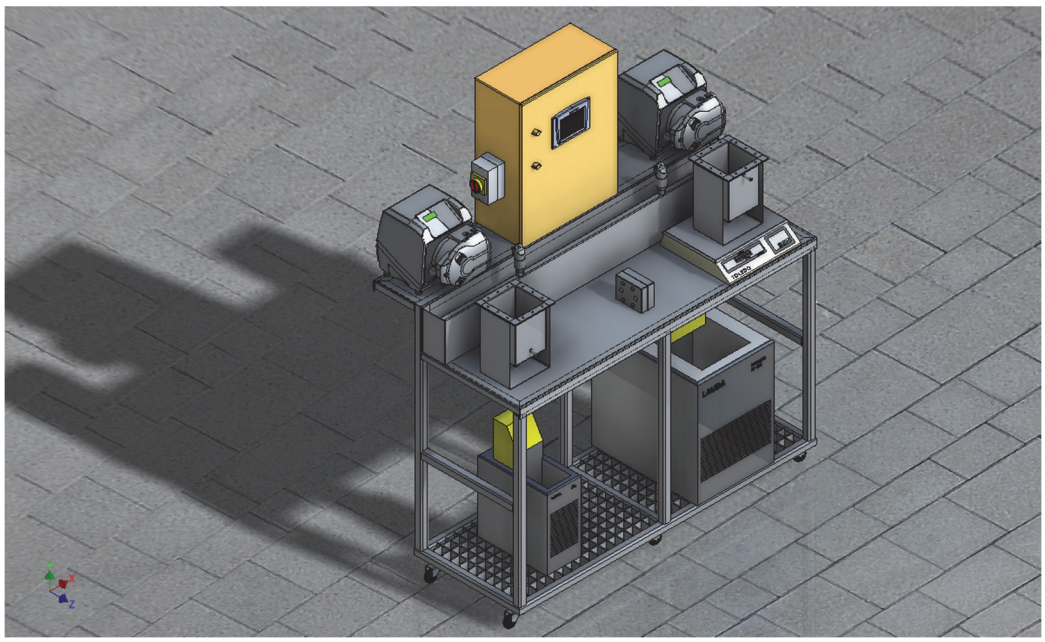

Figure 27: CAD render of the DCMD experimental set up

Figure 28: Photograph of commissioned DCMD experimental set up

Figure 29: Photograph of commissioned DCMD experimental set up

5.2 Experiment Methodology

The experiments were conducted in batch-mode whereby the feed (salt solution) ran co-current to the product (deionised water) with the membrane module separating the two streams. These two systems, i.e. the feed stream and the product stream, were driven by two separate peristaltic pumps. These pumps were calibrated for the specific tubing used in this experiment, so that the volumetric flow rate could be determined for each experiment.[1] The pressure exiting the pumps was monitored to ensure that there were no blockages in the line.

Both the feed and product storage tanks could hold approximately 4L of fluid. This fluid was heated or cooled by a heat exchanger and thermostatic circulating bath, which in this case comprised the jacketed compartment around each tank, allowing the contents to be heated or cooled by pumping hot or cold liquid (anti-freeze) through them. In this experiment two separate heat exchangers were used to heat up and cool down the anti-freeze, which was then pumped through the jackets, to control the tank fluid temperature. The tanks were also fitted with an agitator that was used to ensure a uniform heat distribution within each of the tanks, as well as maintaining a uniform feed concentration. Furthermore, the tanks were wrapped in insulating material to reduce the heat loss from or heat ingress into the system.

Temperatures at the inlet and outlet of the membrane module, for both the feed and product lines were monitored and logged as can be seen in Figure 25. Temperature indicators TI-01 and TI-03 were used to control the temperatures in the tanks by adjusting the respective heat exchanger temperatures accordingly.

Each tank was fitted with an external level, from which the level could be read in cm units. The volumetric change could then be determined by using the calibration value given in Appendix A for each tank. The tanks were also fitted with conductivity probes, to determine the membranes salt rejection, i.e. if any salts were transferred from the feed to the product side, and also to have an indication of the change in feed concentration with time. A pH probe in the product tank monitored the change in product pH characteristics with time.

[1] The pumps were calibrated as per the pump manual. These values are then stored in the pump.

5.2.1 Selection of model brines for the study

A brine solution representing the brine generated from the desalination (via RO) of coal mine pit water was selected for experimentation. The actual composition of the brine solution is given in Chapter 4 – Aqueous Thermodynamic Modelling Table 3, whilst the salt solution used in this experiment is given in Table 6. This was made up using a mixture of sodium bicarbonate ($NaHCO_3$), sodium sulphate (Na_2SO_4), sulphuric acid (H_2SO_4), magnesium chloride ($MgCl_2$) and calcium hydroxide ($Ca(OH)_2$).

Table 6: Analysis of salt solution

Species	mg/L
Sodium ion(+1)	2456.00
Calcium ion(+2)	528.42
Magnesium ion(+2)	451.74
Chloride ion(-1)	1317.88
Bicarbonate ion(-1)	695.12
Sulphate ion(-2)	5850.57

5.2.2 Parameters measurement and data logging

A PLC system measured the temperature of the feed and product in and out of the membrane module. Furthermore, the conductivity in each tank, the pH of the product tank and the pressure after each pump was also recorded. This data logging system was configured to measure and log measurements every 15 seconds.

The agitator speed was controlled via the PLC, and inputs for the given flow rates and heat exchanger temperatures were also manually inputted to record most of the key parameters that influence the system. The tank level was measured and recorded manually. The key parameters that were recorded included the volume change, electrical conductivity, temperatures, flow rates and pressures. The volume change was used to determine the volumetric flux across the membrane by using Equation 9.

$$Flux = \frac{Volume\ of\ water\ extracted\ (ml)}{Membrane\ area\ (m^2) \times Timeperiod(h)} \quad (9)$$

5.3 Experimental Procedure

Trial experiments were first performed to commission the experiment by determining whether the experimental setup needed any adjustments and if all the equipment was operating correctly. This was to ensure that a proper procedure could be put in place for the experiments and to minimise errors during the experimental campaign.

The objectives and outcomes of the commissioning phase are described below, after which a detailed procedure used for this experiment is explained.

5.3.1 Commissioning Results

The commissioning phase was used to investigate the system with various flow rates, membranes, feed concentrations and temperatures in order to:

- Check that all sensors are reading correctly
- Check that there are no leaks in the system
- Ascertain the time required to heat up and cool down the systems with the use of the heat exchangers
- Determine which membranes could be used in the experiments
- Determine if any improvements could be made to the system

The information gathered during the commissioning phase was used to prepare a set of procedures for the actual experiment.

During the initial stages of commissioning, tap water was used as both the feed and product and a PV400 membrane sourced from the European manufacturer Ultura was used. The flow rate was kept equal on the feed and product side, whilst the feed temperature was varied. Subsequent to this an experiment was performed whereby the flow rate of the product side was set to be lower than the feed side. The results from these experiments indicated that there was no change in flux across the membrane with a change in ΔT across the membrane, whilst there was a 5-fold increase in flux with a change of flow rate.

The flow rate is directly proportional to the pressure in the system; therefore a bigger difference in flow rate will result in a bigger pressure differential across the membrane and therefore higher flux rate. Even though an increase in external pressure increases the vapour pressure of water, an increase of 1 atm pressure would only increase the vapour pressure by 0.074% (SALZMAN, W.R., 2004). This would not lead to a drastic increase in flux and this suggested that there was a potential issue with the setup.

Consequently, the preceding experiment was repeated with the addition of NaCl in the feed water in order to determine how the conductivity of the system was affected by the experiment. The results from this experiment indicated that the product electrical conductivity was increasing with time, which meant that there was a transfer of salt ions across the membrane from the feed to the product. This was thought to be due to a leak across the membrane, since this would also explain the fact that the flux increased with an increase in flow rate. The membrane module was checked, replaced and resealed before repeating this experiment. However, the same result was obtained, leading to the conclusion that the membrane was not hydrophobic, which also explained the high increase in flux with an increase in feed flow rate, as the larger pressure differential forced the feed through the membrane.

A new polyethylene (PE) membrane, with a pore size of 0.4 µm from Kubota was then investigated. It was discovered that this membrane only yielded results if a pre-treatment step was performed in which the membrane was first completely wetted by soaking in ethanol followed by soaking in deionised water for a minimum of 16 hours. Immediately before use, membranes were again immersed in ethanol to displace as much water as possible then dried in a vacuum oven for 45 minutes at 34-45°C (DOW, N. et al., 2008).

Additional membranes investigated included:

i) 3M Corp Polypropylene (PP) membranes, with a nominal pore size of 0.45 µm and 110 µm thickness, with no backing layer
ii) Hydranautics, PTFE membranes with a nominal pore size of 0.6 µm and thickness of 25 µm and different backing layers.

Despite the membranes from 3M Corp yielding favourable results; it was decided to only use the Hydranautics membranes. This was due to the fact that they had a support layer, as it was very difficult to work with membranes if they did not have a support layer since they are very delicate and easily damaged.

It should be noted that one of the biggest challenges was to acquire suitable membranes, as there is currently a limited supply of hydrophobic membranes.

During commissioning it became apparent that determining the exact level reading on the tanks at each of the time intervals proved challenging as the tank level fluctuated due to the pulsing action on the meniscus attributed to the characteristic pumping action of the peristaltic pump. Therefore it was decided to take two sets of level readings, firstly whilst the system was running and secondly by stopping the pumps and then taking level measurements and then turning the pumps on again.

Some other improvements to the setup before starting proper experimentation included:

- Keeping the feed and product flow the same, since a difference in flow led to a pressure differential across the membrane, causing the membrane to deform and leading to membrane damage.
- Mounting the feed conductivity meter on an adjustable arm, so that the indicator would stay submerged as the level in the tank dropped.
- Using only the product side level measurements for flux calculations since the feed side had a loss of water due to the minimal evaporation at the surface, since it was an open tank. Precautions were taken to try and cover the surface as far as was practically possible.
- The inclusion of a feed spacer on the feed side to give additional strength to the membrane.

5.3.2 Actual experimental procedure

As previously mentioned, the aim of this experiment was to validate the results obtained from the thermodynamic modelling by using a laboratory-scale MDC experimental rig. Furthermore, the effects of operating (i) temperature, (ii) feed water concentration, (iii) operating flow rates and (iv) antiscalant addition on the water recovery, water purity, salt composition and salt morphology of the system were investigated.

These operating conditions for the experiments can be seen in Table 7. The agitator speed was kept at 600 rpm for all experiments in both the product and feed side.

Table 7: Operating parameters for experiments

Test Number	Feed temperature - T_1 (°C)	Product temperature - T_3 (°C)	ΔT (°C)	Feed flow rate - F_1 (L/hr)	Product flow rate - F_2 (L/hr)	Feed TDS (mg/L)	Membrane Type
1	40	10	30	130	130	11775	NTF-1026-L01
2	40	20	20	130	130	11775	NTF-1026-L01
3	40	30	10	130	130	11775	NTF-1026-L01
4	50	10	40	130	130	11775	NTF-1026-L01
5	50	20	30	130	130	11775	NTF-1026-L01
6	50	30	20	130	130	11775	NTF-1026-L01
7	60	10	50	130	130	11775	NTF-1026-L01
8	60	20	40	130	130	11775	NTF-1026-L01
9	60	30	30	130	130	11775	NTF-1026-L01
10	70	10	60	130	130	11775	NTF-1026-L01
11	70	20	50	130	130	11775	NTF-1026-L01
12	70	30	40	130	130	11775	NTF-1026-L01
13	60	10	50	130	130	11775	NTF-1026-N06
14	60	10	50	130	130	11775	NTF-1026-C02
15	60	10	50	130	130	0.75 x Generic solution	NTF-1026-C02
16	60	10	50	130	130	1.25 x Generic solution	NTF-1026-C02
17	60	10	50	130	130	Deionised Water	NTF-1026-C02
18	60	10	50	200	200	1 x Generic solution	NTF-1026-C02
19	60	10	50	60	60	1 x Generic solution	NTF-1026-C02
20	60	10	50	130	130	1 x Generic solution with Antiscalant 1	NTF-1026-C02
21	60	10	50	130	130	1 x Generic solution with Antiscalant 2	NTF-1026-C02
22	60	10	50	130	130	Brine from Coal Mine	NTF-1026-L01

The feed and product temperatures stipulated in the table above were the temperature requirements at the entrance to the membrane module. These had to be controlled indirectly by adjusting the heat exchanger temperatures. The feed concentration is relative to the Synthetic brine concentration given in Table 6. The characteristics of the membrane types are described below.

Before switching on the experimental apparatus, the valves to the membrane module were closed for both the feed and product side. Four litres of the sample solution with the composition given in Table 6, was prepared and poured into the feed tank. The conductivity probe was submerged into the solution. The product tank was then filled with sufficient deionised water for the conductivity probe to be submerged.

The heat exchangers for each system were then switched on and set to the required temperatures and set to pump at their maximum to achieve the highest heat transfer rate. For the first experiment, the product side temperature was set to 8°C, whilst the feed side was set to 45°C. The membrane and feed spacer were installed into the module together with two rubber gaskets/O-rings to keep the membrane in place and to seal the system.

When the tanks had reached the required operating temperatures, the valves to the membrane module were opened and the pumps switched on. The system was given enough time to stabilise before data logging was

initiated as the temperature of the circulating lines and membrane module had to reach the desired temperature. During this time the inlet temperature for both the feed (T_1) and product (T_3) side into the membrane module were monitored, since these needed to be 40°C and 10°C respectively. The heat exchanger temperatures were adjusted accordingly if T_1 and T_3 were not at the required value.

The tank level readings were recorded at 10-minute intervals. This was done by stopping the pumps for a brief moment, recording the level and switching the pumps on again.

The duration of each experiment was 3 hours.

In addition to the above experiments, Experiments 10, 14 and 20 were repeated and allowed to run for a longer period of time (8 hours) to determine the dynamic variability in the flux rate.

In order to minimise/eliminate the effect of fouling on the membrane performance, the membrane was replaced for each experiment. Furthermore, the product side was flushed with deionised water after every run in order to eliminate the transfer of salts to the product side.

The following three membrane types were investigated:

- NTF1026-N06
  - Membrane: PTFE (25 µm)
  - Backing: Polyester net
  - Pore size: 0.6 µm
  - Membrane total thickness: 75 µm
  - Softening temperature: 240°C
- NTF1026-L01
  - Membrane: PTFE (25 µm)
  - Backing: PE+Polyester nonwoven fabric
  - Pore size: 0.6 µm
  - Membrane total thickness: 123 µm
  - Softening temperature: 80°C
- NTF1026-C02
  - Membrane: PTFE (25 µm)
  - Backing: Polyester cloth
  - Pore size: 0.6 micro
  - Membrane total thickness: 92 µm
  - Softening temperature: 240°C

Due to the limited availability of the number of sheets per membrane type, all the experimental parameters could not be investigated with a single type of membrane; therefore one type of membrane was used to investigate a specific parameter.

5.4 Results and discussion

In all of the results, the flux rate is calculated as given by Equation 1 in Section 2.2 of Chapter 5, which defines it as the volume of water transferred across the area of the membrane every hour.

5.4.1 The effect of operating parameters on permeate flux

5.4.1.1 The effect of temperature on flux

A summary of the flux rates obtained for all experiments performed as described in Table 7 with membrane NTF1026-L01 are given in Figure 30. An average flux rate taken over a duration of 180 minutes of the experiment is presented. The error in the flux measurement over this time period is ± 3.47 L/m^2.hr and mainly attributed to the error associated with accurately reading the water level in the tank. The error was calculated using the error in the first and the last measurements and dividing this by the membrane area and duration over which it was taken. As a result, the longer the duration of the experimental run, the lower the relative error and hence the better the accuracy. Although caution was taken to ensure that the experiment did not run past the point where the flux started to decline due to scaling or fouling.

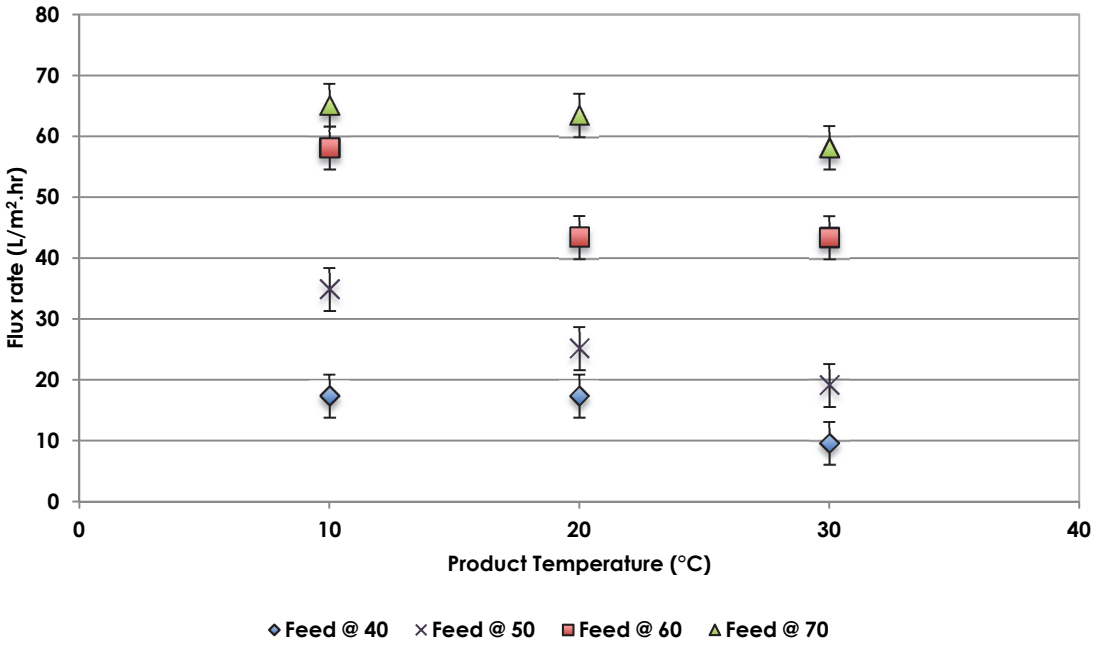

Figure 30: Summary of Effects of Temperature Change on Flux Rate

A 3-dimensional representation of the results showing the effect of a variation in feed and product water temperature on the change in flux can be seen in Figure 31.

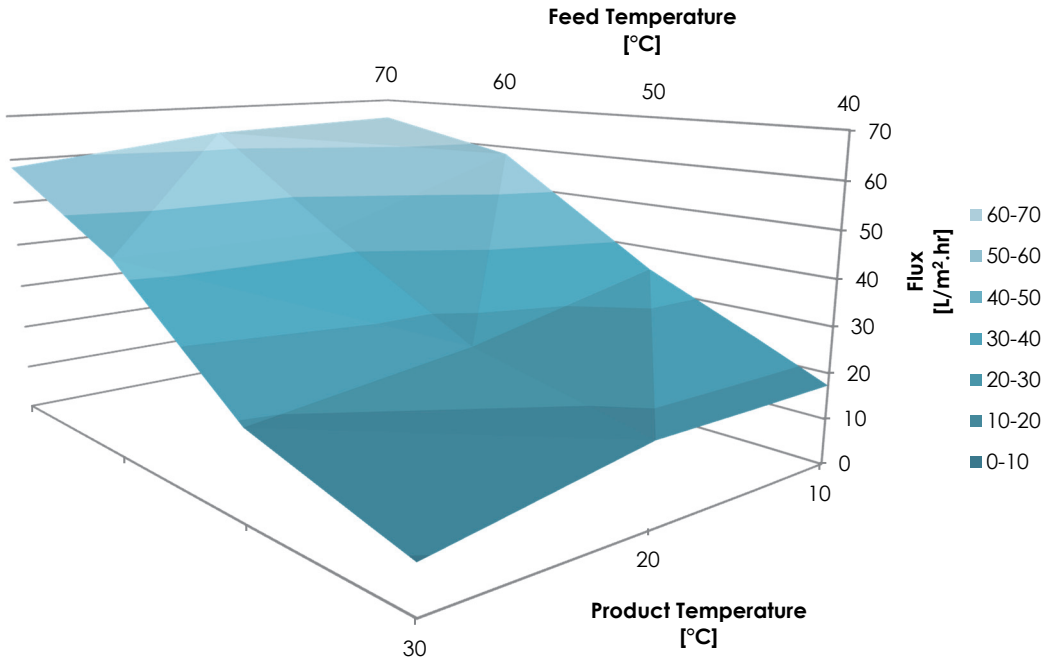

Figure 31: 3-dimensional representation of the effect of a variation in the feed and product temperature on the change in flux

The flux trends for the experiments performed at a constant feed temperature with variation in the product temperature showed that as the product temperature increased, the flux rate decreased. This is in line with what is expected since the ΔT across the membrane decreases with an increase in product temperature, and therefore the vapour pressure difference also decreases. This is explained by the fact that the vapour pressure difference is the main driving force for the mass transfer and therefore there is a resultant decrease in the flux rate.

Similarly, when looking at the flux trends of the experiments performed at a constant product temperature with a variation in feed temperature, it can be seen that as the feed temperature was increased, the flux rate also increased. This is in line with what is expected since the ΔT across the membrane increases with an increase in feed temperature, and therefore the vapour pressure difference also increases, resulting in a higher flux rate.

Based on results presented by Dow, N. et al (2008), at feed and product temperatures of 60°C and 20°C respectively, flux rates of 21 - 24L/m^2.hr were obtained for flat sheet PTFE membranes. (DOW, N. et al., 2008). This article however also suggests that newer generation membranes could obtain flux levels of 50 L/m^2.hr; which is more in line with those achieved in these experiments, i.e. flux rate of 43.4 L/m^2.hr.

When comparing the change in flux with temperature, with the change in vapour pressure difference with temperature (as calculated by using Equation 5), it can be seen (in Figure 32) that the change in flux rate follows a very similar trend to the change in ΔP_{Vapour}.

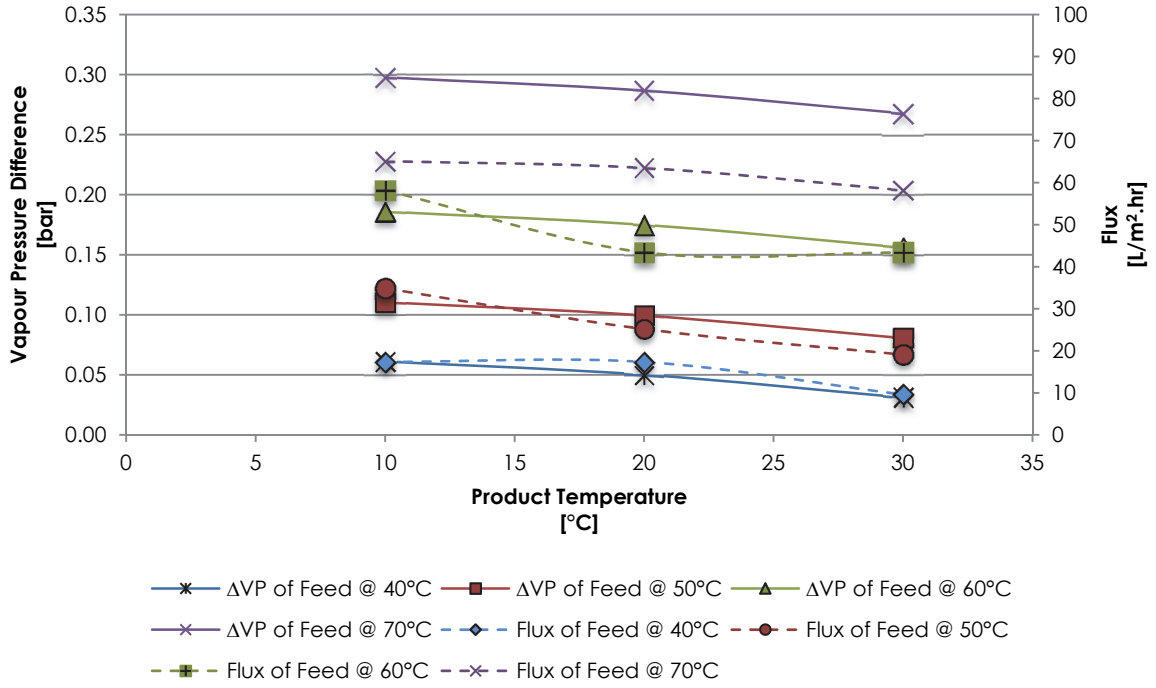

Figure 32: Comparison of Flux Rate and ΔVP at different temperatures

These results also showed that the greatest ΔT does not necessarily mean the greatest mass flux, as the flux obtained when the product temperature was set to 10°C and the feed to 60°C and therefore having a ΔT of 50°C, is similar to the flux obtained at a product temperature of 30°C and a feed temperature of 70°C, with a ΔT of 40°C.

Consequently, further experiments to determine the effect that a constant ΔT at different product temperatures has on the flux rate was investigated. These experiments were performed at feed/product temperatures of 50°C/10°C, 60°C/20°C and 70°C/30°C, to keep a constant ΔT of 40°C, similarly this was done at a constant ΔT of 30°C, with the results given in Figure 33.

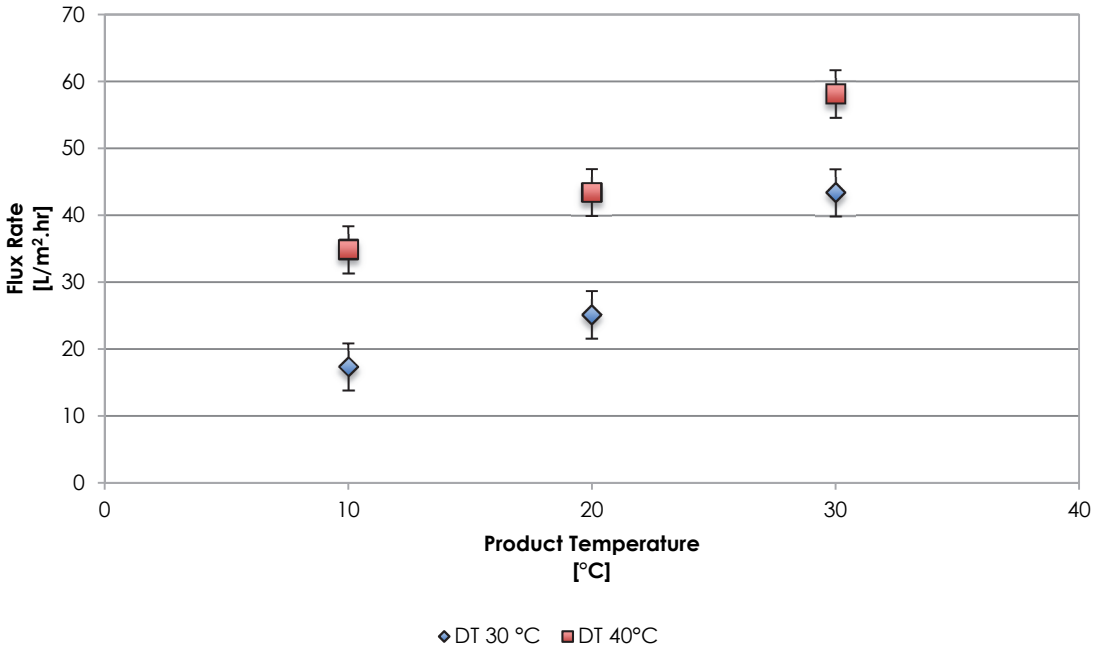

Figure 33: Effects of varying product temperature at constant ΔT of 30 & 40°C on the flux rate

From the results in Figure 33, it can be seen that at a constant ΔT, the flux rate is higher at higher product temperatures. This is in line with what is expected since vapour pressure increases exponentially with an increase in temperature, therefore at higher temperatures, the vapour pressure on the feed side, will have increased more than on the product side, and therefore a greater driving force. This is also represented in Figure 34, where the change in ΔP_{vapour} is compared to the change in flux at a constant ΔT and different product temperatures.

From this it can be concluded that it would be more beneficial to heat up the feed rather than to lower the product temperature in order to improve the flux rate.

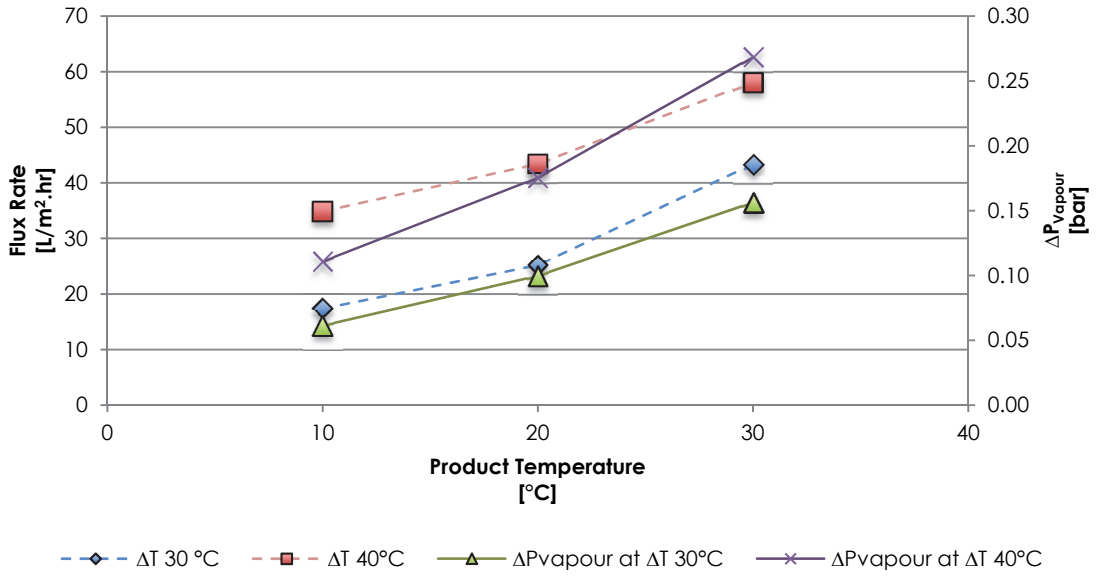

Figure 34: Change in flux rate and ΔP_{vapour} with a change in product temperature at constant ΔT

All of the results obtained were consistent with the theory as described in Sections 2.2.1 & 2.2.2 of Chapter 2, which explains that at a higher feed temperature and lower product temperature will result in the greatest mass flux across the membrane and furthermore that the same ΔT at a higher temperature will result in a higher flux.

This does not necessarily mean that the greatest ΔT or highest working temperature will lead to the best results, since the performance of the MDC process is not only measured on the flux rates but also on the rate of fouling on the membrane and characteristics of the crystals formed in terms of their purity and filterability. The greater the flux rate, the higher the supersaturation and consequently the greater driving force for nucleation rather

than growth of the crystals resulting poorer filterability characteristics of the salt product. Faster crystallisation rates also increase the probability of impurities being integrated within the crystal lattice leading to impure crystals, which negatively impacts on the usability of the final crystal product.

The salt crystal analysis is given in Section 5.4.3.

A key practical consideration is the availability of waste heat for use on the feed side or alternatively the cost of generating the heat and providing cooling on the product side, which increases with an increase in ΔT. The most ideal temperatures will be dependant on the resources available to supply the heat to the system, since it might be easier to obtain temperatures of 60°C and 10°C for the feed and product side respectively in certain industries and areas, whilst in other cases it would be easier to obtain temperatures of 70°C and 30°C for the feed and product side respectively, each of which resulted in the same flux for this membrane.

5.4.1.2 The effect of membrane type on flux rate

Each of the three membranes, namely NTF1026-N06, NTF1026-C02 and NTF1026-L01 were run at a feed temperature of 60°C and product temperature of 10°C, whilst keeping all other parameters constant. The only difference between these membranes is that they had a different backing layer, which in turn affected their overall thickness and also their softening temperature as shown below:

- NTF1026-N06
  - Membrane: PTFE (25 µm)
  - Backing: Polyester net
  - Pore size: 0.6 µm
  - Membrane total thickness: 75 µm
  - Softening temperature: 240°C
- NTF1026-L01
  - Membrane: PTFE (25 µm)
  - Backing: PE+Polyester nonwoven fabric
  - Pore size: 0.6 µm
  - Membrane total thickness: 123 µm
  - Softening temperature: 80°C
- NTF1026-C02
  - Membrane: PTFE (25 µm)
  - Backing: Polyester cloth
  - Pore size: 0.6 micro
  - Membrane total thickness: 92 µm
  - Softening temperature: 240°C

The results of the effect of membrane type on the flux are provided in Table 8:

Table 8: Flux rates obtained for different membranes

Membrane Type	Flux rate ($L/m^2.hr$)
NTF1026-N06	46.54
NTF1026-L01	58.20
NTF1026-C02	42.56

Based on the relationship between flux and membrane characteristics as explained in Section 2.2.6 of Chapter 2, the results in Table 8 are contrary to the expected results since the thickest membrane exhibits the highest flux rate. A possible explanation for this apparent dichotomy could be the permeability characteristics of the backing-layer of each of the membranes and specific manufacturing conditions, details of which could not be obtained. Further research into this is required to determine the exact cause.

5.4.1.3 The effect of feed water concentration on flux rate

To determine the effects that a change in feed concentration has on the flux rate, three solutions of varying concentrations were prepared and investigated with membrane NTF1026-C02. These solutions were based on 0.75, 1 and 1.25 times the original TDS of the Synthetic brine solution in Table 6 and were predetermined based on the supersaturation limits achievable with the antiscalants used in this study. In addition to this, a control experiment with deionised water on both the feed and product side, i.e. essentially having a concentration of 0 mg/L was performed. The results can be seen in Figure 35.

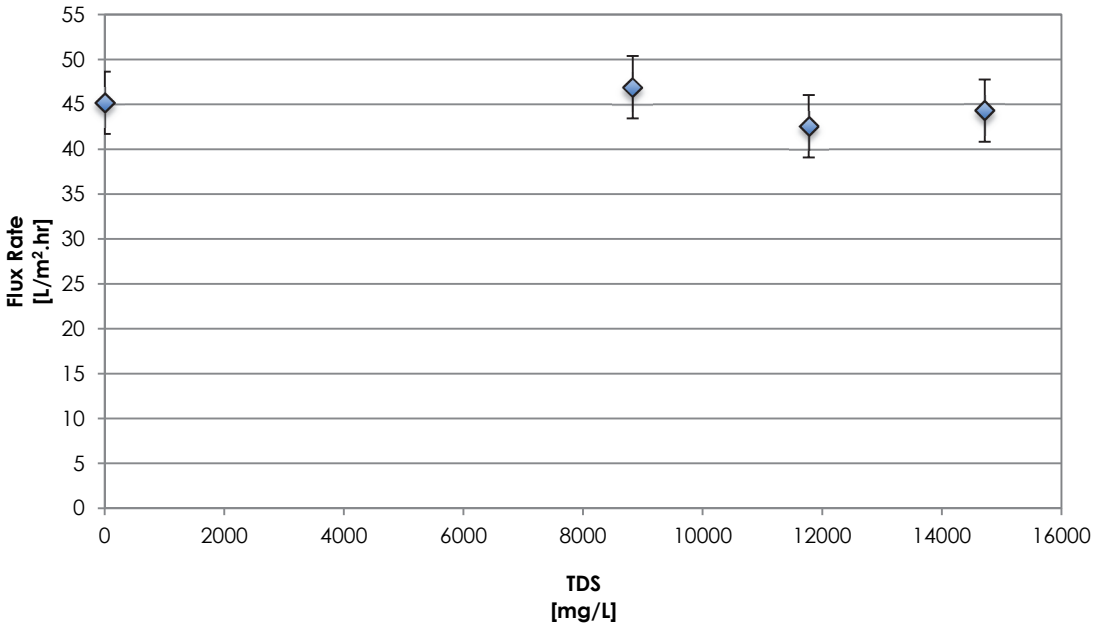

Figure 35: Effects of concentration on flux rate

This graph indicates that there is not much variance in flux with a change in concentration, especially if you take into account the 3.47 L/m^2.hr error in measurement. This is expected since according to Raoult's Law given in Equation 7, the vapour pressure is negligibly affected by the amount of solute in the solution but rather based on the solvent molal concentration and because the solvent molal concentrations for the concentrated solutions are all above 99%, the vapour pressure is not expected to change a significantly for these solutions as seen in Figure 36.

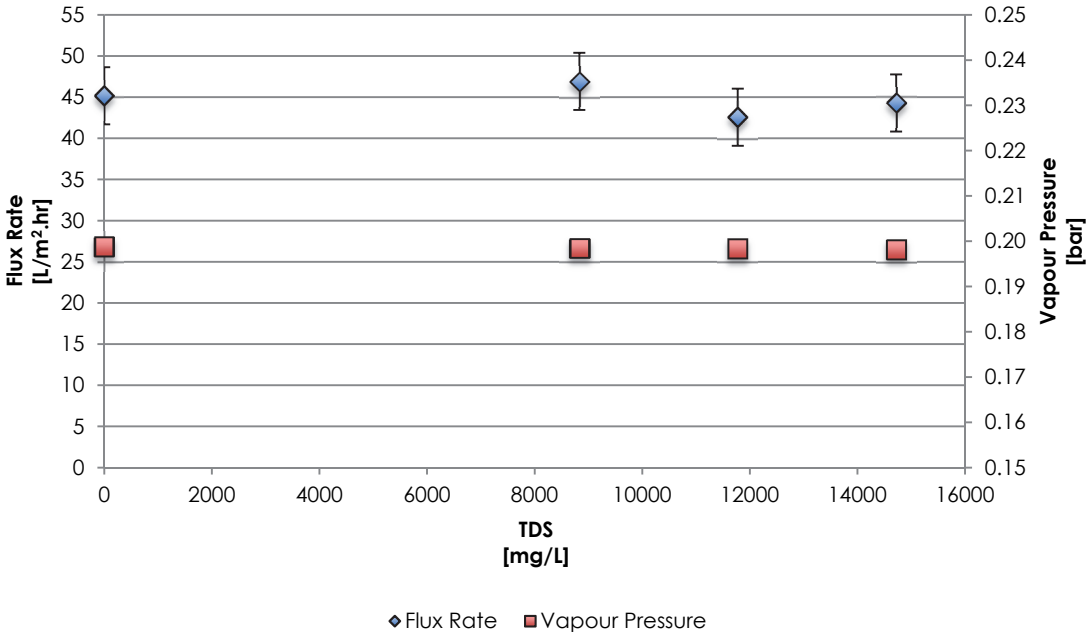

Figure 36: Comparison of Flux rate and Vapour Pressure at varying concentrations

Therefore, in order for the concentration to have a 10% effect on the vapour pressure, the initial brine concentration would have to be approximately 60 times more concentrated.

5.4.1.4 The effect of feed cross flow velocity and product sweep velocity on flux rate

The flow rate was limited by the fact that higher flow rates resulted in deformation of the membrane due to increased pressure on the membrane. Therefore the flow rates were limited to 60 l/hr, 130 l/hr and 200 l/hr, which are equivalent to 0.15 m/s, 0.32 m/s and 0.49 m/s respectively in the circulation piping of the system. Membrane NTF1026-C02 was used for these experiments, with the results given in Figure 37:

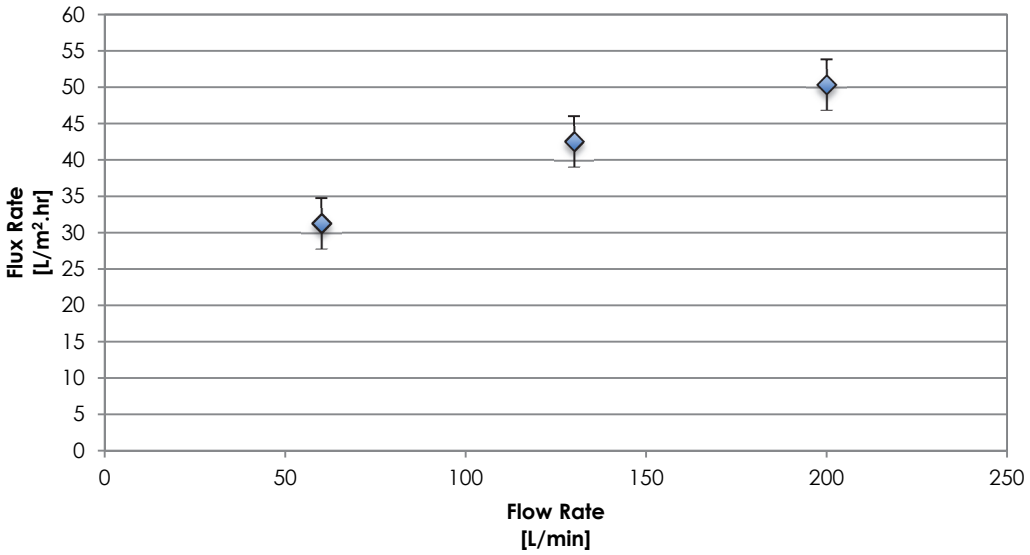

Figure 37: Effects of flow rate on Flux Rate

The overall trend from this experiment clearly shows that the flux rate increases with an increase in flow rate. This can mainly be attributed to an increase in turbulence due to the higher flow rate. This in turn reduces the effect of temperature polarisation at the membrane surface and thereby results in a higher vapour pressure difference across the membrane. Furthermore, by having an increased flow, the fluid is in contact with the membrane surface and membrane module for a shorter period of time, thereby reducing the effects of heat transferred to and from the liquid.

5.4.1.5 The effect of the addition of antiscalant on the flux rate

The effects of two antiscalants on the flux rate were investigated. These antiscalant are described as follows:

a. Antiscalant 1 - Containing organic functional groups
b. Antiscalant 2 - That is aqueous phosphonic acid based

The flux obtained from the experiments using the two different antiscalant was compared to the flux using the Synthetic brine solution without antiscalant in Table 9:

Table 9: Effects of Antiscalants on Flux Rate

Antiscalant	Flux rate ($L/m^2.hr$)
No Antiscalant	42.56
Antiscalant 1	36.48
Antiscalant 2	46.91

Based on the results from concentration experiments, a change in flux rate is not expected with the presence of an antiscalant, since the concentration has been shown to have a negligible effect on the flux rate according to Raoult's Law.

However, a decrease in flux was observed with the Antiscalant 1. Therefore, whilst the decline in the flux was not expected to be attributed to a decrease in the vapour pressure, it could be attributed to the fact that with the organic functional groups within the antiscalant could have caused organic fouling on the membrane. Owing to the fact that the exact composition of the antiscalant is proprietary to the manufacturer, further work is required to confirm these results and to provide a plausible explanation.

The effect of the Antiscalant 2 on the flux showed a slight increase in the flux. However, the increase could be negligible when one takes the error in measurement into account. As Antiscalant 2 is characterised as an aqueous solution of neutralised phosphonic acid, this would further strengthen the suggestion that antiscalants with organic functional groups are in sufficiently high concentrations in RO brines to cause membrane fouling and a flux reduction in MDC processes.

5.4.1.6 The effect of fouling on the flux rate

To determine the effect of fouling resulting from a dynamic increase in the feed water concentration on the flux rate, an additional experiment was performed at 70°C feed temperature and 10°C for 8 hours. The flux rate

monitored by observing the change in level in the product tank. These parameters were chosen since they had the highest flux rate in order to reduce the experimental time, since the focus was on the change in flux rate. The flux rate as a function of water recovered from the feed can be seen in Figure 38.

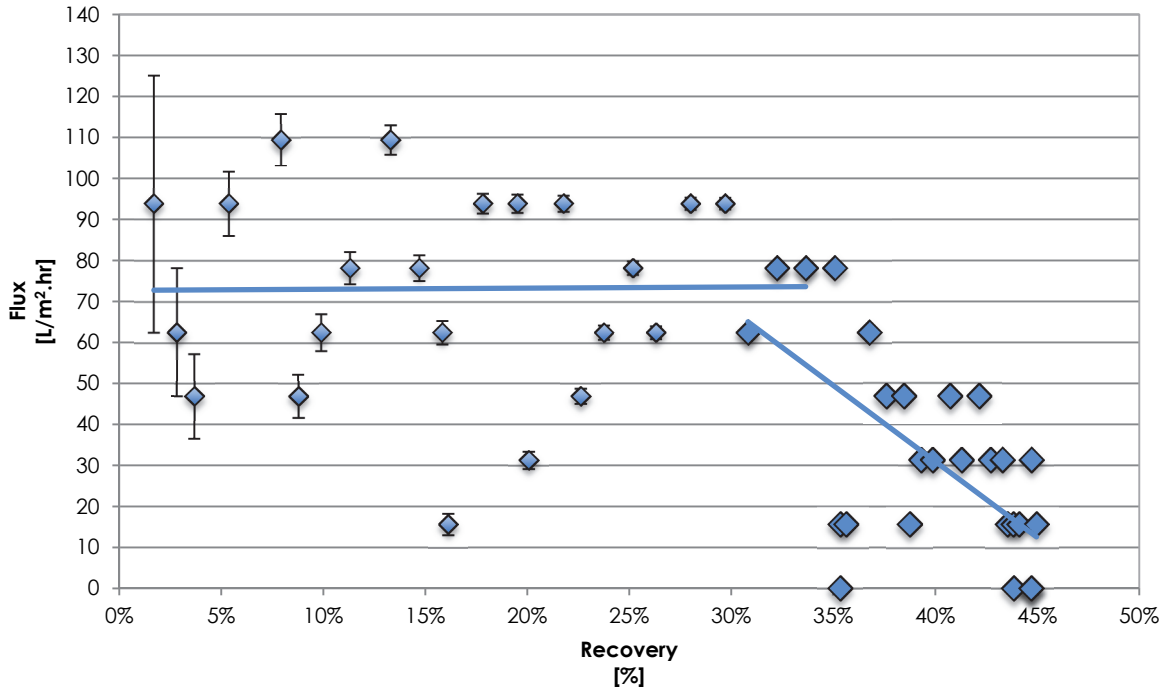

Figure 38: Flux as a function of Water Recovery (NTF1026-L01).

This x-axis of this graph can also be seen as a timeline; since readings were taken every 10 minutes and the recovery increases the longer the experiment is run. Therefore, the closer the data points are to one another, the smaller the increase in recovery over the same time period. Furthermore at a low recovery, there is a larger error in measurement since there was smaller time frame over which the flux was calculated and as mentioned at the beginning of Section 4.1, the error decreases with time. Furthermore the concentration of points at a specific recovery indicates the number of readings taken at that recovery and therefore also the amount of time that the recovery stayed at a certain value.

It can be seen that at higher recoveries, the change in recovery decreased compared to the lower recoveries, as the points are closer together.

From this graph it can be deduced that the flux rate is consistent up to approximately 35% water recovery, after which it starts to decline at an increasing rate. This is to be expected due to the fact that as more water is transferred across the membrane from the feed to the product side, the feed becomes more concentrated and the saturation limit of some of the salts is reached. When this happens, the salts start to crystallise out and consequently deposit onto the membrane surface, resulting in membrane scaling. This scaling in turn decreases the surface area of the membrane through which the water can be transferred, and therefore reduces the amount of water that is transferred.

Figure 39 further supports the point that scaling is occurring, as we can see that there is an increase in salt passage with an increase in recovery due to scaling of the membrane surface, thereby reducing the hydrophobicity at these points and allowing water to pass though.

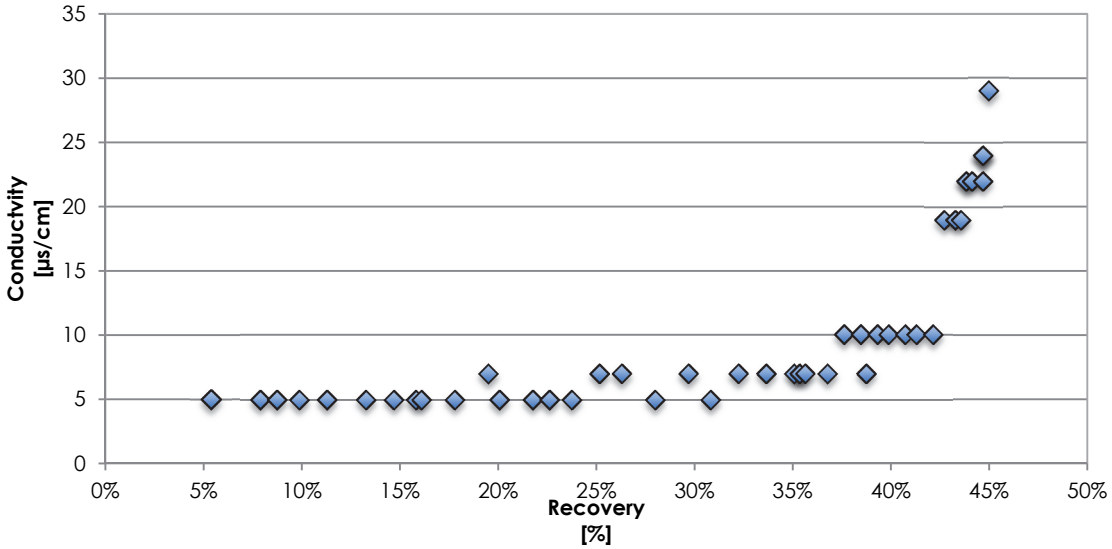

Figure 39: Change in product conductivity with recovery (NTF1026-L01)

These results further highlight the point that the highest flux is not necessarily the optimum method of running an MDC process, since this may lead to faster membrane fouling.

Two additional long runs were performed, both with a product and feed temperatures of 10°C and 60°C respectively and both with the use of an NTF1026-C02 membrane. The only difference being that the one experiment included the use of an antiscalant (Antiscalant 1), whilst the other did not. The experiments with the antiscalant are labelled as "60-10 with Antiscalant" whilst the other two will be labelled "60-10" and "70-10" accordingly. These results are presented together, along with the previous long run in Figure 40, furthermore their product conductivities are presented in Figure 41.

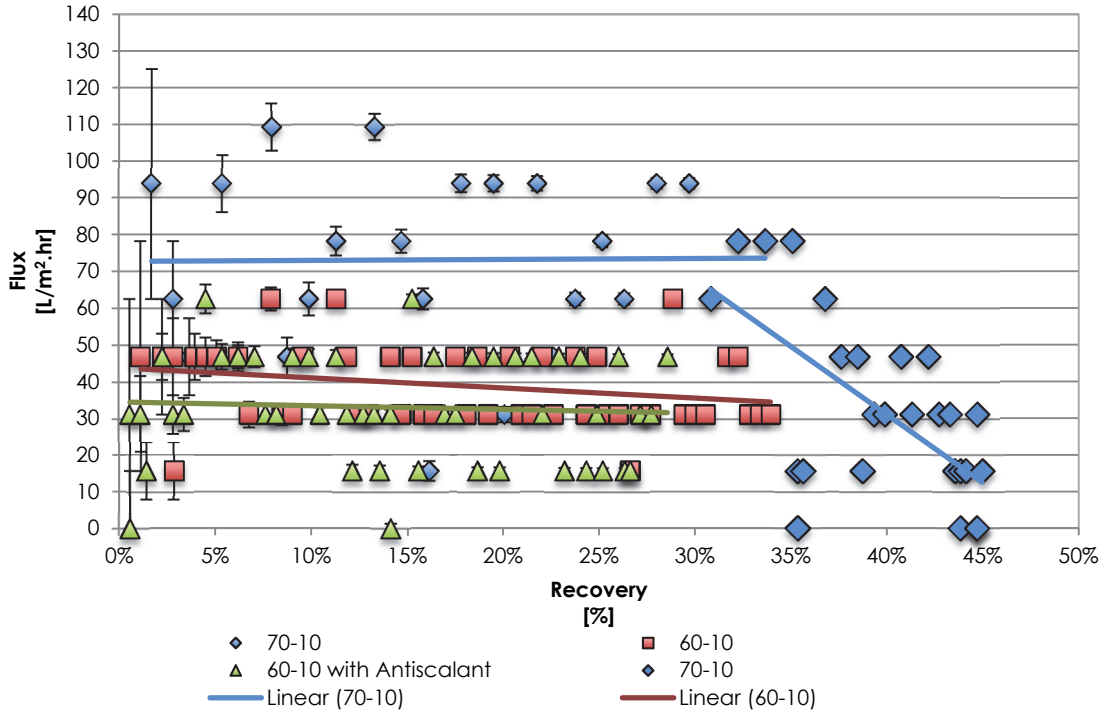

Figure 40: Flux as a function of recovery for three long runs

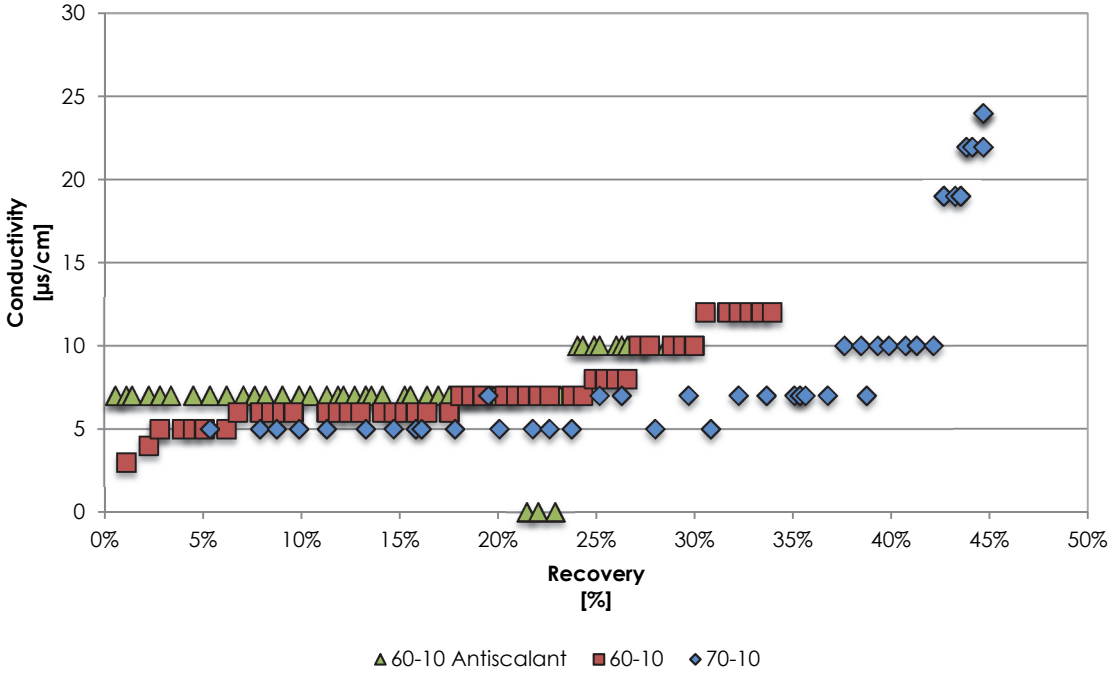

Figure 41: Change in product conductivity with recovery

These results indicate that firstly the amount of water recovered was less in the "60-10" experiment and the least in the "60-10 with Antiscalant" experiment, but this was expected since this follows the fact that these two experiments had lower flux rates. At first glance the two "60-10" experiments seem to be better than the "70-10" due to the fact that they do not have a sudden drop in flux rate. The possible reason that these two experiments did not see a sudden drop in flux rate could be attributed to the fact that not enough water had been recovered after 8 hours and therefore the saturation limit had not been reached yet, which could have led to salt crystallisation and possibly membrane fouling. Additional experiments are required at higher water recoveries to confirm this.

It should also be noted that the "60-10 with antiscalant" experiment had a slower decline in flux rate than the "60-10" experiment, which could be explained by the dispersant effect of the antiscalant, minimising scaling. However as previously mentioned, additional longer experiments are required to confirm this.

5.4.2 The effect of using actual Brine on the flux rate

An experiment using actual brine from a coal mine, with water characteristics as given in Table 10, was also performed. This was done at a feed temperature of 60°C and product temperature of 10°C and using membrane NTF1026-L01, whilst all other parameters stayed the same as the experiments performed in Section 5.4.1.1.

The flux obtained after 180 minutes was 45.71 L/m^2.hr. This was considerably less than the 58.2 L/m^2.hr that was obtained with the Synthetic brine solution under the same conditions. This discrepancy could be due to all the additional ions and organic matter that the actual brine has compared to the Synthetic.

Since no major flux decline was observed during this experiment, an additional experiment was performed over an 8-hour period to determine if there would be a drop in flux, with the results presented in Figure 42 and Figure 43.

Table 10: Brine water characteristics

Parameter	Units	Value
pH – Value at 25°C	-	8.3
Electrical Conductivity at 25°C	mS/m	1188
Total Dissolved Solids at 180°C *	mg/L	11900
Suspended Solids at 105°C *	mg/L	<1.0
Turbidity	NTU	0.4
Total Alkalinity as $CaCO_3$	mg/L	464
Bicarbonate Alkalinity as $CaCO_3$ *	mg/L	464
Chloride as Cl	mg/L	342
Sulphate as SO_4	mg/L	7713
Fluoride as F	mg/L	1.9
Nitrate as N	mg/L	0.5
Nitrite as N	mg/L	0.9
Silica as SiO_2 *	mg/L	17
Total Organic Carbon as C [s]	mg/L	2.9
Chemical Oxygen Demand as O_2 (Total)	mg/L	26
Total Coliform Bacteria	/ 100 mL *	3300
E. Coli	/ 100 mL *	0
Free & Saline Ammonia as N	mg/L	0.9
Sodium as Na	mg/L	2091
Potassium as K	mg/L	60
Calcium as Ca	mg/L	622
Magnesium as Mg	mg/L	492
Aluminium as Al	mg/L	<0.10
Barium as Ba *	mg/L	0.086
Boron as B *	mg/L	4.63
Chromium as Cr	mg/L	<0.025
Copper as Cu	mg/L	0.016
Iron as Fe	mg/L	0.044
Manganese as Mn	mg/L	0.042
Phosphorus as P *	mg/L	0.3
Strontium as Sr *	mg/L	15
Zinc as Zn	mg/L	0.066

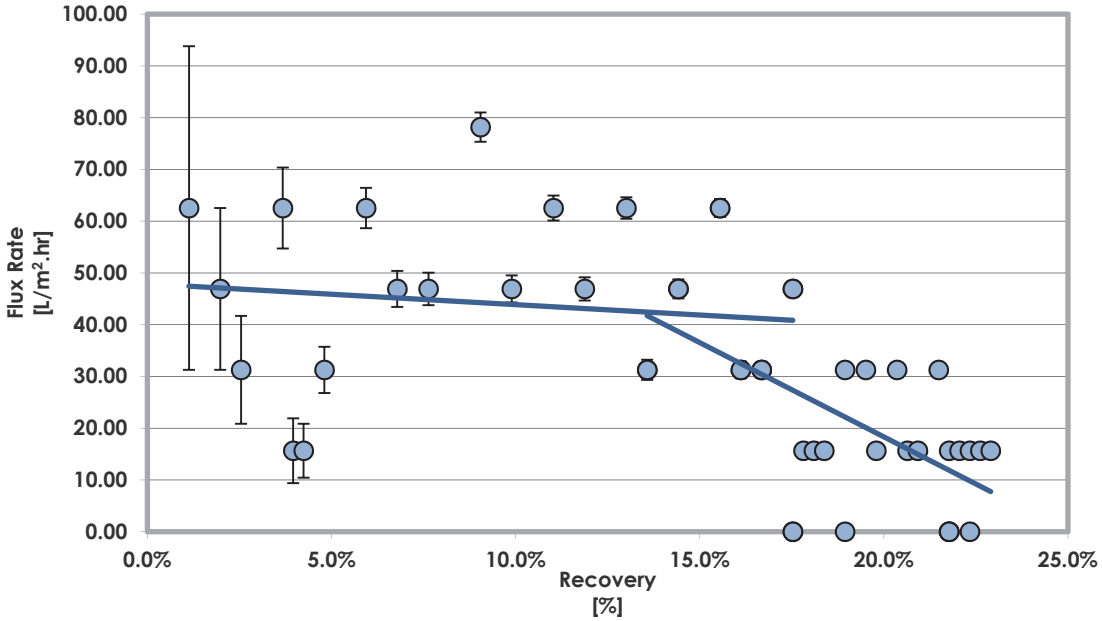

Figure 42: Flux rate as a function of water recovery for brine from a coalmine

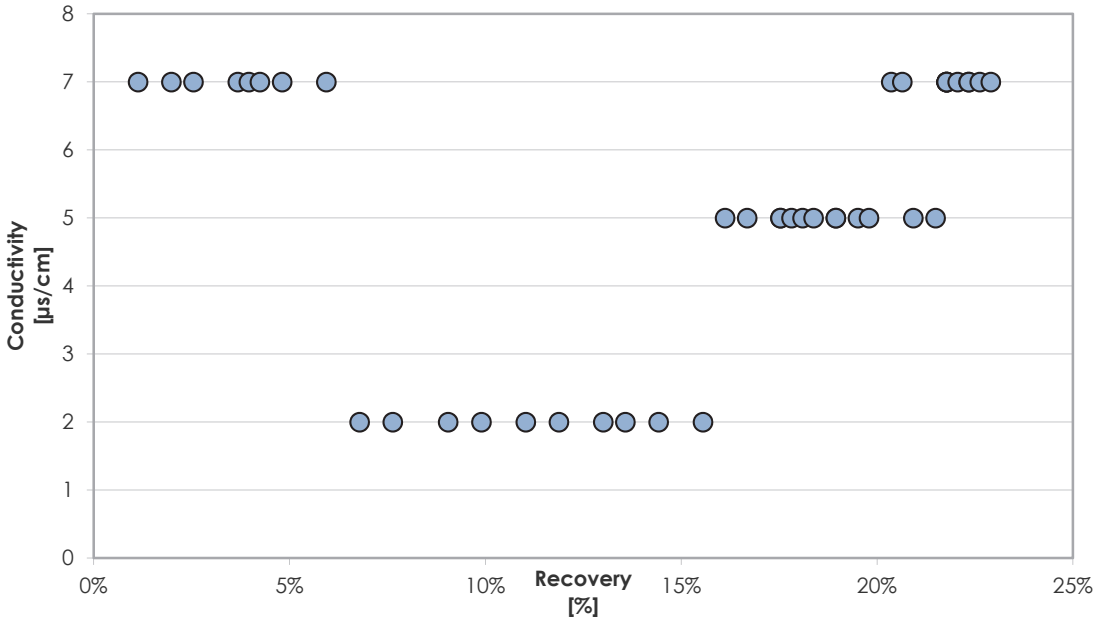

Figure 43: Product Conductivity as a function of Water recovery for brine from a coalmine

The results in Figure 42 indicate that the flux rate dropped after a recovery of approximately 16-18%, which is also the point at which the product conductivity starts to increase, which most likely be due to membrane fouling or scaling. The initially measured higher product conductivity may have been attributed to the measurement of a stagnant slug of water from a previous experiment that was trapped within the probe's measurement cavity and had not been properly displaced. The uncharacteristic elevated conductivity measurement issue was resolved after soaking the probe in deionised water for a few minutes.

The flux rate for the actual brine dropped off at a much lower recovery than the synthetic brine, again indicating that the extra ions and organics in the actual brine affect the flux and fouling rate of the membrane. In order to determine if a constant flux rate can be maintained at a constant recovery, a continuous process would be required as opposed to the current batch set-up.

5.4.3 The effect of operating conditions (and flux rates) on crystal morphology and size

To check the effects of how a change in parameters affects the crystal structure, 6 crystal samples from key experiments were chosen for Scanning Electron Microscope (SEM) analysis to determine the structure of the crystals, as well as Energy Dispersive X-rays (EDX) to determine the elements present in the salts formed.

The six samples that were chosen were namely:

Table 11: Sample characteristics

	Feed Temperature (°C)	Product Temperature (°C)	ΔT (°C)	Flow Rate (L/hr)	Antiscalant	Motivation
Sample 1	70	10	60	130	None	Determine the effect of high ΔT
Sample 2	40	30	10	130	None	Determine the effect of lower ΔT
Sample 3	60	10	50	200	None	Determine the effect of high cross flow velocity and lower temperature polarisation
Sample 4	60	10	50	60	None	Determine the effect of low cross flow velocity and higher temperature polarisation
Sample 5	60	10	50	130	Antiscalant 2	Determine the effect of an aqueous phosphonic acid based antiscalant
Sample 6	60	10	50	130	Antiscalant 1	Determine the effect of an antiscalant with organic functional groups

5.4.3.1 The effects of temperature on crystal formation

Samples 1 and 2 were analysed to determine effects of a higher and lower temperature difference between on the feed and product sides on the crystal formation. When looking at the general consistency of the product at 2000x zoom as seen in Figure 44 and Figure 45, the two products look quite similar. The crystal morphology can be characterised as amorphous with a wide particle size distribution.

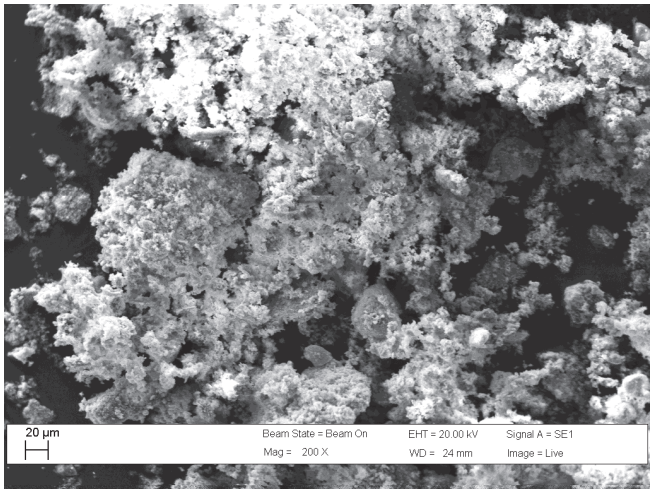

Figure 44: SE Micrograph of Sample 1 (ΔT = 60°C)

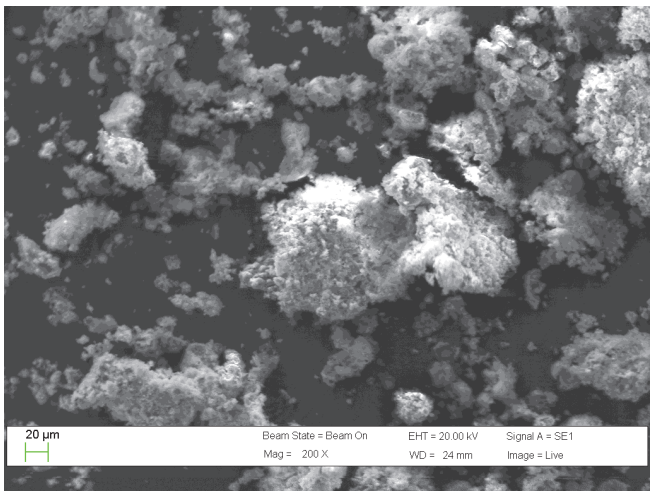

Figure 45: SE Micrograph of Sample 2 (ΔT = 10°C)

Similarly when zooming in 5000x as seen in Figure 46 and Figure 47, the crystal structures still look quite similar.

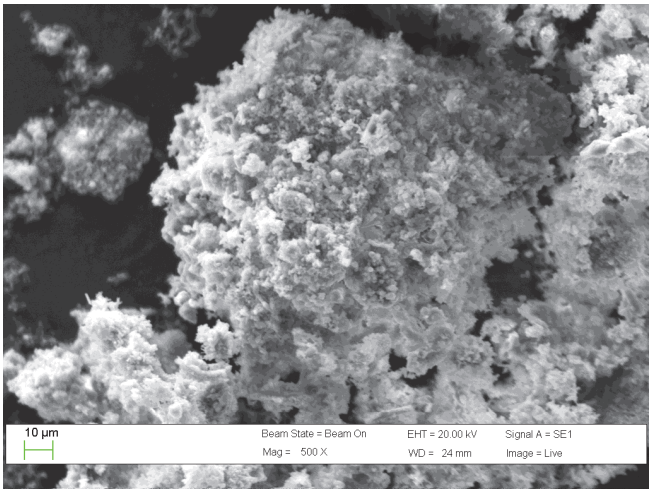

Figure 46: SE Micrograph of Sample 1 (ΔT = 60°C)

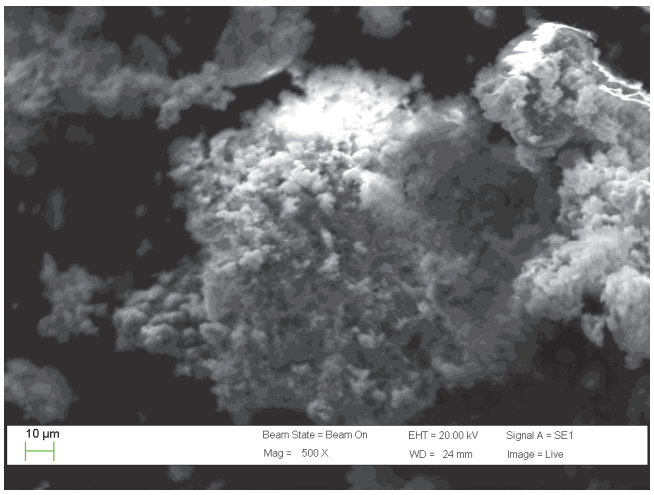

Figure 47: SE Micrograph of Sample 2 (ΔT = 10°C)

Again, the crystal morphology can be characterised as amorphous with a wide particle size distribution.

The results from Sample 1 are consistent with a high flux rate and higher supersaturation resulting in a high concentration of smaller nucleated particles, agglomerated into clusters. The results for Sample 2 (lower temperature difference between the feed and product sides), albeit at a 7 times lower flux rate also yielded a high concentration of smaller nucleated particles, agglomerated into clusters.

A possible explanation for the similarity in the particle morphologies and sizes could be that the constant agitation speed in the feed reactor of 600 rpm had a high shearing effect on the particles as well as due to the milling effect caused by the peristaltic pump.

Furthermore for all the experiments performed to determine the effects of temperature on the flux rate, the samples were filtered through filter paper, which took up to an hour to filter the whole feed sample during which time the temperature of the feed sample dropped considerably. This could have had an impact on the crystal characteristics. All subsequent crystal samples were filtered with the aid of a vacuum pump and a Buchner funnel, and thereby reducing the filtration time and the possible effects of sample cooling.

5.4.3.2 The effects of flow rate on crystal structure

In order to see the effects of flow rate on crystal formation, the two extreme flow rates were chosen for analysis, namely 60 L/hr and 200 L/hr. The SE Micrographs can be seen in Figure 48 to Figure 51.

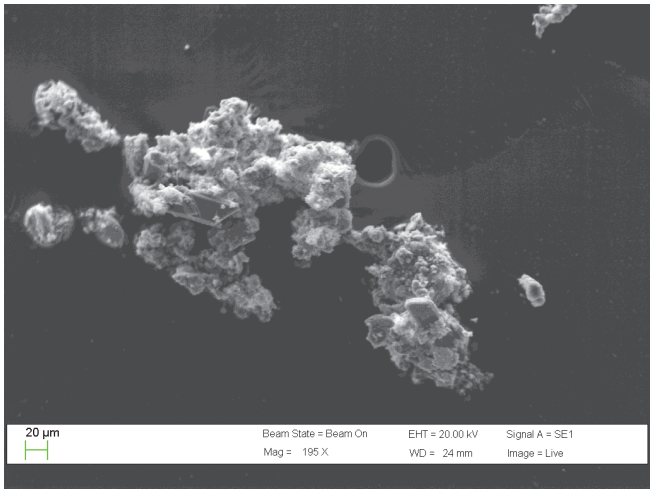

Figure 48: SE Micrograph of Sample 3 (200 L/hr)

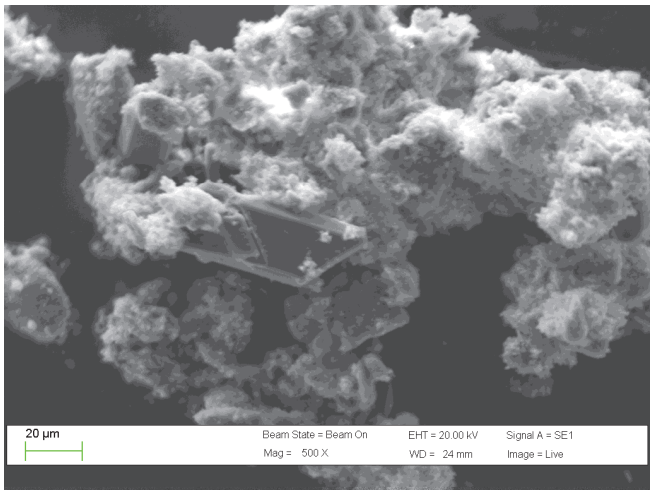

Figure 49: SE Micrograph of Sample 3 crystal (200 L/hr)

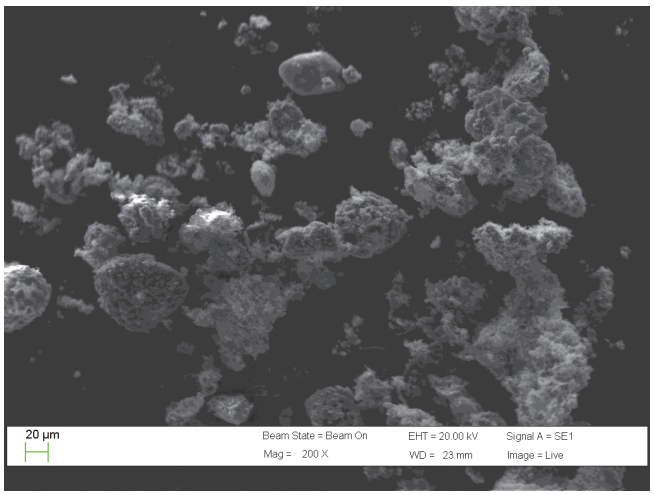

Figure 50: SE Micrograph of Sample 4 (60 L/hr)

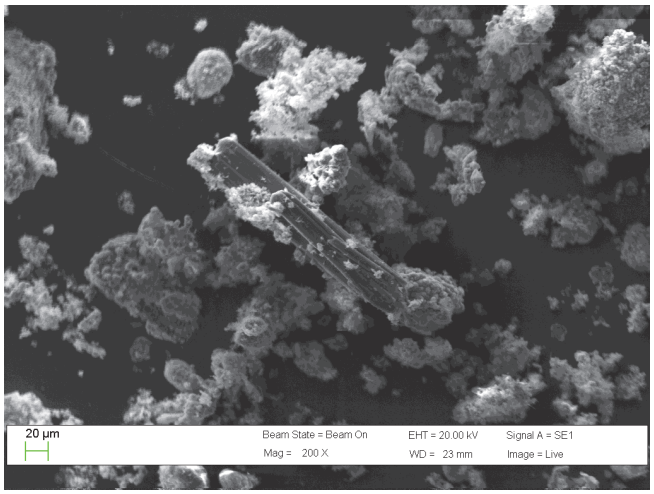

Figure 51: SE Micrograph of Sample 4 crystal (60 L/hr)

Again, the crystal morphology can be characterised as amorphous with a wide particle size distribution. However, there are signs of more structured crystalline particles for both operating conditions.

In this case, it was expected that Sample 4 would have larger more defined crystals than Sample 3 due to the lower flux rate. However, Samples 3 and 4 had very similar appearances to each other and furthermore both samples generally had a very similar appearance to Samples 1 and 2, with most of the sample having a fluffy, agglomerated, amorphous crystalline morphology with a wide particle size distribution. A possible explanation for the similarity in the particle morphologies and sizes could be that the constant agitation speed in the feed reactor of 600rpm had a high shearing effect on the particles as well as due to the milling effect caused by the peristaltic pump.

One dissimilarity to Samples 1 and 2 was the presence of very defined crystals as mentioned previously. This is discussed in Section 4.3.2.

5.4.3.3 The effects of antiscalant on crystal structure

In order to determine the effects of antiscalant on the system, samples from both antiscalant experiments were analysed. The crystal growth was expected to be similar to each other, but smaller than the other samples due to the dispersive effect of the antiscalant. The SE Micrographs can be seen in Figure 52 and Figure 53.

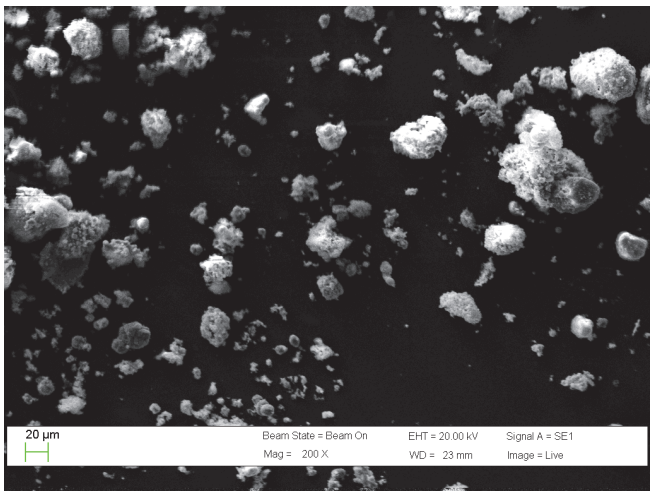

Figure 52: SE Micrograph of Sample 5 (Antiscalant 2)

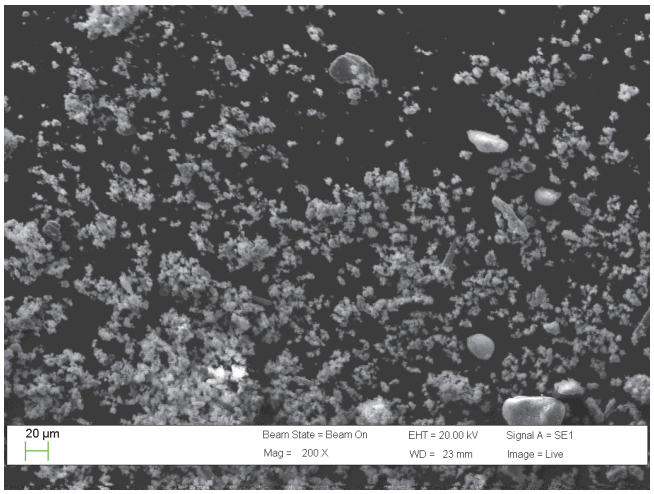

Figure 53: SE Micrograph of Sample 6 (Antiscalant 1)

These images are consistent with what was expected in that the agglomerates are significantly smaller and well dispersed in the presence of an antiscalant. Sample 6 (Antiscalant 1) which produced smaller agglomerates would have been expected to have a lower impact on the flux reduction in an MDC process due to the fouling/scaling effect. However, the fact that it had an effect on reducing flux in the MDC process, further strengthens the case for the negative effect that antiscalants with organic functions groups have on the organic fouling of MDC membranes. No defined crystals were observed in Sample 5, whilst they could be seen in Sample 6, although they were smaller than in Samples 3 and 4. There were also some smooth crystals that were observed in Sample 6. The analysis of these images fits in with what was said in Section 2.1.5, in that the antiscalant causes crystal modifications and some have a dispersive property.

From this analysis it can be said that the antiscalant works well as a dispersant, which could help in reducing membrane fouling, provided that there is no detrimental effect of any organic functional groups that may cause organic fouling of the MDC membranes. Generally, with an antiscalant the salt crystals are a lot smaller and can be swept away by the cross flow. Furthermore, the salt that does deposit on the membrane surface will be less likely to grow into bigger crystals due to the dispersive nature of the antiscalant, and therefore it will take longer for the membrane to be scaled with salt crystals.

5.4.4 The effect of operating conditions on the chemical composition of crystals formed

5.4.4.1 The effects of temperature on crystal composition

Based on the thermodynamic modelling in Chapter 4, Sample 2 was expected to have a high concentration of $CaCO_3$, since the recovery over this time period was only 3% and the temperature was 40°C. Whereas Sample 1 was expected to have a high concentration of $CaSO_4$ since the recovery was 21% at 70°C. The EDX analysis for these two samples, as given in Table 12, correspond with the thermodynamic modelling to certain degree, in that Sample 2 has a much higher Carbon concentration than Sample 1. However Sample 1 was expected to have a higher sulphur content than observed, according to the thermodynamic modelling.

Table 12: EDX analysis of Samples 1 and 2

Element	Elemental % of Sample 1 (relating to Figure 44)	Elemental % of Sample 2 (relating to Figure 45)
Oxygen	74.07	66.31
Calcium	21.32	17.74
Carbon	2.73	14.60
Sodium	0.93	0.65
Sulphur	0.69	0.51
Magnesium	0.27	0.13

An X-ray powder diffraction (XRD) analysis was also performed on these samples. The analysis of Sample 1 indicated the presence of Aragonite, Calcite and Gypsum, whilst in Sample 2; only aragonite and calcite were detected, which is in line with the thermodynamic modelling.

In order to check if the whole sample has a uniform density distribution, an image using the Backscatter Detector (BSD) was obtained as seen in Figure 54, which showed uniformity of the whole sample. This was done for all samples to confirm that they all exhibited a uniform density distribution as can be seen in Appendix B.

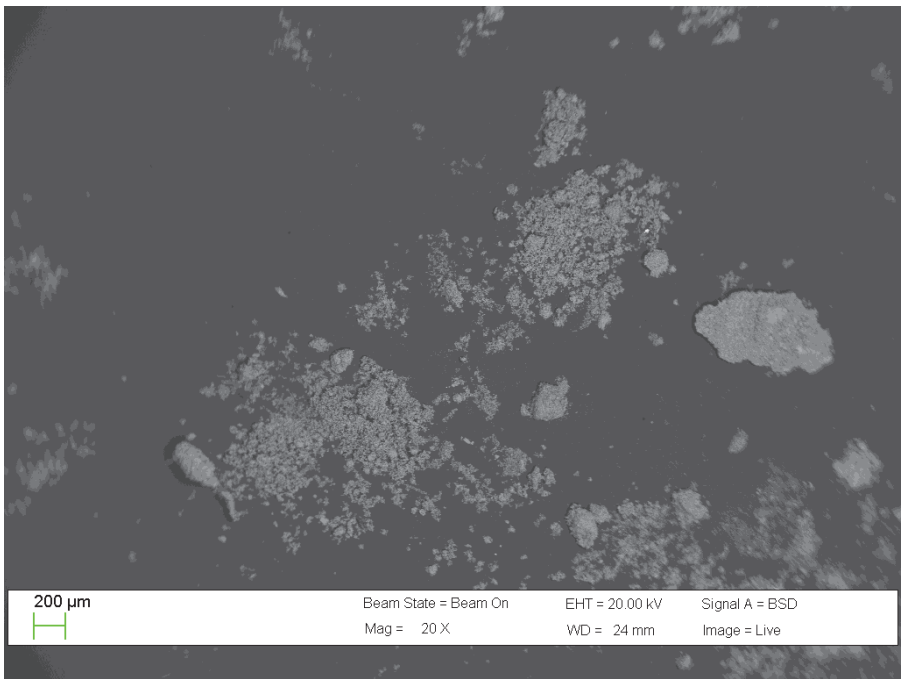

Figure 54: BSD of Sample 1

5.4.4.2 The effects of flow rate on crystal composition

Due to the fact that the samples were run at 60°C and had recoveries of 16.4% and 10.2% for Samples 3 and 4 respectively, the predominant salt was expected to be $CaSO_4$, according to the thermodynamic modelling. However, the results from the EDX performed on these samples, as can be seen in Table 13, suggest that the fluffy crystals had a similar composition to Sample 1, indicating a predominance of $CaCO_3$ whereas the defined crystal is more likely to be $CaSO_4$.

Table 13: EDX analysis of Samples 3 and 4

	Fine		Crystal	
Element	Elemental % of Sample 3 (relating to Figure 48)	Elemental % of Sample 4 (relating to Figure 50)	Elemental % of Sample 3 (relating to Figure 49)	Elemental % of Sample 4 (relating to Figure 51)
Oxygen	67.94	75.30	71.03	78.87
Calcium	25.22	19.68	17.26	10.96
Carbon	5.86	4.22	0.95	0.35
Sulphur	0.98	0.80	10.76	9.82

The XRD analysis detected the presence of Aragonite, Calcite and Gypsum for Sample 3, whilst in Sample 4, Anhydrite was also detected. This is consistent with the thermodynamic results.

5.4.4.3 The effects of antiscalant on crystal composition

Since these samples were also run at 60°C and had recoveries of 15.3% and 11.9% for Sample 5 and 6 respectively, the predominant salt was expected to be $CaSO_4$ according to the thermodynamic modelling.

The EDX analysis, as seen in Table 14, of the bulk crystal formation in Sample 5, again suggested a predominant presence of $CaCO_3$, instead of $CaSO_4$. When the bulk portion of Sample 6 was analysed a surprisingly high content of carbon was observed and it is unclear as to what this can be attributed to. Whilst the defined crystal indicated a similar quantity of $CaCO_3$ and $CaSO_4$, and the smooth crystal seemed to be predominantly $CaCO_3$.

Table 14: EDX analysis of Samples 5 and 6

	Fine		Crystal	Smooth
Element	**Elemental % of Sample 5 (relating to** Figure 52**)**	**Elemental % of Sample 6 (relating to** Figure 53**)**	**Elemental % of Sample 6 (relating to** Figure 53**)**	**Elemental % of Sample 6 (relating to** Figure 53**)**
Oxygen	64.59	56.71	70.92	64.56
Calcium	15.44	7.72	11.69	17.93
Carbon	16.46	35.17	10.12	16.92
Sulphur	0.65	0.40	7.28	0.58

The XRD analysis of Sample 5 indicated the presence of Aragonite, Calcite and Anhydrite, Sample 6 on the other hand did not indicate the presence of Anhydrite, however it did indicate the presence of Gyspum. This was not expected and could possibly be attributed to the influence of the antiscalants on the crystal formation.

CHAPTER 6 - Conclusions

The investigations into the effects of (i) operating temperature, (ii) operating feed water concentration, (iii) operating flow rates, and (iv) antiscalant addition on the permeate flux rates all yielded the following results:

i) Increased feed temperatures and increased temperature difference led to the highest flux rates
ii) A flux rate of 9.6 L/m^2.hr was achieved for feed and product temperatures of 40°C and 30°C respectively
iii) A flux rate of 65.2 L/m^2.hr was achieved for feed and product temperatures of 70°C and 10°C respectively
iv) Changes in feed water concentrations (at TDS's of 8000-16000 mg/L) did not have any significant effect on the flux rates.
v) Increased flow rates (ranging from 0.15 m/s to 0.49 m/s in the main feed pipe) led to improved flux rates, increasing from 31.3 L/m^2.hr to 50.4 L/m^2.hr.
vi) Phosphonic based antiscalants did not have an effect on the flux rates, whilst the organic based antiscalant resulted in a slight reduction in the flux rate from 42.6 L/m^2.hr to 36.5 L/m^2.hr.

The flux rates obtained also varied depending on the type of membrane backing layer that was used in that membranes with a PE + Polyester non-woven fabric backing layer achieved the highest flux rate (58.2 L/m^2.hr) whilst the polyester cloth backing layer achieved the lowest flux rate (42.6 L/m^2.hr).

The investigations into the effects of (i) operating temperature, (ii) operating feed water concentration, (iii) operating flow rates, and (iv) antiscalant addition on the water purity produced good results, in that for all of these parameters the product waters had extremely low conductivity and only started to increase once scaling on the membrane surface and pore wetting caused a decrease the flux rate.

Limited distinction could be made with respect to the differences in the morphology between the various factors investigated. This was most likely due to the constant agitation speed in the feed reactor of 600rpm, which had a high shearing effect on the particles, as well as due to the potential milling effect caused by the peristaltic pump. However, the addition of antiscalant did yield good results in that the agglomerates were significantly smaller and well dispersed in the presence of an antiscalant.

When looking at the composition of salts formed, only Sample 2 yielded result that were consistent with thermodynamic modelling results. The higher carbon concentration was indicative of $CaCO_3$ being formed rather than $CaSO_4$.

Importantly, the flux rates obtained from these experiments are significantly higher than those reported in literature and indicates a definite possibility that membrane distillation could be used to increase water recovery from RO brines whilst generating usable salts as a by-product. However, further research needs to be undertaken into the development of cheaper membranes for this purpose, since currently hydrophobic membranes are being used more for laboratory scale use as opposed to large-scale operations. Furthermore, there is a trade-off between maximising flux and minimising the rate of scaling/fouling. Increased flux implies less membrane surface area is required and consequently a lower CAPEX, however, increased flux results in increased propensity for scaling and fouling, which has a negative impact on OPEX.

CHAPTER 7 - Recommendations

Based on the results obtained from these experiments, there are a few areas that have been identified as being key to improve the understanding of MDC.

1) One of the biggest issues with performing these experiments was the difficulty in finding the correct membranes that were suitable for the experiments. There are many aspects of a membrane that could affect the flux rate and furthermore some membranes may have greater tendency to scale than others. Therefore additional research is required to identify which membrane characteristics would be most suitable for an MDC application.

2) The crystallisation aspects of this project did not always yield the expected results in terms of the particle size distribution of the crystals formed. A possible reason for this is the high shear force imparted by the agitator, which resulted in crystal breakage and attrition. Further experiments at a lower agitation rate and with different impeller configurations are recommended.

3) Even though the experiments were run for up to 8 hours, this was not always long enough to see a sudden drop in flux rate, most likely due to the fact that the supersaturation point had not been reached for certain salts. By performing longer tests, the supersaturation point for different systems could be determined, and furthermore at which point scaling or fouling becomes a concern.

4) A limitation to the current system is that it was designed as a batch system, which means that once the point of supersaturation had been determined, it could not be indefinitely maintained at this point. Consequently, further investigations into a continuous-mode of operation would provide further valuable insights into scaling this process up to pilot scale and eventually industrial scale.

5) The experiment performed with the brine from a coal mine indicated that the membrane fouled/scaled a quicker than the synthetic brine, which could be as a result of the effect of some of the minor elements in the brine and leaves room to further explore which water characteristics would lead to the highest fouling/scaling rate.

6) Due to the fact that many of the membranes tested were very delicate and therefore could not be used for experimentation with the current set-up, it would be advisable to perform additional tests to see the effect of different types of feed and product spacers (used to strengthen and support the membrane) would have on the flux and also additionally on the fouling rate.

7) Following on from Point (6), the delicacy of the membranes meant that the flow rate was limited, since the increased flow rate resulted in an increased pressure on the membranes, resulting in deformation. Therefore, if suitable feed and product spacers are found, the flow rate could be increased such that they are more closely aligned to industrial flow rates (which are expected to be in the region of 2 m/s).

8) The applicability of MDC for AMD, particularly in the context of South African mining, suggests that the effects of pH on the system would be of great value.

9) In order to determine the energy efficiency of the system, a detailed energy balance over the system should be considered.

CHAPTER 8 - References

ALKHUDHIRI, A., N. DARWISH, and N. HILAL. 2012. Membrane distillation: A comprehensive review. *Desalination*. **287**, 2-18.

BALASUBRAMANIAN, P. 2013. A brief review on best available technologies for reject water (brine) management in industries. *International Journal Of Environmental Sciences*. **3**(6), 2010-2018.

CAMACHO, L.M., L. DUMÉE, J. ZHANG et al. 2013. Advances in Membrane Distillation for Water Desalination and Purification Applications. *Water*. **5**, 94-196.

DOW, N., J. ZHANG, M. DUKE et al. 2008. *Membrane Distillation of Brine Wastes*. Adelaide: Water Quality Research Australia Limited.

DOW, N., Z. ZHANG, M. DUKE et al. 2008. *Membrane Distillation of Brine Wastes*. Adelaide: Water Quality Research Australia Limited.

ECOLOGYDICTIONARY.ORG. 2008. *EcologyDictionary.org*. [online]. [Accessed 23 Jul 2015]. Available from World Wide Web: http://www.ecologydictionary.org/MYPgV/EPA-Terms-of-Environment-Dictionary/BRINE

EMIS. 2010. *Membrane distillation*. [online]. [Accessed 04 Mar 2015]. Available from World Wide Web: http://emis.vito.be/techniekfiche/membrane-distillation?language=en

GRYTA, M. 2001. Direct Contact Membrane Distillation with Crystallization Applied to NaCl Solutions.

KHALIFA, A. E. and D. U. LAWAL. 2014. Flux Prediction in Direct Contact Membrane Distillation. *International Journal of Materials, Mechanics and Manufacturing*. **2**(4), 302-307.

KHAYET, M. *Desalination by Membrane Distillation*. [online]. [Accessed 03 Mar 2015]. Available from World Wide Web: http://www.desware.net/DESWARE-SampleAllChapter.aspx

KONIG, A. and D. WECKESSER. 2005. Membrane Based Evaporation Crystallization. *In*: *16th International Symposium on Industrial Crystallization 2005*., 1171-1176.

KULLAB, A. 2011. *Desalination Using Membrane Distillation*. Stockholm.

LENNTECH, B.V. *Scaling and Antiscalants*. [online]. [Accessed 14 January 2016]. Available from World Wide Web: http://www.lenntech.com/antiscalants.htm

LILEY, E.L., G. H. THOMSON, D. G. FRIEND et al. 1999. Section 2: Physical and Chemical Data. *In*: D. W. GREEN, (ed). *Perry's Chemical Engineers' Handbook*, McGraw-Hill.

MARIAH, L. 2006. *Membrane Distillation Of Concentrated Brines*. Durban.

MCCABE, W. L., J.C. SMITH, and P. HARRIOTT. 1993. Unit Operations of Chemical Engineering. Fifth Edition. New York: McGraw-Hill Book Co, 882-923.

ONSEKIZOGLU, P. 2012. Membrane Distillation: Principle, Advances, Limitations and Future Prospects in. *In*: S. ZERESHKI, (ed). *Distillation - Advances from Modeling to Applications*, Intech, 233-266.

QTAISHAT, M.R. and F. BANAT. 2012. Desalination by solar powered membrane distillation systems. *Desalination*. **308**, 186-197.

SALEHI, M.A. and R. ROSTAMANI. 2013. Review of membrane distillation for the production of fresh water from saline water. *Journal of Novel Applied Sciences*. **2**, 1072-1075.

SALZMAN, W.R. 2004. *The Melting Curve for Water; Vapor Pressure*. [online]. [Accessed 06 Apr 2016]. Available from World Wide Web: http://www.chem.arizona.edu/~salzmanr/480a/480ants/watvp/watvp.html

TUN, C.M., A.G. FANE, J.T. MATHEICKAL, and R. SHEIKHOLESLAMI. 2005. Membrane distillation crystallization of concentrated salts—flux and crystal formation. *Journal of Membrane Science*. **257**(1-2), 144-155.

UNIVERSITY OF COLORADO AT BOULDER. 2015. *Organic Chemistry at CU Boulder*. [online]. [Accessed 21 Apr 2015]. Available from World Wide Web: http://orgchem.colorado.edu/Technique/Procedures/Crystallization/Crystallization.html

VAN NESS, H. C. and M. M. ABOTT. 1999. Section 4: Thermodynamics. *In*: D. W GREEN, (ed). *Perry's Chemical Engineerrs' Handbook*, McGraw-Hill.

WORLD BANK GROUP. *Introduction to Wastewater Treatment Processes*. [online]. [Accessed 03 Mar 2015]. Available from World Wide Web: http://water.worldbank.org/shw-resource-guide/infrastructure/menu-technical-options/wastewater-treatment

ZENG, L. and C. GAO. 2010. The prospective application of membrane distillation in the metallurgical industry. *Membrane Technology*. **2010**(5), 6-10.

Appendix A: Tank level calibration

Table A1: Feed Tank Level Calibration

Level (cm)	ΔL (cm)	Volume added (ml)	ml/cm
404		0	
406.3	2.3	480	208.7
408.6	2.3	495	215.2
410.8	2.2	474	215.5
412.9	2.1	475	226.2
		Average	**216.4**

Table A2: Product Tank Level Calibration

Level (cm)	ΔL (cm)	Volume added (ml)	ml/cm
435.5	0	0	0.0
433.3	2.2	482	219.1
431.2	2.1	486	231.4
428.9	2.3	491	213.5
426.9	2	482	241.0
		Average	**226.2**

Appendix B: BSD Images

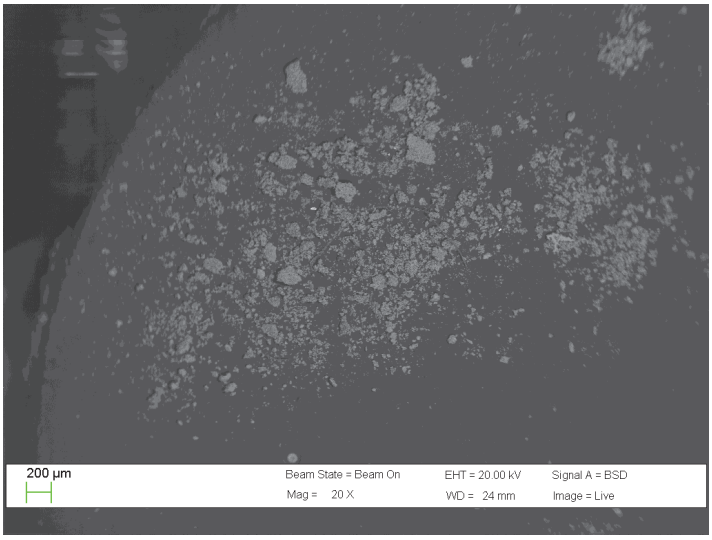

Figure 55: BSD of Sample 2

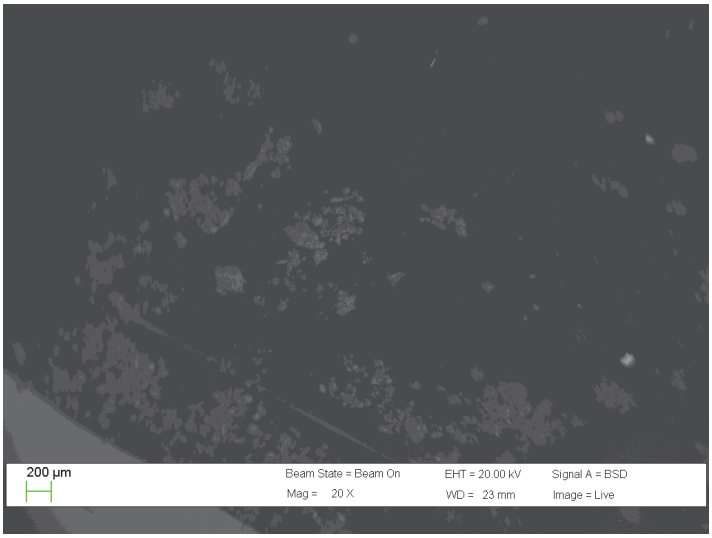

Figure 56: BSD of Sample 3

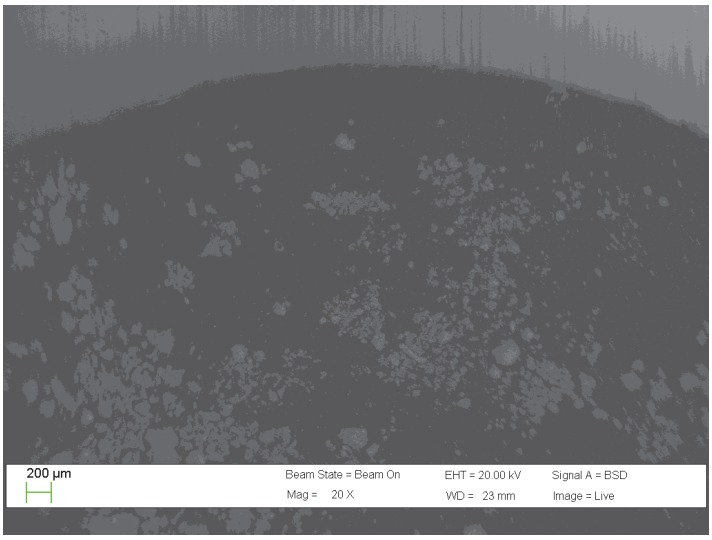

Figure 57: BSD of Sample 4

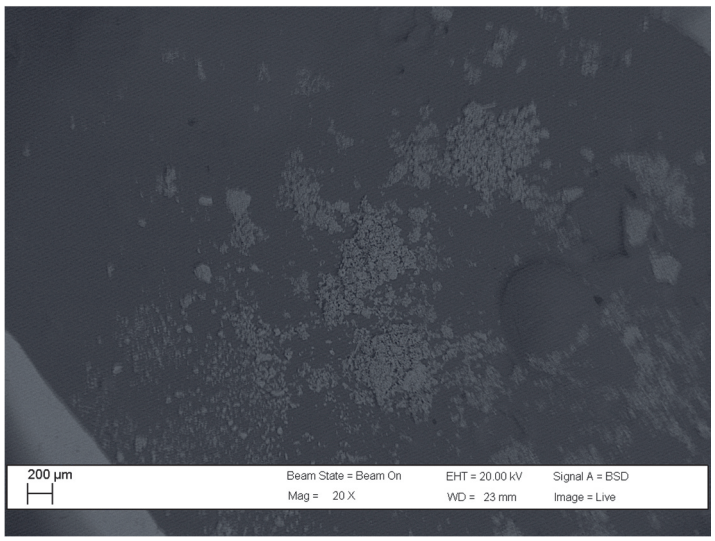

Figure 58: BSD of Sample 5

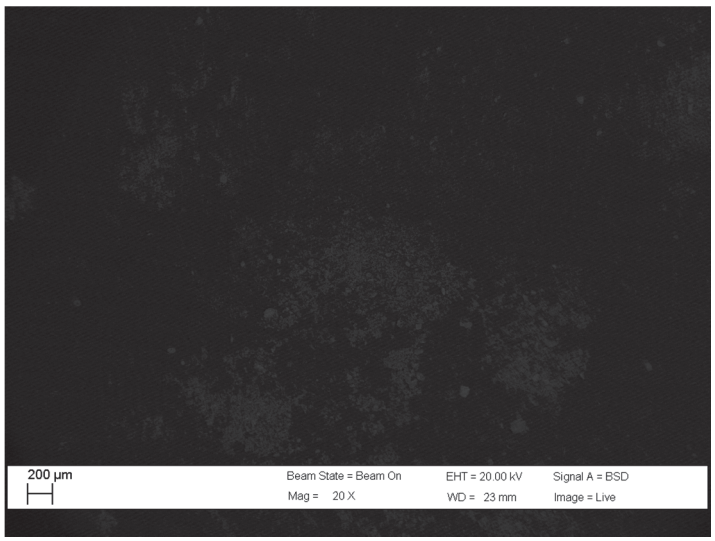

Figure 59: BSD of Sample 6